Integrated Trajectory-Tracking and Vibration Control of Kinematically-Constrained Warehousing Cable Robots

by

Hamed Jamshidifar

A thesis
presented to the University of Waterloo
in fulfillment of the
thesis requirement for the degree of
Doctor of Philosophy
in
Mechanical and Mechatronics Engineering

Waterloo, Ontario, Canada, 2018

Examining Committee Membership

The following served on the Examining Committee for this thesis. The decision of the Examining Committee is by majority vote.

External Examiner	NAME: Philippe Cardou
	Title: Professor, Department of Mechanical Engineering, Laval University
Supervisors	NAME: Amir Khajepour
	Title: Professor, Department of Mechanical and Mechatronics Engineering, University of Waterloo
	NAME: Baris Fidan
	Title: Associate Professor, Department of Mechanical and Mechatronics Engineering, University of Waterloo
Internal Member	NAME: Jan Huissoon
	Title: Professor, Department of Mechanical and Mechatronics Engineering, University of Waterloo
Internal Member	NAME: Ehsan Toyserkani
	Title: Professor, Department of Mechanical and Mechatronics Engineering, University of Waterloo
Internal-external Member	NAME: John Zelek
	Title: Associate Professor, Department of Systems Design Engineering, University of Waterloo

Author's Declaration

This thesis consists of material all of which I authored or co-authored: see Statement of Contributions included in the thesis. This is a true copy of the thesis, including any required final revisions, as accepted by my examiners.

I understand that my thesis may be made electronically available to the public.

Statement of Contributions

The following co-authors have contributed to the current work:

Professor Amir Khajepour and Professor Baris Fidan supervised this Ph.D. thesis.

Mr. Mitch Rushton assisted with coding and performing different tests.

Dr. Saeid Khosravani assisted with designing the controller.

Abstract

With the explosion of e-commerce in recent years, there is a strong desire for automated material handling solutions including warehousing robots. Cable driven parallel robots (CDPRs) are a relatively new concept which has yet to be explored for high-speed pick-&-place applications in the industry. Compared to rigid-link parallel robots, a CDPR possesses significant advantages including: large workspace, low moving inertia, high-speed motion, low power consumption, and incurring minimal maintenance cost. On the other hand, the main disadvantages of the CDPRs are the cable's unilateral force exerting capability and low rigidity which is resulting in undesired vibrations of their moving platform. Kinematically-constrained CDPRs (KC-CDPRs) include a special class of CDPRs which provide a considerably higher level of stiffness in undesired degrees of freedom (DOFs) via connecting a set of constrained cables to the same actuator. Nevertheless, undesired vibrations of the moving platform are still their main problem which request more attention and investigation.

Dynamic modeling, stiffness optimization, vibration and trajectory-tracking control, and stiffness-based trajectory-planning of redundant KC-CDPRs are studied in this thesis. As a new technique, we separate the moving platform's vibration equations from its desired (nominal) equations of motion. The obtained vibration model forms a linear parametric variable (LPV) dynamic system which is based for the following contributions:

1) Proposing a new tension optimization approach to minimize undesired perturbations under external disturbances in a desired direction; and demonstrating the effectiveness of kinematically-constrained actuation method in vibration attenuation of CDPRs in undesired DOFs. 2) Providing the opportunity of using a wide class of well-established robust and optimal LPV-based control methods, such as $H\infty$ control techniques, for trajectory-tracking control of CDPRs to minimize the effect of disturbances on the robot operation; and showing the effectiveness of kinematically-constrained actuation method in control design simplification of such robots. 3) Proposing the concept of stiffness-based trajectory-planning to find the stiffness-optimum geometry of trajectories for KC-CDPRs; and designing a time-optimal zero-to-zero continuous-jerk motion to track such trajectories.

All the proposed concepts are developed for a generic KC-CDPR and verified via numerical analysis and experimental tests of a real planar warehousing KC-CDPR.

Acknowledgements

First and foremost, I would like to thank my supervisors, Prof. Amir Khajepour and Prof. Baris Fidan for their support, guidance, and encouragement.

I am deeply thankful to my family members, specially my wife, Maryam Salehi, whose support is truly appreciated. My whole experience would not have been complete without the help and collaboration of my friends and colleagues, Mitch Rushton, Saeid Khosravani, and Iman Fadakar. I would like to appreciate their support and dedication.

I also would like to acknowledge Jeff Graansma and Jeremy Reddekopp for their technical supports.

Dedication

To my parents, my wife, and my little son.

Table of Contents

List of Figures

List of Tables

Chapter 1
Introduction

1.1 Motivations

In recent years, e-commerce explosion has fueled the growth of automated warehousing solutions. According to eMarketer [1], ecommerce is the only trillion-dollar industry growing at a double-digit percentage each year. Nowadays, consumers are requesting shorter delivery time and lower shipping costs. Reported by RJMETRICS [2], 110,000 English language websites are making a meaningful revenue on the internet which 70% of them require warehousing. Reported by MarketsAndMarkets [3], the market of automated material handling equipment was valued at 28.31 Billion $US in 2016 and is predictable to grow at a compound annual growth rate of 7.8% between 2017 and 2023. Such growth of automated warehousing applications provides a unique opportunity for different robotic ideas to be developed in industrial scales.

In automated warehousing tasks, similar to other robotic applications, maximizing the accuracy of the end-effector and the size of workspace as well as minimizing the power consumption and maintenance costs are of a great importance. High stiffness of the manipulators usually leads to precise motions but calls for heavy and bulky mechanisms resulting in low speeds, small workspaces and high-power consumptions. Weight reduction of a manipulator usually increases its speed and enlarge the workspace; however, reduces the mechanism's stiffness level which results in undesired vibrations.

Cable driven parallel robots (CDPRs) are a good example of light weight manipulators which are suffering from undesired vibrations. In the structure of such robots, a rigid platform is connected to the land-fixed winches via flexible cables where by controlling the length and/or tension of the cables, the platform's motion is controlled. Large workspaces, low moving inertias, high-speed motions, low power consumptions and small-size actuators are the most significant advantages of CDPRs. Nevertheless, CDPRs' cables can only provide unidirectional tensions and the stiffness of their structures is considerably low. Accordingly, the platform's undesired vibrations is their main problem.

Among different types of CDPRs, redundant CDPRs are distinguished by having more actuators than the moving platform's degrees of freedom (DOFs). Redundancy of actuators not only can provide a larger workspace, but also can increase the platform's stiffness level. In addition to the redundancy of actuators, a CDPR can benefit from kinematically-constrained actuation method. Such actuation

technique constrains the CDPR in undesired DOFs, attenuates undesired vibrations in those directions, and provide a considerably higher level of stiffness in other directions.

In a commonly actuated CDPR with desired translational motion, as illustrated in Figure 1-1 (with considering only the solid-lines as the cables), each cable is connected to an individual actuator. On the other hand, in a kinematically-constrained CDPR (KC-CDPR), as illustrated in Figure 1-1 (with considering both the solid-lines and dashed-lines as the cables), two sets of actuators are used to move the platform. The first set of actuators (top actuators) are connected to a set of cables which are used to determine the position of the moving platform. In the second set of actuators (bottom actuators), each cable is connected to an individual actuator where its tension is controlled to hold and optimize the tension of top cables. Such arrangement of cables, restricts the rotational DOF and provides a considerably higher level of stiffness for the moving platform in translational DOFs.

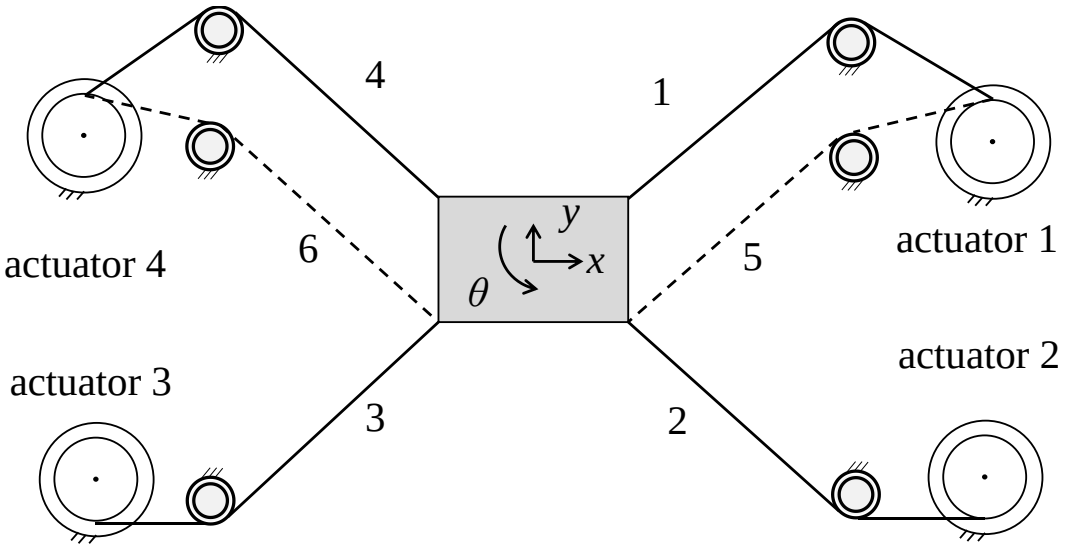

Figure 1-1: Layout of a redundant planar CDPR with kinematic constraints.

As illustrated in Figure 1-2, kinematically-constrained actuation method can be used for 3D CDPRs with translational motion as well. In this figure, each actuation unit consists of multiple winches which are actuated by a single actuator via a power transition system (actuation unit). Position control of the actuator of each unit provides equal lengths for its connected cables. Such arrangement of cables restricts the platform rotational DOFs and provides a considerably higher level of translational stiffness for the platform where the number of actuators is the same and a small cost increase is imposed to the system.

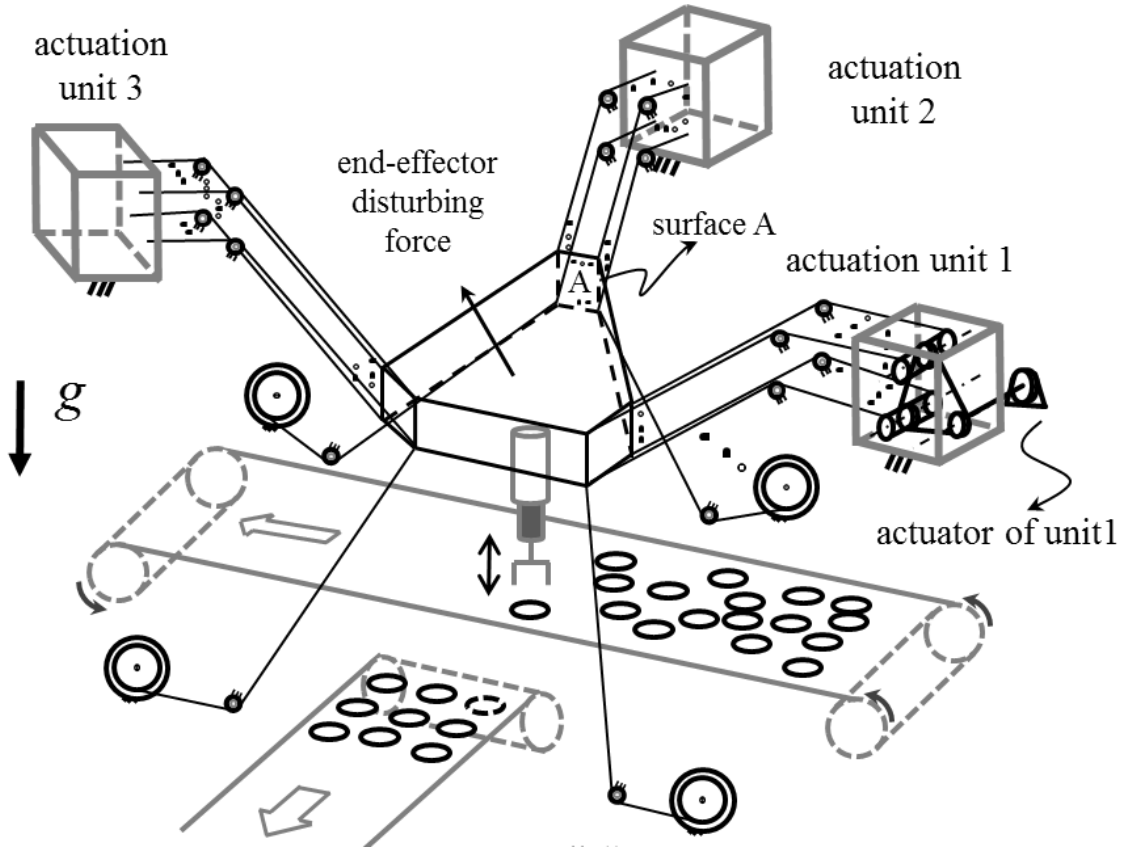

Figure 1-2: A 3D KC-CDPR for pick-&-place applications.

Literature of the CDPRs includes different aspects such as: workspace analysis, kinematic and dynamic modelling, wrench feasibility and tension optimization, stiffness and vibration analysis, trajectory tracking and vibration control, and optimal trajectory-planning which have attracted many researchers for years. Nevertheless, such aspects have received few attention for KC-CDPRs. Specifically, dynamic modeling, stiffness optimization, trajectory-tracking and vibration control, as well as optimal trajectory-planning of KC-CDPRs have not received enough attention. Accordingly, such aspects are studied in this thesis.

1.2 Objectives

The main objectives of this thesis are:

1) Providing a new approach for dynamic modeling of redundant KC-CDPRs, formulating the tension redundancy problem and providing a tension optimization approach to maximize the directional stiffness of such robots. The effects of axial flexibility of cable as well as redundant tensions of cables are required to be considered in the modeling approach where the vibration and motion equations of the platform are needed to be derived. Based on the obtained vibration equations, the concept of directional stiffness optimization needs to be developed and corresponding objective functions need to be derived. Accordingly, time-efficient optimization algorithms need to be proposed. In order to validate the proposed modeling and tension optimization methods, experimental results are required to be provided and discussed.
2) Providing a robust control structure for vibration and trajectory-tracking control of KC-CDPRs. Based on the developed dynamic model, a new robust control approach for KC-CDPRs needs to be proposed and its effectiveness in minimizing the effect of external disturbances on the trajectory-tracking performance of such robots should be demonstrated. In addition, the beneficial effects of kinematically-constrained actuation method on vibration attenuation as well as control design simplification of KC-CDPRs should be demonstrated. Experimental results are required to be provided and compared with other common control techniques in the literature.
3) Investigating the concept of stiffness-based trajectory-planning for the KC-CDPR to find the geometry of optimum trajectories with minimum perturbations under external disturbances and also investigating the concept of time-optimal zero-to-zero continuous-jerk motion design to minimize the motion time in tracking of such trajectories. Rest-to-rest motion of KC-CDPRs needs to be considered and the directional structural stiffness of the moving platform should be formulated as a function of platform's trajectory. The effects of disturbance force/moment on the perturbations of the moving platform need to be considered and used to define the corresponding optimization functions. Minimizing the average and also maximum directional perturbations need to be formulated in form of an optimization problem and a time-efficient solution needs to be proposed which finds the optimum trajectory between the desired points. After providing the geometry of stiffness-optimum trajectory, the concept of time-optimal zero-to-zero continuous-jerk motion design needs to be investigated.

Limitations of the cables' velocity, acceleration and tension need to be considered and the minimum motion time to track the trajectory with optimal geometry should be obtained. In order to demonstrate the effectiveness of the proposed approaches, numerical and experimental results need to be provided.

1.3 Thesis Outline and Contributions

The literature of CDPRs and KC-CDPRs is reviewed in the second chapter of this thesis.

In the third chapter, a new dynamic modeling of KC-CDPRs is presented, where platform's vibration equations are decoupled from the desired (nominal) equations of motion in form of a linear parametric varying (LPV) system. Based on the stiffness matrix of the platform in the obtained LPV vibration model, the magnitude of directional stiffness of moving platform is formulated as a linear objective function of cables' tension and is maximized using linear programming (LP) approach. The proposed vibration model and stiffness optimization technique are experimentally validated on an actual planar warehousing KC-CDPR.

In the fourth chapter, robust trajectory-tracking control problem of KC-CDPRs has been studied. The developed LPV model let us to use a wide class of well-established robust and optimal vibration control techniques. Accordingly, LPV-H_∞ control design techniques are used for the development of vibration controller to optimally attenuate the effect of external disturbances on the robot's trajectory-tracking performance. In this chapter, experimental results are provided which confirm the effectiveness of modelling and proposed control approach. Moreover, the advantages of the kinematically-constrained actuation method in eliminating undesired DOFs and control design simplification are demonstrated.

In fifth chapter, the concept of stiffness-based trajectory-planning of the KC-CDPRs is proposed and investigated to provide the geometry of a stiffness-optimum trajectory for KC-CDPRs. Regarding the direction of external disturbance force/moment, directional perturbation of the moving platform is defined as an objective function to be minimized. By providing a set of smooth trajectories between desired points, different external disturbance are considered and corresponding optimized trajectories are proposed and optimized. By providing the stiffness-optimum trajectory, the problem of time-optimal zero-to-zero continuous-jerk motion design along the determined trajectory is investigated in this chapter. Considering the limitation of cables' velocity, acceleration and tension, the minimum time to track the stiffness-optimum trajectory is found.

Finally, conclusions and future work are discussed in Chapter 6.

Chapter 2: Background and Literature Review

2.1 Cable Driven Parallel Robots

A cable driven robot, as illustrated in Figure 2-1, is a special type of parallel mechanisms which via several flexible cables manipulates a rigid mobile platform. In the literature, CDPRs are titled with different names such as: cable-based robots, wire-driven manipulators, tendon-based parallel robots, parallel wire robots, and cable robots.

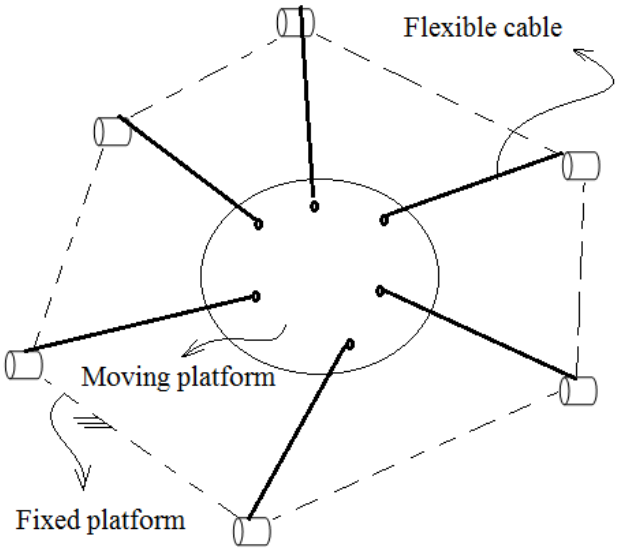

Figure 2-1: General configuration of a cable driven parallel robot.

If a CDPR with λ DOFs is driven by n cables while $n \leq \lambda$, it is classified as an under-constrained CDPR, where as if $n \geq \lambda+1$, it is classified as a fully-constrained CDPR [4]. Any under-constrained CDPR needs an external wrench to provide all the expected DOFs; however, a fully-constrained CDPRs can provide desired DOFs by using the cables only. Cable-suspended robots are a special type of under-constrained CDPRs which rely on the gravity to keep the tension of their cables and produce their expected DOFs [5]. If any cable of a fully-constrained CDPR has its own independent actuator, (n-λ) indicates the CDPR degree of redundancy. In several studies, fully constrained CDPRs with one degree of redundancy are named completely-restrained CDPRs and those with more degrees of redundancy are titled redundantly-restrained CDPRs. Based on that definition, redundantly-restrained CDPRs have more than cables required for providing the desired DOFs.

2.2 Cable Modeling

A sufficiently precise mathematical model of a flexible mechanism is a necessary part of kinematic and dynamic analyzes and also controller design. A great number of studies related to flexible mechanisms have focused on flexible beam-made mechanisms. A flexible beam under bending is a continuous structure with infinite DOFs. Flexible beams are usually simplified into a finite-DOF system using different techniques including finite element methods (FEM), assumed mode shapes, and lumped parameter models [6]–[8].

In front of beam-made flexible mechanisms, moving platform and connecting cables are two basic components of a CDPR. Because of high rigidity of the CDPRs' moving platform, this part is considered as a rigid body in different modeling approaches. On the other hand, the cables' model plays the main role in modelling of a CDPR. CDPR cables are unilateral force exerting flexible parts, which depending on the focus of each study, are modelled differently. For example in [9]–[11], the cables have been assumed as non-stretchable massless segments, while in [3], [10], and [11], mass, elasticity, damping and sagging of cables have been considered the modeling approach. In CDPRs that the cables' weight is comparable to the applied tensions, mass of the cables can result in cables sagging [5]. Therefore, mass distribution in cables is considered in the modeling approach. Cable sagging changes the uniform force distribution in a cable and complicates the CDPRs' model and control design. Receiver support CDPRs for large radio telescopes [14], [15], large cranes [16], search and rescue systems [17], maintenance systems for large buildings [18] are examples of suspended CDPRs with considerable cable sagging. In [3] and [10] in addition to cables' sagging, cables' flexibility has been also considered in the modelling. Compared to suspended CDPRs, fully-constrained CDPRs can provide higher forces. Such forces can keep the cables as a line. Accordingly, in such CDPRs, cables are usually modelled as a line segment link. As an example, in fully-constrained CDPRs of [19]–[28], cables have been modelled as massless non-stretchable lines. In studies related to stiffness and vibration analyzes [29]–[32] and also vibration control of fully-constrained CDPRs [13], [33]–[37], cables have been modelled by massless elastic linear springs. In addition to cable axial flexibility, mass of cables has been considered for more precise dynamic, vibration analyzes and control design in [38]–[40]. In these studies, any cable has been modelled as a distributed lumped mass-spring part. Modelling cables by FEM or lumped mass-spring methods will increase the computational time which can results in low performance of controllers [12].

2.3 Kinematics

The relation between position and velocity of the moving platform and the cables (actuators) is the subject of kinematic analysis. Inverse kinematics gives the cables' length and velocity where the moving platform position and velocity are provided. Forward kinematics gives the moving platform's position and velocity using cables' length and velocity. Modelling cables by non-stretchable and straight lines has simplified the kinematic analysis in many studies including [31], [41], [42]. Considering the cables flexibility requires the elongation of cables for kinematic analysis. In kinematic model of [35], cables have been modelled by linear springs where their total length is measured by string pot. Laser tracker and CCD camera are two other devices which have been used for measuring the position and velocity of the moving platform in [15], [27], [43], [44]. Some of these measurement instruments need a wide space for installation which is impractical in many industrial applications.

2.4 Singularity

Singularity is a common problem that may occur in both serial and parallel mechanisms. In the CDPRs, when the platform falls into the neighborhood of a singular configuration, it cannot hold the tension in all cables which means the platform is not controllable. In such conditions, the moving platform stability can be lost [45]. For maintaining the controllability of the robot, singular configurations must be avoided in control strategy or eliminated in the design process. Gosselin and Angeles categorized different types of singularity points of closed-loop chains into three classes [46], and 4 years later, Zlatanov et al. have presented a more generalized categorization [47]. Because of unilateral force driving capability of the cables, direct application of the conventional singularity analysis methods for CDPRs is not possible. Dino et al. have proposed two types of singularities for CDPRs [48]: 1- Jacobian singularity: Similar to other robots, when the Jacobian matrix of a CDPRs becomes rank deficient, 2- Force-closure singularity: When the Jacobian matrix is still full rank but the cables' tension fail to counterbalance the moving platform's external wrench. In these definitions, Jacobian singularity is defined based on the CDPR's kinematics while the force-closure singularity is defined based on the dynamics of a CDPR [48]. For resolving the Jacobian singularity problems, the CDPR configuration should be redesigned. However, for solving the force-closure singularity upper bound of cables' tension should be increased.

2.5 Dynamics

Dynamic modeling of CDPRs is completely related to the model of cables while the moving platform is usually modelled as a rigid body. A massless non-stretchable line segment is the simplest model of cables which reduces the dynamic model of a CDPR into the moving platform's dynamics. Considering mass, damping and/or axial flexibility of cables make the dynamic model more complicated. In [49]–[53] elasticity, mass and damping of cables have been ignored in dynamic modelling. In [54], because of moving platform's low mass and accelerations, the mass of cables has been considered in the cables' model. In [33]–[35], [55], cables have been modelled by massless linear springs with variable stiffness coefficients. Total elasticity of the cable-pulley-gear system has been modelled by a third order polynomial in [56]. In [13], it has been shown that adding the cables elasticity and damping has a significant influence on the dynamic behavior of the CDPR. In [57] and [40], a lumped mass-spring model with finite number of elements has been presented for the cables. A discretized finite element model has been introduced in [58] and [59] for dynamic modelling of cable-suspended robots by considering sagging effects. By adding damping elements to lumped mass-spring model, another discretized dynamic model has been presented in [60] .

The Newton-Euler and the Lagrange approaches are two common methods of deriving the CDPR dynamic equations. In cases with a simple cable model, the Newton-Euler method has usually been preferred. However, for CDPR with discretized cable model, Lagrange method is commonly used.

2.6 Wrench Closure and Wrench Feasible Criteria

Unilateral force exerting characteristics of cables have made tension analysis of CDPRs as one the most attractive subjects in different studies [4]. Because of such characteristic, the moving platform's set of poses where the cables can balance external wrenches are limited [61]. In determination of balanceable poses of a CDPR, according to the cables' forces bounds and also the moving platform's external wrench, the following definitions are provided. A CDPR in a specific location is said to have wrench-closure condition if any external wrench applied to the moving platform can be balanced [48]. Based on the mentioned definition, wrench-closure workspace (WCW) is the set of poses in which a platform can balance any arbitrary external wrench with no upper bound on the cables' forces. By consideration of the cables' tension limits and the external wrench upper bounds, the WCW is transformed into wrench-feasible workspace (WFW) [62]. The shape and size of WFW depend on the geometry of the CDPR, specific external wrench and the allowable tension of cables, where, those of WCW depend on the CDPR's geometry only [61]. Based on the provided definitions, the WCW can

be analyzed only for fully constrained CDPRs [63]. Static and dynamic workspace are special types of WFW that in them the moving platform's weight and inertia forces play the role of external wrenches [64].

2.7 Tensions Redundancy and Optimization Approaches

Wrench closure and wrench feasible conditions check the potential and practical existence of an all positive solution for cables' tension, respectively. Existence of a solution for a fully-constrained CDPR usually means having redundancy in solution of cables' tension. Tensions' redundancy is a desirable feature of manipulators although it can add to the computational cost of CDPRs for real time applications [65]. Jacobian pseudo inverse method is the most used redundancy resolution technique in robotic applications, which has been originally introduced by Whitny [66] and improved by Liegise [67]. The complexity of redundancy resolution is increased by adding the cables' tension limits in CDPRs. Barrette and Gosselin have shown that redundancy resolution of CDPRs can be studied as an optimization problem with inequality and equality constraints [64].

According to the desired characteristic of the CDPRs, different objective functions of cables' tension, such as 1st-norm, ∞-norm, and p-norm ($1<p<\infty$) [68], [69], have been proposed and studied by different researchers. Shiang et al. have considered the summation of cables' tension as an optimization objective function, and have used the linear programming approach for redundancy resolution [70]. Pott et al. have focused on Euclidian norm of cables' tension as the optimization objective function and have studied different optimization technique to minimize such norm [71]. A few studies have focused on stiffness-related objective functions. Yu et al. have studied the idea of holding a predetermined stiffness level for the moving platform [72]. In another study, the same group has developed an algorithm to control a lower bound of stiffness via holding the smallest eigenvalue of the stiffness matrix larger than a predefined positive value [73].

The computational cost has always been an important factor in solving an optimization problem. Majority of the optimization resolution techniques which are used for CDPRs are using iterative techniques. Hassan and Khajepour have used the Dykstra method for finding the minimum second norm of tensions [74]. Based on Karush–Kuhn–Tucker (KKT) theorem, Taghirad and Bedoustani are using an analytic-iterative approach for optimizing the second norm of tensions [65]. A non-iterative approach is presented by Mikelsons et al. in [75] where guarantee the continuity of the cables' tension.

2.8 Stiffness, Stability and Natural Frequency

Stiffness is one of the most important characteristic of CDPRs which can directly affect the natural frequencies and vibrations of such robots [32]. Stiffness of parallel manipulator with no internal force in their links has been studied by Gosselin [76]. Griffis and Duffy [77] have studied the effects of internal force in stiffness matrix of Stewart manipulator. An equivalent four-spring model has been proposed by Behzadipour and Khajepour in [32], which shows the effect of cables' stiffness and tension in formation of the CDPRs' stiffness matrix.

Stiffness stability of a manipulator has been generally defined in [78] as "the likelihood that an external disturbance will disturb the end-effector from a given equilibrium pose". A CDPR's stability conditions is evaluated based on its tendency to restore an original configuration when it undergoes a displacement [79]. Svinin et al. have studied the necessary and sufficient conditions of CDPR's stability based on the positive definiteness of the stiffness matrix [80], [81]. They have shown that the stiffness matrix can be considered as the summation of two different matrices. The first matrix is formed by the cables' compliance and the second one arisens from cables' tension. Behzadipour and Khajepour have presented the necessary conditions to have stiffness stability in CDPRs. They have shown a CDPR with all cables in tension can be unstable [32].

In addition to the stability conditions, natural frequency of the moving platform is another important characteristic of a CDPR which is obtained based on the stiffness matrix. Having high natural frequency is a desirable characteristic for a CDPR. Hassan and Khajepour have optimized the dimensions of a CDPR to maximize the minimum natural frequency of the moving platform [21]. Using a similar approach, Torres-Mendez and Khajepour have proposed an optimal design for a warehousing CDPR [82], [83].

2.9 Trajectory-Tracking and Vibration Control

Maximizing the accuracy of the end-effector has always been a desirable characteristic in robotic applications. Having a flexible structures makes CDPRs more susceptible to external disturbances resulting in undesired vibrations. For decades, different types of solutions have been proposed and applied on different flexible mechanisms. The proposed solutions can be classified into three categories: 1- Hardware design/ redesign, 2- Command shaping or feed forward control, and 3- Feedback control. In comparison to two other methods, feedback control is the most common approach in attenuation of the undesired vibrations in flexible structures. Most of such studies have

focused on beam-made serial or parallel mechanisms. Almost all of these studies ignore all flexible motion of the beams except the lateral motion under bending moments. Benosman and Vey [84] have reviewed and classified the flexible manipulators control objectives into four categories which in order of difficulty are: 1- End-effector regulation [85], [86]: in such approach, the controller minimizes the end-effector residual oscillation during a point to point motion. 2- Rest-to-rest motion of end-effector in a certain time [87], [88]: the control objective of such approach is the same as previous method while complete elimination of oscillation in a certain final time is added to desired conditions. 3- Joint space trajectory-tracking [89] : in this approach, the robot joints have to track a desired trajectory to cause the end-effector to follow its desired path. 4- Workspace trajectory-tracking: in this trend, the end-effector have to follow the desired trajectory in the operational workspace and reach the final equilibrium point with minimum oscillations. Because of the non-minimum phase nature of the non-collocated system dynamics, the last one is the most difficult approach [84], [90].

Similar to the beam-made flexible mechanisms, position and vibration control of CDPRs attracted the attention of a considerable number of researchers. The proposed control approaches for CDPRs can be classified into two different categories:1-Task space control including [26], [35], [36], [41], [50], [57], [60], [68], [91]–[93] and joint space control including [33], [55], [56], [94], [95]. In the joint space control approach, the controller tries to hold each joint in its desired position while the end-effector position is not considered in the control design process. On the other hand, task space controllers try to keep the moving platform on a desired trajectory. In cases that the flexibility of cables is negligible and the motion has small accelerations, the joint space controllers have shown satisfying performances. However, using CDPRs for high speed motions and considering the effects of external disturbances, such methods cannot guarantee a high performance for such robots. Similar to beam-made flexible manipulators, different algorithm are used for feedback control of CDPRs. In [73], computed torque or feedback linearization technique has been used for finding the actuator forces based on the CDPR inverse dynamics. This technique has been combined with proportional-derivative controllers in [91] and also with adaptive controllers in [96]. A proportional-derivative controller has been designed by Kawamura et al. in joint space [56] of FALCON-7 robot. This controller has shown satisfying rest-to-rest experimental results. Ghasemi et al. have used a model predictive controller beside the input-output linearization method for trajectory-tracking control of a CDPR in task space [97]. The performance of this controller has been evaluated by simulation results. An efficient inverse dynamics controller in joint space of a 6 DOF redundant robot has been studied

by Gholami et al. in [98]. Khosravi et al. have proposed a PD controller in joint space for a planar CDPR, where the vibration regulation results are evaluated by simulation [55]. Alikhani and Vali proposed a robust sliding mode [19] and also a computed torque [41] controller for task space control of a fully constrained CDPR [41]. Caverly and Forbes have designed a non-collocated controller for a planar CDPR based on the passivity analysis [40]. Their model consists of flexible cables with distributed lumped mass points which are connected by linear spring elements [57]. They have evaluated their controller performance in simulation. Duchaine et al. have proposed a computationally efficient model predictive controller for a suspended CDPR [99]. Khosravi and Taghirad designed a robust PID controller for a planar CDPR without considering the flexibility of the cables. Their experimental results showed proper performance of their controller [26]. According to this study, they have investigated their controller performance for CDPR with flexible cables in simulation [37]. Kino et al. have studied feed-forward positioning with frictional and gravitational compensation [100]. Zeinali and Khajepour have proposed and implemented a chattering-free sliding mode controller on a new CDPR [96].

In the mentioned studies, in order to provide a real-time solution for the cables' tension, different optimization objective functions and resolution techniques are developed and used for different CDPRs. For example [68] minimize the summation of cables' tension for a CDPR with one degree of redundancy. Yu et al. in [73] and [72] introduced a lower bound task stiffness within the control scheme to improve the trajectory-tracking and disturbance rejection performance in CDPRs. Oh and Agrawal in [50] have minimized both linear and quadratic functions of cables' tension, where Meunier et al. in [60] have minimized the infinite norm of tensions.

2.10 Trajectory-Planning

Time-optimization has always been one of the most attractive problems in robotic applications. The idea of time-optimal and smooth trajectory-planning of industrial manipulators along a specified trajectory has been proposed by Constantinescu and Croft in [101]. In this study, they have considered the torque limitations and jerk smoothness for the motion of each actuator and developed a generic approach which minimizes the robot's motion time. Gasparetto and Zanotto have studied the problem of time-jerk optimal planning of robotic manipulators [102]. They have proposed a new objective function which takes into account the upper bound of the actuators' velocity, acceleration, and jerk as well as the total time of motion. The problem of time-optimization of a holonomic

scleronomic mechanical system on a prescribed trajectory has been studied by Obradovic et al. in [103].

Undesired vibration of cable robots can be directly stimulated by the non-smoothness of the moving platform's jerk and acceleration along a desired trajectory. Accordingly, design of smooth and optimal-time motions for CDPRs has attracted the attention of different researches. The problem of time-optimal trajectory-planning of high-speed cable-based parallel manipulators has been studied by Behzadipour and Khajepour [104]. In this study a generic time-optimal trajectory-planning technique has been adapted for cable-based parallel manipulators where the cables' tension limitations is considered and represented as a constraint on the acceleration of the actuators. In addition, the inherent acceleration and velocity limitation of each actuators are considered in the optimization approach where no limitation on the motion jerk has been applied. Time-optimal trajectory-tracking of redundant planar cable-suspended robots by considering both the tension and velocity limitations has been studied by Fahham et al. [105]. Using their proposed algorithm, the limitation of the cables' tension and velocity are transformed into the bounds of speed and acceleration along a desired trajectory. Accordingly, by using a hybrid genetic algorithm and a bang-bang control technique, the optimum trajectory with minimum motion time is found. In a recent study, Barbazza et al. have proposed an optimal trajectory-planning approach for cable-suspended robots with pick-&-place applications [106]. In their proposed approach, an objective function of motion time and platform's jerk has been defined and optimized along a desired trajectory. Barnett and Gosselin have integrated minimum-time trajectory shaping technique with the cable-tension constraints to provide a time-optimal trajectory-planning for cable-suspended robots [107]. Sharifi and Taghirad have proposed a new approach for time-optimal trajectory-planning of cable-suspended robots which considers the moving platform's dynamics and the limit of cables' tension and also counteracts unwanted velocity inputs in such robots [108]. The idea of time-energy optimal trajectory-planning of cable-suspended robots has been proposed by Bamdad in [109], where the objective function has been chosen as a weighted function of motion time and the required energy for the motion.

In most of the mentioned studies, a predetermined trajectory has been considered for the moving platform path, where finding an optimum geometry as the trajectory of the moving platform has received a few attention. Moreover, to the best of author's knowledge, having a zero-to-zero continuous-jerk in rest-to-rest motion of CDPRs has not been studied so far. Regarding the

susceptibility of the CDPRs to undesired vibration, such motion can decrease the stimulating effects of jerk non-continuity along the motion.

2.11 Kinematically-Constrained CDPRs

In most of the studied cable robots, ranging from the FALCON [30] to the recent CDPRs [110], [111], there is no kinematic constraint in the cables' actuation. In recent years, KC-CDPRs have attracted more attention. A design approach is provided by Behzadipour and Khajepour for a KC-CDPR to restrict the rotational DOFs of a flat moving platform [112]. Bosscher et al. have proposed the conceptual design of a suspended KC-CDPR as a search and rescue robotic system [17]. In this study, the rotational DOFs of a moving platform are constrained to provide a pure translational motion over a 3D workspace. Torres-Mendez and Khajepour have introduced a KC-CDPR for warehousing applications [82]. Adaptive control problem of a simplified version of the introduced CDPR is studied in [113]. Saber has demonstrated the effects of kinematic constraints on improvement of CDPRs' workspace [114]. A similar actuation technique, named cable differentials, is proposed by Khakpour et al. to improve the workspace and kinetostatic properties of CDPRs [115]. In this method, using multiple idle pulleys, mounted on the moving and the fixed platforms of a CDPR, multiple connection points are made for each individual cable.

2.12 Summary and Discussion

As the literature review showed, different aspects of CDPRs have attracted the attention of large number of researches for years. Most of the researchers have focused on CDPRs with no kinematic constraint. A small number of studies have focused on stiffness-related objective functions for the cable's tension optimization; whereas the CDPRs suffer from their low stiffness in different applications. The beneficial aspects of KC-CDPRs have received few attention. Specifically, dynamic modeling, stiffness analysis, control design, and optimal trajectory-planning of such robots have not received enough attention. Robust control design of KC-CDPRs needs more investigation, where the effects of kinematically-constrained actuation method on the simplification of such controllers require more studies. In the most of the previous studies, trajectory-planning optimization of CDPRs have been studied for trajectories with predetermined geometry, where, optimizing the geometry of the trajectory has received a few attention. Moreover, providing a continuous-jerk motion for the CDPRs has not received enough attention.

Chapter 3: Kinematic and Dynamic Modeling, Redundancy Analysis and Stiffness Optimization

3.1 Introduction

This chapter reviews the kinematic and dynamic model of CDPRs and develops a new dynamic modeling approach for such robots. In the developed model, assuming an axially flexible model for the cables, platform's motion equations are derived and used to separate the linear vibration equations of the moving platform from its desired (nominal) equations of motion. Accordingly, the stiffness matrix of the moving platform during the motion is formed as a function of cables' tension and axial stiffness. In order to show the effects of kinematic constraints on the obtained stiffness matrix, the concept of such actuation is reviewed and the substantial effects of constrained cables and the potential effects of cables' tension on the stiffness improvement of CDPRs are shown. In order to minimize the effects of external disturbances in a desired direction, the magnitude of directional stiffness of moving platform is formulated as a linear objective function of cables' tension and is maximized using linear programming (LP) approach, allowing real-time implementation. The proposed actuation method and stiffness optimization approach are experimentally evaluated on an actual planar warehousing KC-CDPR.

The following sections of this chapter are based on previously published works of "Kinematically-Constrained Redundant Cable-Driven Parallel Robots: Modeling, Redundancy Analysis, and Stiffness Optimization, IEEE/ASME Transactions on Mechatronics, 2017" [116] and "Vibration Decoupled Modeling and Robust Control of Redundant Cable-Driven Parallel Robots IEEE/ASME Transactions on Mechatronics, 2018" [117] by "Hamed Jamshidifar et al." and are reproduced with permission, from IEEE. Accordingly, the copyright of the following sections is owned by IEEE. This thesis author specific contribution to these paper is to: "prepare all the graphics and results, prepare the final manuscript. These papers are co-authored by Dr. Amir Khajepour and Dr. Baris Fidan as supervisors. Also, Mitch Rushton, in assisting with experimental setup and testing, and Saeid Khosravani, in control design analysis. In reference to IEEE copyrighted material which is used with permission in this thesis, the IEEE does not endorse any of [university/educational entity's name goes here]'s products or services. Internal or personal use of this material is permitted.

3.2 Kinematics and Dynamics of Commonly-Actuated CDPRs

Figure 3-1 illustrates a general configuration of a CDPR with *n* actuators where each actuator pulls its individual cable.

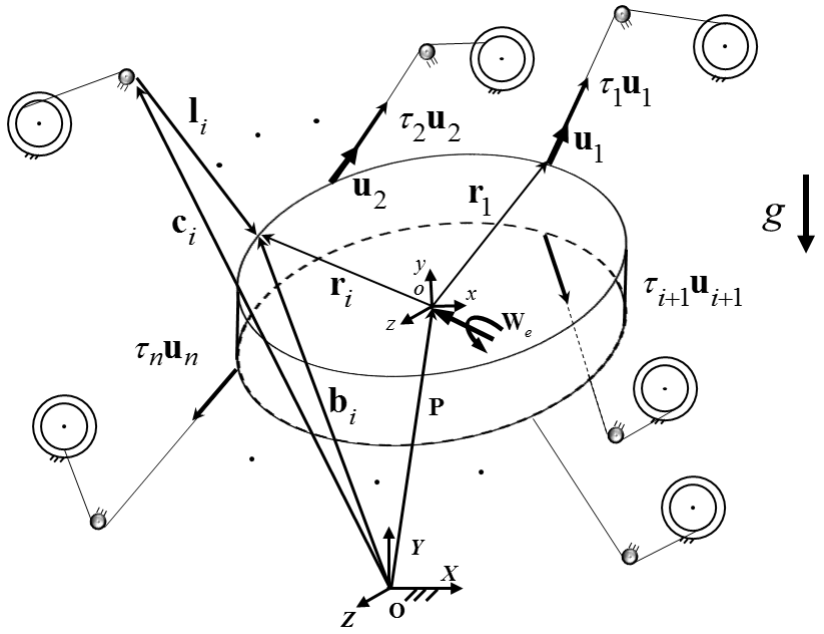

Figure 3-1: Configuration of a generic commonly-actuated CDPR.

In Figure 3-1, *O* is the origin of global coordinate system of *XYZ* where *o* indicates the origin of *xyz* frame which is fixed to the platform's center of mass. l_i, $\mathbf{u}_i$ and $\mathbf{r}_i$ denote cable *i* total length, unit and anchor vectors with respect to the center of mass. Position vector of the moving platform's center of mass is denoted by **p**, where the connection point of cable *i* to the moving and fixed platforms are denoted by $\mathbf{b}_i$ and $\mathbf{c}_i$.

Based on the presented vectors in Figure 3-1, $\mathbf{l}_i$ as the illustrated vector of cable *i* is obtained as

$$\mathbf{l}_i = (\mathbf{p} + \mathbf{r}_i) - \mathbf{c}_i \tag{3-1}$$

where $\mathbf{p}=[x,y,z]^T$ denotes the vector of translational coordinates. Accordingly, l_i is obtained as

$$l_i = \|\mathbf{l}_i\| = \|(\mathbf{p} + \mathbf{r}_i) - \mathbf{b}_i\| \tag{3-2}$$

which gives

$$\mathbf{u}_i = -\frac{\mathbf{l}_i}{l_i}. \tag{3-3}$$

By differentiating both sides of (3-1) with respect to time, we have

$$-\dot{l}_i\mathbf{u}_i - \dot{\boldsymbol{\theta}}_i \times l_i\mathbf{u}_i = \dot{\mathbf{p}} + \dot{\boldsymbol{\theta}} \times \mathbf{r}_i \tag{3-4}$$

where $\boldsymbol{\theta}=[\theta_x,\theta_y,\theta_z]^T$ is the moving platform's angular coordinates vector and $\boldsymbol{\theta}_i=[\theta_{xi},\theta_{yi},\theta_{zi}]^T$ denotes such vector for cable *i*. By multiplication of both sides of (3-4) by $\mathbf{u}_i^T$, we have

$$-\dot{l}_i = \mathbf{u}_i^T(\dot{\mathbf{p}} + \dot{\boldsymbol{\theta}} \times \mathbf{r}_i - \dot{\boldsymbol{\theta}}_i \times l_i\mathbf{u}_i) \tag{3-5}$$

which can be simplified into

$$-\dot{l}_i = \mathbf{u}_i^T\dot{\mathbf{p}} + (\mathbf{r}_i \times \mathbf{u}_i)^T\dot{\boldsymbol{\theta}}\ . \tag{3-6}$$

Summarizing (3-6) for all cables gives

$$-\begin{bmatrix} \dot{l}_1 \\ \dot{l}_2 \\ \vdots \\ \dot{l}_n \end{bmatrix}_{n\times 1} = \begin{bmatrix} \mathbf{u}_1^T & (\mathbf{r}_1 \times \mathbf{u}_1)^T \\ \mathbf{u}_2^T & (\mathbf{r}_2 \times \mathbf{u}_2)^T \\ \vdots & \vdots \\ \mathbf{u}_n^T & (\mathbf{r}_n \times \mathbf{u}_n)^T \end{bmatrix}_{n\times 6} \begin{bmatrix} \dot{\mathbf{p}} \\ \dot{\boldsymbol{\theta}} \end{bmatrix}_{6\times 1} = \mathbf{J}_{n\times 6}\begin{bmatrix} \dot{\mathbf{p}} \\ \dot{\boldsymbol{\theta}} \end{bmatrix}_{6\times 1} \tag{3-7}$$

where **J** is the Jacobian matrix of the CDPR that relates the platform's velocity vector to the velocity of cables. Deriving the Newton-Euler dynamic equations for the illustrated mechanism of Figure 3-1, with a symmetric moving platform gives

$$\begin{aligned} &\sum_{i=1}^{n}\tau_i\mathbf{u}_i + = \mathbf{M}_{\mathrm{m}}(\ddot{\mathbf{p}}) - \mathbf{f}_e,\ \mathbf{M}_{\mathrm{m}} = m_{mp}\mathbf{I}_{3\times 3} \\ &\sum_{i=1}^{n}\tau_i(\mathbf{r}_i \times \mathbf{u}_i) = \mathbf{I}_{\mathrm{cm}}\ddot{\boldsymbol{\theta}} + \dot{\boldsymbol{\theta}} \times (\mathbf{I}_{\mathrm{cm}}\dot{\boldsymbol{\theta}}) - \mathbf{m}_e, \mathbf{I}_{\mathrm{cm}} = diag(I_{xx}, I_{yy}, I_{zz}) \end{aligned} \tag{3-8}$$

where $\mathbf{M}_{\mathrm{m}}$ and $\mathbf{I}_{\mathrm{cm}}$ are the moving platform mass and inertia matrices, $\mathbf{f}_e$ and $\mathbf{m}_e$ are the external force and moment vectors applied on the moving platform. The gravity effects has been in included in $\mathbf{f}_e$ where its acceleration is denoted by *g*. m_{mp}, I_{xx}, I_{yy} and I_{zz} denote the mass and rotational inertia of the moving platform around *x*, *y*, and *z* axes where **I** denotes the identity matrix. (3-8) can be summarized as

$$\mathbf{J}^T{}_{6\times n}\boldsymbol{\tau}_{n\times 1} = \begin{bmatrix} \mathbf{M}_{\mathrm{m}} & \mathbf{0} \\ \mathbf{0} & \mathbf{I}_{\mathbf{cm}} \end{bmatrix}_{6\times 6}\begin{bmatrix} \ddot{\mathbf{p}} \\ \ddot{\boldsymbol{\theta}} \end{bmatrix}_{6\times 1} + \begin{bmatrix} \mathbf{0} \\ \dot{\boldsymbol{\theta}} \times (\mathbf{I}_{\mathbf{cm}}\dot{\boldsymbol{\theta}}) \end{bmatrix}_{6\times 1} - \begin{bmatrix} \mathbf{f}_{\mathbf{e}} \\ \mathbf{m}_{\mathbf{e}} \end{bmatrix}_{6\times 1}, \tag{3-9}$$

where

$$\mathbf{J}^T(\mathbf{x})_{6\times n} = \begin{bmatrix} \mathbf{u}_1 & \dots & \mathbf{u}_{1n} \\ \mathbf{r}_1 \times \mathbf{u}_1 & \dots & \mathbf{r}_n \times \mathbf{u}_n \end{bmatrix}, \tag{3-10}$$

and

$$\boldsymbol{\tau} = \left[\tau_1, \ldots, \tau_n\right]^T \tag{3-11}$$

denotes the vector of cables' tension.

Considering each cable as a massless linear spring with the stiffness coefficient

$$k_i = \frac{A_i E}{l_i}, \tag{3-12}$$

where A_i and E denote the cables cross section area and modulus of elasticity, we have

$$\tau_i = k_i (l_i - l_{oi}) \tag{3-13}$$

as the relation between τ_i, as the magnitude of tension in cable i, l_i as the total length and l_{oi} as the initial (non-stretched) length of such cable.

3.2.1 Vibration Decoupled Modeling

Let us denote the platform's vector of coordinates by $\mathbf{x} = [\mathbf{p}^T, \boldsymbol{\theta}^T]^T$. Assuming infitiesmal perturbation for the moving platform, we can write $\mathbf{x} = \bar{\mathbf{x}} + \mathbf{x}_\delta$ where $\bar{\mathbf{x}} = [\bar{\mathbf{p}}^T, \bar{\boldsymbol{\theta}}^T]^T$ and $\mathbf{x}_\delta = [\mathbf{p}_\delta^T, \boldsymbol{\theta}_\delta^T]^T$ denote the coordinates of desired trajectory and its perturbation, respectively. Accordingly, (3-9) can be written as

$$\begin{bmatrix} \mathbf{M}_m & 0 \\ 0 & \mathbf{I}_{cm} \end{bmatrix} \begin{bmatrix} \ddot{\bar{\mathbf{p}}} + \ddot{\mathbf{p}}_\delta \\ \ddot{\bar{\boldsymbol{\theta}}} + \ddot{\boldsymbol{\theta}}_\delta \end{bmatrix} + \begin{bmatrix} 0 \\ (\dot{\bar{\boldsymbol{\theta}}} + \dot{\boldsymbol{\theta}}_\delta) \times \mathbf{I}_{cm} (\dot{\bar{\boldsymbol{\theta}}} + \dot{\boldsymbol{\theta}}_\delta) \end{bmatrix} = \mathbf{J}^T (\bar{\mathbf{x}} + \mathbf{x}_\delta) \boldsymbol{\tau} (\bar{\mathbf{x}} + \mathbf{x}_\delta) + \mathbf{w}_e, \mathbf{w}_e = [\mathbf{f}_e^T \quad \mathbf{m}_e^T]^T. \tag{3-14}$$

Let us assume the level of moving platform's stiffness is high enough such that the second order terms of $(\dot{\boldsymbol{\theta}}_\delta) \times \mathbf{I}_{cm} (\dot{\boldsymbol{\theta}}_\delta)$ can be ignored. Accordingly, (3-14) can be written as

$$\begin{aligned} &\mathbf{M}\ddot{\bar{\mathbf{x}}} + \mathbf{M}\ddot{\mathbf{x}}_\delta + \begin{bmatrix} 0 \\ (\dot{\bar{\boldsymbol{\theta}}}) \times \mathbf{I}_{cm} (\dot{\bar{\boldsymbol{\theta}}}) \end{bmatrix} + \mathbf{Q}\dot{\mathbf{x}}_\delta = \mathbf{J}^T (\bar{\mathbf{x}}) \boldsymbol{\tau} (\bar{\mathbf{x}}) + \left(\frac{\partial \mathbf{J}^T}{\partial \mathbf{x}} \boldsymbol{\tau} + \frac{\partial \boldsymbol{\tau}}{\partial \mathbf{x}} \mathbf{J}^T \right) \Big|_{\mathbf{x}=\bar{\mathbf{x}}} \mathbf{x}_\delta + \mathbf{w}_e, \\ &\mathbf{Q} = \begin{bmatrix} 0 & 0 \\ 0 & \mathbf{Q}_r (\dot{\bar{\boldsymbol{\theta}}}) \end{bmatrix}, \mathbf{Q}_r (\dot{\bar{\boldsymbol{\theta}}}) \dot{\boldsymbol{\theta}}_\delta = \dot{\boldsymbol{\theta}}_\delta \times (\mathbf{I}_{cm} \dot{\bar{\boldsymbol{\theta}}}) + \dot{\bar{\boldsymbol{\theta}}} \times (\mathbf{I}_{cm} \dot{\boldsymbol{\theta}}_\delta). \end{aligned} \tag{3-15}$$

Based on [32], we represent $-\left(\frac{\partial \mathbf{J}^t}{\partial \mathbf{x}} \boldsymbol{\tau} + \frac{\partial \boldsymbol{\tau}}{\partial \mathbf{x}} \mathbf{J}^t \right) \Big|_{\mathbf{x}=\bar{\mathbf{x}}}$ by $\mathbf{K}(\bar{\mathbf{x}}, \bar{\boldsymbol{\tau}})$. Then, by rewriting $\boldsymbol{\tau}$ as $\boldsymbol{\tau} = \bar{\boldsymbol{\tau}} + \boldsymbol{\tau}_\delta$, where $\bar{\boldsymbol{\tau}}$ is the vector of nominal tensions and $\boldsymbol{\tau}_\delta$ denotes difference between the nominal and actual cables' tension, one can separate the moving platform's desired motion equations

$$\mathbf{M}\ddot{\bar{\mathbf{x}}}+\begin{bmatrix}0^T & (\dot{\bar{\boldsymbol{\theta}}}\times(\mathbf{I}_{cm}\dot{\bar{\boldsymbol{\theta}}}))^T\end{bmatrix}^T=\mathbf{J}^T(\bar{\mathbf{x}})\bar{\boldsymbol{\tau}}(\bar{\mathbf{x}}) \tag{3-16}$$

from the vibration equations

$$\mathbf{M}\ddot{\mathbf{x}}_\delta+\mathbf{Q}(\dot{\bar{\boldsymbol{\theta}}})\dot{\mathbf{x}}_\delta+\mathbf{K}(\bar{\mathbf{x}},\bar{\boldsymbol{\tau}})\mathbf{x}_\delta=\mathbf{J}^T(\bar{\mathbf{x}})\boldsymbol{\tau}_\delta(\bar{\mathbf{x}})+\mathbf{w}_e\ . \tag{3-17}$$

It has been shown in [32] that the stiffness matrix of a moving platform can be written as

$$\mathbf{K}(\bar{\mathbf{x}},\bar{\boldsymbol{\tau}})=\mathbf{K}_k(\bar{\mathbf{x}})+\mathbf{K}_{\bar{\tau}}(\bar{\mathbf{x}},\bar{\boldsymbol{\tau}}) \tag{3-18}$$

where

$$\mathbf{K}_k=\sum_{i=1}^{m}k_i\begin{bmatrix}\mathbf{u}_i\mathbf{u}_i^T & \mathbf{u}_i\mathbf{u}_i^T[\mathbf{r}_i\times]^T\\ [\mathbf{r}_i\times]\mathbf{u}_i\mathbf{u}_i^T & [\mathbf{r}_i\times]\mathbf{u}_i\mathbf{u}_i^T[\mathbf{r}_i\times]^T\end{bmatrix} \tag{3-19}$$

is the moving platform's structural stiffness resulted from inherent stiffness of the cables and

$$\mathbf{K}_{\bar{\tau}}=\sum_{i=1}^{m}\frac{\bar{\tau}_i}{l_i}\begin{bmatrix}\mathbf{I}-\mathbf{u}_i\mathbf{u}_i^T & (\mathbf{I}-\mathbf{u}_i\mathbf{u}_i^T)[\mathbf{r}_i\times]^T\\ [\mathbf{r}_i\times](\mathbf{I}-\mathbf{u}_i\mathbf{u}_i^T) & [\mathbf{r}_i\times](\mathbf{I}-\mathbf{u}_i\mathbf{u}_i^T)[\mathbf{r}_i\times]^T\end{bmatrix}+\sum_{i=1}^{n}\bar{\tau}_i\begin{bmatrix}0 & 0\\ 0 & -[\mathbf{u}_i\times][\mathbf{r}_i\times]\end{bmatrix} \tag{3-20}$$

is formed by the tension of cables. In these equations

$$[\mathbf{r}_i\times]=\begin{bmatrix}0 & -r_{zi} & r_{yi}\\ r_{zi} & 0 & -r_{xi}\\ -r_{yi} & r_{xi} & 0\end{bmatrix}_{3\times3},\mathbf{r}_i=\begin{bmatrix}r_{xi}\\ r_{yi}\\ r_{zi}\end{bmatrix}, \tag{3-21}$$

and $[\mathbf{u}_i\times]$ and $\mathbf{u}_i$ have similar equations. It is worth mentioning, equation (3-19) and (3-20) are provided for the static equilibrium conditions where each cable is fixed at its connection point with the ground holding its desired tension. Accordingly, the axial stiffness and tension of all cables have been involved in calculation of $\mathbf{K}_k$ and $\mathbf{K}_{\bar{\tau}}$. However, along the motion of the moving platform, involvement of all cables in $\mathbf{K}_k$ and $\mathbf{K}_{\bar{\tau}}$ is not valid. In the common type of actuation, where only the tension of each cable is under control, $\mathbf{K}_{\bar{\tau}}$ is the only part of **K**. However, if any cable of the CDPRs are held under position control, as long as it is under tension, inherent stiffness of such cable is involved in **K**. Such concept justifies the kinematically-constrained actuation technique which holds a considerable number of cables in position control to improve the stiffness level of the moving platform.

3.3 Kinematically-Constrained Cable-Driven Robots

In this section, with the help of an illustrative example, we review the concept of kinematically-constrained actuation method in the CDPRs. In order to move the platform of a common redundant CDPR, such as the planar CDPR of Figure 3-2 with four cables of 1 to 4, three DOFs of *x, y,* θ_z and a

desired translational motion, each cable force is controlled by an individual actuator to provide a desired tension. In such conditions, the moving platform's stiffness within the motion is formed by the cables' tension.

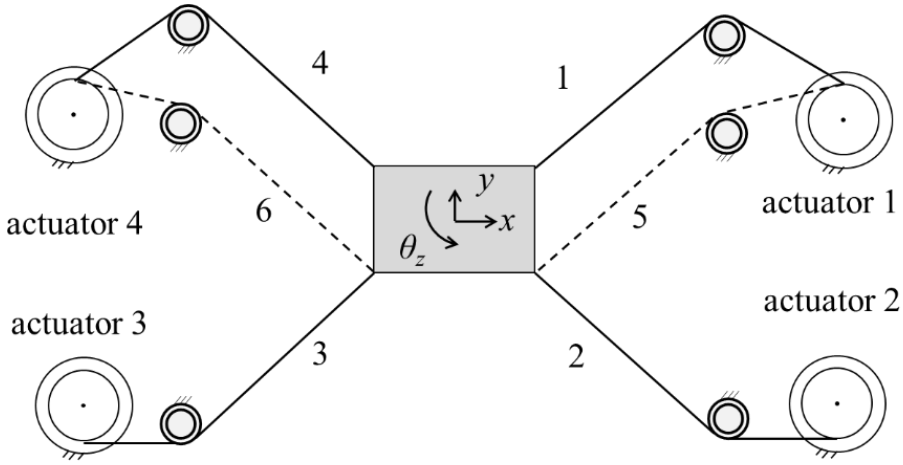

Figure 3-2: Layout of a redundant planar CDPR with kinematic constraints in 2D.

By adding two cables of 5 and 6, driven by actuators of 1 and 2, we can add a kinematic constraint to the moving platform to restrict the undesirable rotational DOF θ_z. To move the platform using 6 cables, consider top actuators under position control to provide the non-stretched length of top cables. Simultaneously, to make the desired tension of top cables, consider the tension of bottom cables are provided by their individual actuators. In such arrangement, the platform's stiffness along the motion is improved by axial stiffness of the constrained cables which can be considerably high in θ_z direction. Figure 3-3 illustrates the same example where, in order to limit the moving platform's out-of-plane motions, other unnecessary DOFs are restricted via kinematically-constrained actuation method. In such arrangement of the cables, in addition to θ_z, θ_x, θ_y and z are also restricted.

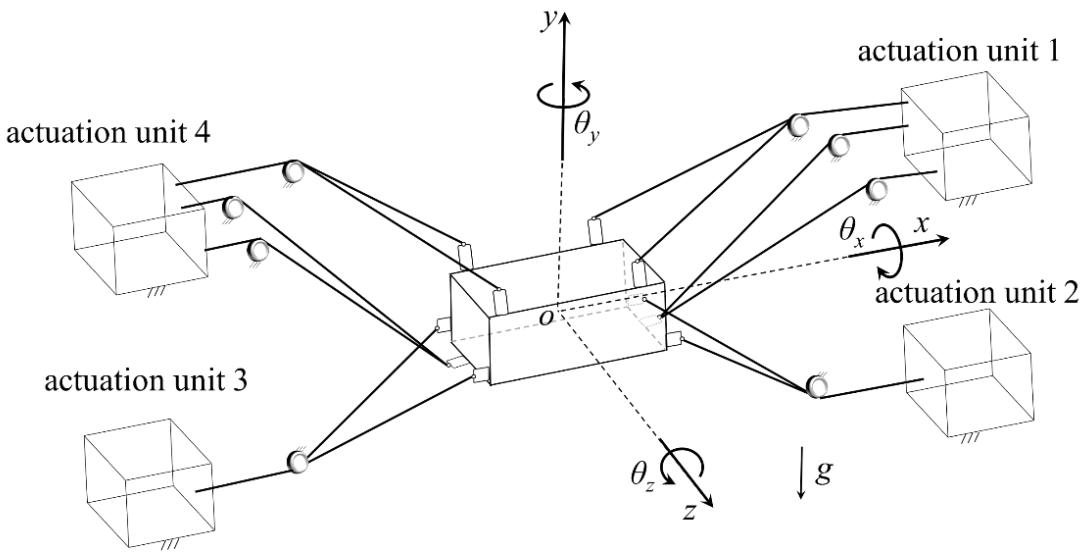

Figure 3-3: Layout of a planar KC-CDPR with kinematic constraints in 3D.

3.3.1 General Model of KC-CDPRs

A general flexible KC-CDPR is represented in this section and its dynamics, tensions redundancy, and stiffness optimization problems are studied. Based on the actuations of the cables in KC-CDPRs, each constrained cable is modeled with a massless linear spring where the damping effects and slackness of the cables are ignored. On the other hand, each non-constrained cables is replaced with its tension. It is assumed that all cables of each constrained actuator have an equal initial (non-stretched) length and also all actuators are perfect in providing the initial length or tension of the cables.

Figure 3-4 and Figure 3-5 illustrate the general layout and model of a 3D redundant KC-CDPR with $n=n'+n''$ actuators and $m=m_1+\ldots+m_{n'}+n''$ cables, where n' and n'' denote the number of actuators of constrained and non-constrained cables. In this configuration, initial and total lengths of cable j driven by actuator i, are denoted by l_{oi} and l_{ji}. The unit and anchor vectors (with respect the moving platform center of mass) for the same cable are designated by $\mathbf{u}_{ji}$ and $\mathbf{r}_{ji}$. The tension vector of each cable is along $\mathbf{u}_{ji}$ and has magnitude τ_{ji}. The number of constrained cables of the ith actuator is denoted by m_i and. Similar to commonly actuated CDPR, assuming a known position and orientation for the moving platform, the magnitudes of the tension is $\tau_{ji}=k_{ji}(l_{ji}-l_{oi})$ that in which $k_{ji}=A_iE/l_{ji}$.

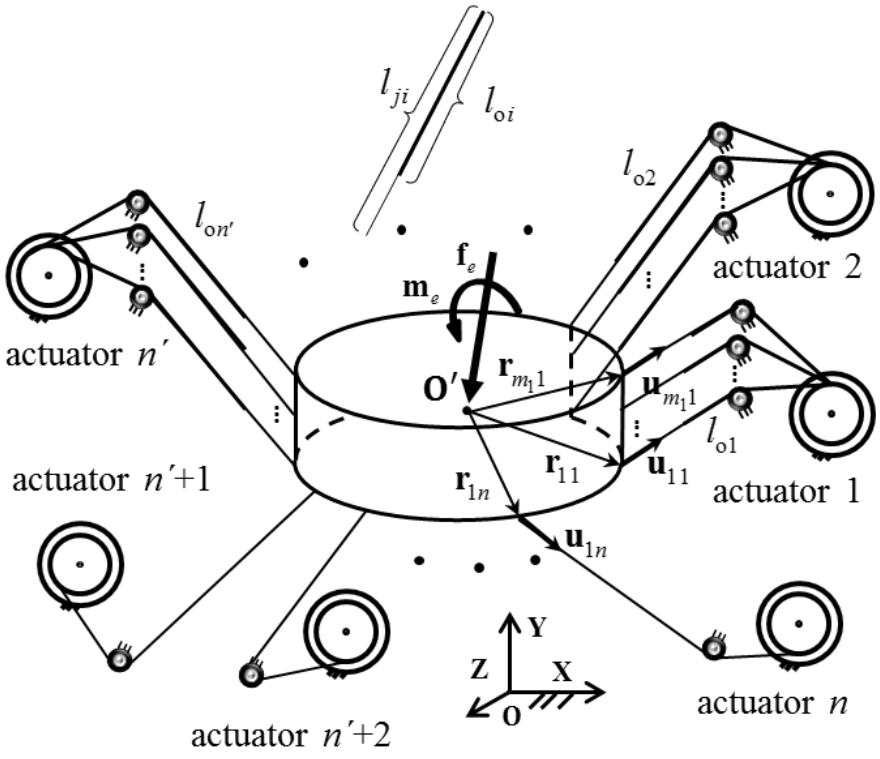

Figure 3-4: The general layout of a generic KC-CDPRs.

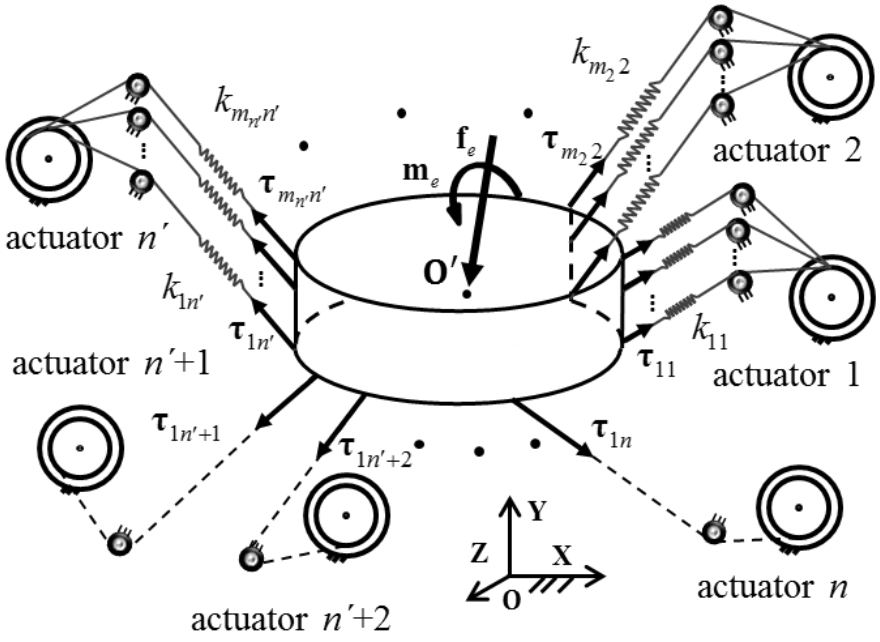

Figure 3-5: The general model of the generic KC-CDPRs.

In the nominal conditions of the moving platform, we have no perturbation in the position or orientation of the moving platform. In such conditions, the total length of all cables of each constrained actuator are equal. Accordingly, the connection points of constrained cables need to be selected such that this condition holds all over the workspace. In addition, the spool system of each constrained actuator needs to provide equal lengths for its connected cables. Applying large enough tensions, via non-constrained cables, holds all the constrained cables under tension to act as a strong spring which, by proper selection of the cables' connection points, can highly improve the moving platform's stiffness in desired directions. The Newton-Euler equations of motion for the moving platform of KC-CDPR, illustrated in Figure 3-5, gives the same motion equations (3-9), where **J** and **τ** for the KC-CDPR are obtained as

$$\mathbf{J}^T(\mathbf{x})_{6\times m}=\begin{bmatrix} \mathbf{u}_{11} & \cdots & \mathbf{u}_{m_{n'}n'} & \mathbf{u}_{1n'+1} & \ldots & \mathbf{u}_{1n} \\ \mathbf{r}_{11}\times\mathbf{u}_{11} & \cdots & \mathbf{r}_{m_{n'}n'}\times\mathbf{u}_{m_{n'}n'} & \mathbf{r}_{1n'}\times\mathbf{u}_{1n'} & \ldots & \mathbf{r}_{1n}\times\mathbf{u}_{1n} \end{bmatrix} \tag{3-22}$$

and

$$\boldsymbol{\tau}_{m\times 1}(\mathbf{x})=[\tau_{11},\ldots,\tau_{m_{n'}n'},\tau_{1n'+1},\ldots,\tau_{1n}]^T. \tag{3-23}$$

Apply the decoupling approach provides the same equations of (3-16) and (3-17), where based on the actuation of the cable in KC-CDPRs, $\mathbf{K}_k$ and $\mathbf{K}_{\bar{\tau}}$ for such robots are obtained as

$$\mathbf{K}_k=\sum_{i=1}^{n'}\sum_{j=1}^{m_i}k_{ji}\begin{bmatrix} \mathbf{u}_{ji}\mathbf{u}_{ji}^T & \mathbf{u}_{ji}\mathbf{u}_{ji}^T[\mathbf{r}_{ji}\times]^T \\ [\mathbf{r}_{ji}\times]\mathbf{u}_{ji}\mathbf{u}_{ji}^T & [\mathbf{r}_{ji}\times]\mathbf{u}_{ji}\mathbf{u}_{ji}^T[\mathbf{r}_{ji}\times]^T \end{bmatrix}_{6\times 6} \tag{3-24}$$

and

$$\begin{aligned}\mathbf{K}_{\bar{\tau}}=&\sum_{i=1}^{n}\sum_{j=1}^{m_i}\frac{\bar{\tau}_{ji}}{l_{ji}}\begin{bmatrix} \mathbf{I}-\mathbf{u}_{ji}\mathbf{u}_{ji}^T & (\mathbf{I}-\mathbf{u}_{ji}\mathbf{u}_{ji}^T)[\mathbf{r}_{ji}\times]^T \\ [\mathbf{r}_{ji}\times](\mathbf{I}-\mathbf{u}_{ji}\mathbf{u}_{ji}^T) & [\mathbf{r}_{ji}\times](\mathbf{I}-\mathbf{u}_{ji}\mathbf{u}_{ji}^T)[\mathbf{r}_{ji}\times]^T \end{bmatrix}_{6\times 6} \\ &+\sum_{i=1}^{n}\sum_{j=1}^{m_i}\bar{\tau}_{ji}\begin{bmatrix} 0 & 0 \\ 0 & -[\mathbf{u}_{ji}\times][\mathbf{r}_{ji}\times] \end{bmatrix}_{6\times 6}.\end{aligned} \tag{3-25}$$

According to (3-24) and (3-25), arrangement of constrained cables and the magnitude of tensions can be used to improve the moving platform's stiffness level and reduce its undesired vibrations. Accordingly, tension redundancy and stiffness optimization of the moving platform is studied in the sequel.

3.4 Tensions Redundancy Formulation

Based on the desired motion of the moving platform and (3-16), the redundant solution of $\bar{\boldsymbol{\tau}}$ can be found which is used in formulation of $\mathbf{K}(\bar{\mathbf{x}},\bar{\boldsymbol{\tau}})$. If the left hand side of (3-16) is defined as the CDPR total wrench and is represented by $\boldsymbol{\Omega}$, this equation can be rewritten in brief as

$$\boldsymbol{\Omega}_{6\times1}=\bar{\mathbf{J}}^{T}_{6\times m}\bar{\boldsymbol{\tau}}_{m\times1}, \tag{3-26}$$

where $\bar{\mathbf{J}}^{T}_{6\times m}=\mathbf{J}^{T}_{6\times m}(\bar{\mathbf{x}})$. For a determined motion or position of the moving platform, $\bar{\mathbf{J}}$ and $\boldsymbol{\Omega}$ are the known parts of (3-26). In case of $m > 6$, we have m-6 degrees of redundancy in the solution of $\bar{\boldsymbol{\tau}}$. Since there are n actuators that provide n independent actuation inputs, the degree of redundancy needs to be reduced to n-6. Regarding the nominal conditions of the moving platform, we can assume equal nominal tensions for all constrained cables of each actuator. Accordingly, replacing the identical tension of actuator i cables by $\bar{\tau}_i$ simplifies (3-26) to the following equation with desired redundancy degree n-6

$$\boldsymbol{\Omega}_{6\times1}=\bar{\mathbf{J}}'^{T}_{6\times n}\bar{\boldsymbol{\tau}}'_{n\times1} \tag{3-27}$$

where

$$\bar{\mathbf{J}}'^{T}_{6\times n}=\begin{bmatrix} \sum_{j=1}^{m_1}\mathbf{u}_{j1} & \cdots & \sum_{j=1}^{m_{n'}}\mathbf{u}_{jn'} & \mathbf{u}_{1n'+1} & \cdots & \mathbf{u}_{1n} \\ \sum_{j=1}^{m_1}(\mathbf{r}_{i1}\times\mathbf{u}_{i1}) & \cdots & \sum_{j=1}^{m_{n'}}(\mathbf{r}_{in'}\times\mathbf{u}_{in'}) & \mathbf{r}_{1n'}\times\mathbf{u}_{1n'} & \cdots & \mathbf{r}_{1n}\times\mathbf{u}_{1n} \end{bmatrix}, \bar{\boldsymbol{\tau}}'_{n\times1}=[\bar{\tau}_1\ldots\bar{\tau}_{n'}\,\bar{\tau}_{1n'+1}\ldots\bar{\tau}_{1n}]^{T}. \tag{3-28}$$

In real applications, for avoiding the cables' slackness and also considering the actuators' maximum torque, there is a minimum and maximum bound on the tension's magnitude of each cable. Denoting the minimum and maximum acceptable tension values for cables of actuator i by $\tau_{i\min}$ and $\tau_{i\max}$, the allowable tension range of the cables can be written as

$$0\le\tau_{i\min}\le\bar{\tau}_i\le\tau_{i\max}. \tag{3-29}$$

Regarding the dimension of $\bar{\mathbf{J}}'$ in (3-27), in case of $n > 6$, $\boldsymbol{\tau}'$ has a solution with the limitations of (3-29). This solution in general form can be written as

$$\bar{\boldsymbol{\tau}}'_{n\times1}=\bar{\mathbf{J}}'^{T+}_{n\times6}\boldsymbol{\Omega}_{6\times1}+\mathbf{H}_{n\times(n-6)}\boldsymbol{\alpha}_{(n-6)\times1} \tag{3-30}$$

where $\bar{\mathbf{J}}'^{T+}$ is the pseudo inverse of $\bar{\mathbf{J}}'^{T}$, $\boldsymbol{\alpha}=[\alpha_1,\alpha_2,\ldots,\alpha_{n-6}]^{T}$ is the vector of arbitrary variables, $\mathbf{H}=[\mathbf{h}_1\ \mathbf{h}_2\ldots\ \mathbf{h}_{n-6}]$, where $\mathbf{h}_1$ to $\mathbf{h}_{n-6}$ denote the basis unit vectors of null space of $\bar{\mathbf{J}}'^{T}$. Using (3-30), the cables' tension limitation (3-29) can be written as

$$\boldsymbol{\tau}_{\min} - \bar{\mathbf{J}}'^{T+}\boldsymbol{\Omega} \le \mathbf{H}\boldsymbol{\alpha} \le \boldsymbol{\tau}_{\max} - \bar{\mathbf{J}}'^{T+}\boldsymbol{\Omega} \tag{3-31}$$

which form a polytope in space $\boldsymbol{\alpha}$, where $\boldsymbol{\tau}_{\min}=[\tau_{1\min},\tau_{2\min},\ldots,\tau_{n\min}]^T$ and $\boldsymbol{\tau}_{\max}=[\tau_{1\max},\tau_{2\max},\ldots,\tau_{n\max}]^T$ are the vectors of cables' minimum and maximum allowable tensions.

3.5 Redundancy Resolution

In this thesis, it is aimed to find the optimum $\boldsymbol{\alpha}$ in polytope (3-31), which maximizes the stiffness of the moving platform in a desired direction. To find the desired direction, two different scenarios are considered. In the first scenario we consider that the moving platform interaction with its environment or a tool mounted on it, makes a disturbance force $\mathbf{f}_e$ or moment $\mathbf{m}_e$ in a known direction. In such a case, the corresponding objective function is derived based on the translational or rotational part of $\mathbf{K}$ in direction of $\mathbf{f}_e$ or $\mathbf{m}_e$ and then is maximized. Accordingly, we can expect to have the minimum translational or rotational deviation under disturbance $\mathbf{f}_e$ or $\mathbf{m}_e$ in their applied directions. In the second scenario, in absence of any knowledge about the disturbance force/moment, we first have considered the coupled structural stiffness matrix $\mathbf{K}_k$ to define the softest direction of the stiffness matrix. Next, the corresponding objective function of softest direction is defined and maximized.

3.5.1 Maximization of Directional Stiffness

Regarding the nominal conditions for the stiffness matrix in (3-17), in addition to replacing τ_{ji}s by τ_i, k_{ji} and l_{ji} can also be replaced by their nominal values of k_i and l_i in (3-24) and (3-25). Accordingly, the translational and rotational stiffness matrices of the moving platform are given by

$$\mathbf{K}_{tr\,3\times3} = \sum_{i=1}^{n'}\sum_{j=1}^{m_i} k_i \mathbf{u}_{ji}\mathbf{u}_{ji}^T + \sum_{i=1}^{n}\sum_{j=1}^{m_i} \frac{\tau_i}{l_i}(\mathbf{I} - \mathbf{u}_{ji}\mathbf{u}_{ji}^T) \tag{3-32}$$

and

$$\begin{aligned}\mathbf{K}_{ro\,3\times3} = &\sum_{i=1}^{n'}\sum_{j=1}^{m_i} k_i [\mathbf{r}_{ji}\times]\mathbf{u}_{ji}\mathbf{u}_{ji}^T[\mathbf{r}_{ji}\times]^T \\ &+ \sum_{i=1}^{n}\sum_{j=1}^{m_i} \frac{\tau_i}{l_i}([\mathbf{r}_{ji}\times](\mathbf{I} - \mathbf{u}_{ji}\mathbf{u}_{ji}^T)[\mathbf{r}_{ji}\times]^T - l_i[\mathbf{u}_{ji}\times][\mathbf{r}_{ji}\times]).\end{aligned} \tag{3-33}$$

According to (3-30), τ_is and hence the entries of translational and rotational stiffness matrices in (3-32) and can be written as linear combinations of α_is and can be used to develop an objective function.

To derive the translational stiffness objective function, consider the moving platform in a desired position and let $\boldsymbol{\beta}_t=[\beta_{tx},\beta_{ty},\beta_{tz}]^T$ be the unit vector of desirable translational stiffness direction. The translational stiffness of the moving platform in direction of $\boldsymbol{\beta}_t$ is given by

$$K_{tr\beta t} = \frac{\delta F_{\beta t}}{\delta P_{\beta t}} \tag{3-34}$$

where δF_{β} denotes the magnitude of small force variation in direction of $\boldsymbol{\beta}_t$ for having a small translational displacement of $\delta P_{\beta t}$ in the same direction. Based on the translational stiffness matrix definition, denoting the vector of required external force for having the translational deviation of $\delta\mathbf{p}$ by $\delta\mathbf{F}$, we have

$$\delta\mathbf{F} = \mathbf{K}_{tr}\delta\mathbf{p}. \tag{3-35}$$

Accordingly, the required force vector for having δP_{β} displacement in $\boldsymbol{\beta}_t$ direction is obtained as

$$\delta\mathbf{F}_{\beta t} = \mathbf{K}_{tr}\boldsymbol{\beta}_t\delta P_{\beta t}. \tag{3-36}$$

By projecting $\delta\mathbf{F}_{\beta}$ in $\boldsymbol{\beta}_t$ direction, $\delta F_{\beta t}$ is obtained as

$$\delta F_{\beta t} = \boldsymbol{\beta}_t^T\delta\mathbf{F}_{\beta t}. \tag{3-37}$$

Substituting (3-36) in (3-37), gives

$$\delta F_{\beta t} = \boldsymbol{\beta}_t^T\mathbf{K}_{tr}\boldsymbol{\beta}_t\delta P_{\beta t}. \tag{3-38}$$

Therefore based on (3-34), we have

$$K_{tr\beta t} = \boldsymbol{\beta}_t^T\mathbf{K}_{tr}\boldsymbol{\beta}_t. \tag{3-39}$$

Having $\mathbf{K}_{tr}$ as a linear function of α_is, $K_{tr\beta t}$ is also a linear combination of α_is. Accordingly, the optimization problem of maximizing the translational stiffness in direction $\boldsymbol{\beta}_t$ is formulated as finding

$$K^*_{tr\beta t} = \max_{\boldsymbol{\alpha}} K_{tr\beta t}(\boldsymbol{\alpha}). \tag{3-40}$$

Similar to the translational stiffness, maximizing the rotational stiffness of the moving platform can be formulated as finding

$$K^*_{ro\beta\theta} = \max_{\boldsymbol{\alpha}} K_{ro\beta\theta}(\boldsymbol{\alpha}) \tag{3-41}$$

where $K_{ro\beta\theta} = \boldsymbol{\beta}_\theta{}^T\mathbf{K}_{ro}\,\boldsymbol{\beta}_\theta$ and $\boldsymbol{\beta}_\theta=[\beta_{\theta x},\beta_{\theta y},\beta_{\theta z}]^T$ is the unit vector of desirable rotational stiffness direction.

3.5.2 Stiffness Maximization in the Softest Direction

To define the softest direction of a CDPR, we have assumed that the moving platform's stiffness matrix $\mathbf{K}$ is made only by the structural part $\mathbf{K}_k$. In such conditions, a wrench of $\delta\mathbf{W}=[\delta\mathbf{F}^T, \delta\mathbf{M}^T]^T=\delta D_{\beta}\boldsymbol{\beta}$ makes the perturbation $\delta X_{\beta}\boldsymbol{\beta}$, where $\boldsymbol{\beta}=[\boldsymbol{\beta}_t^T,\boldsymbol{\beta}_\theta^T]^T$ is a unit vector. The softest direction of the moving platform is defined as the vector $\boldsymbol{\beta}$ for which $\delta X_{\beta}/\delta D_{\beta}$ has its maximum value. Noting $\mathbf{K}_k$ as a positive definite symmetric matrix [32], it can be shown that $\boldsymbol{\beta}=\boldsymbol{\eta}_{\min}$ where $\boldsymbol{\eta}_{\min}$ is the eigenvector of $\mathbf{K}_k$ minimum eigenvalue $\eta_{\min}$. Accordingly, the maximum value of $\delta X_{\beta}/\delta D_{\beta}$ is obtained as $1/\eta_{\min}$. Noting the total stiffness matrix $\mathbf{K}=\mathbf{K}_k+\mathbf{K}_{\bar{\tau}}$, in order to minimize $\delta X_{\beta}/\delta D_{\beta}$ in $\boldsymbol{\beta}$ direction, maximization of the objective function

$$K_\beta = \boldsymbol{\beta}^T \mathbf{K} \boldsymbol{\beta},\ \boldsymbol{\beta} = \boldsymbol{\eta}_{\min} \tag{3-42}$$

is formulated as

$$K_\beta^* = \max_{\boldsymbol{\alpha}} K_\beta(\boldsymbol{\alpha}). \tag{3-43}$$

Utilizing the linearity of the obtained objective functions, linear programming techniques can be used as the redundancy resolution technique for the developed objective functions. As an example, this algorithm for the translational stiffness can be written as

$$\begin{aligned} &\text{maximize } K_{tr\beta}(\boldsymbol{\alpha}) \\ &\text{over } \boldsymbol{\alpha} \in \mathbb{R}^{n-6} \\ &\text{subject to } \boldsymbol{\tau}_{\min} - \bar{\mathbf{J}}'^{T+}\boldsymbol{\Omega} \le \mathbf{H}\boldsymbol{\alpha} \le \boldsymbol{\tau}_{\max} - \bar{\mathbf{J}}'^{T+}\boldsymbol{\Omega}. \end{aligned} \tag{3-44}$$

Solving (3-44) gives $\boldsymbol{\alpha}^*$ as the optimized vector of $\boldsymbol{\alpha}$. Substituting $\boldsymbol{\alpha}^*$ in (3-30), provides the optimum $\boldsymbol{\tau}'$ which is used in actuators' input calculation. In addition, based on the optimized $\boldsymbol{\tau}'$, the stiffness matrix $\mathbf{K}$ can be obtained and used in vibration equations (3-17). Accordingly, the free vibration of the moving platform in all of its six DOFs can be modeled for different initial position and velocity conditions. It should be noted that the provided approach for maximizing the stiffness assumes that the CDPR is in a stable configuration. The necessary and sufficient geometrical conditions for stability of a CDPR are discussed in [32].

3.6 Application on the Warehousing CDPR

In this section, the developed approach is used for stiffness maximization of a planar warehousing robot over its workspace. Figure 3-6 illustrates the prototype of studied CDPR that has been fabricated based on an optimized design reported in [82].

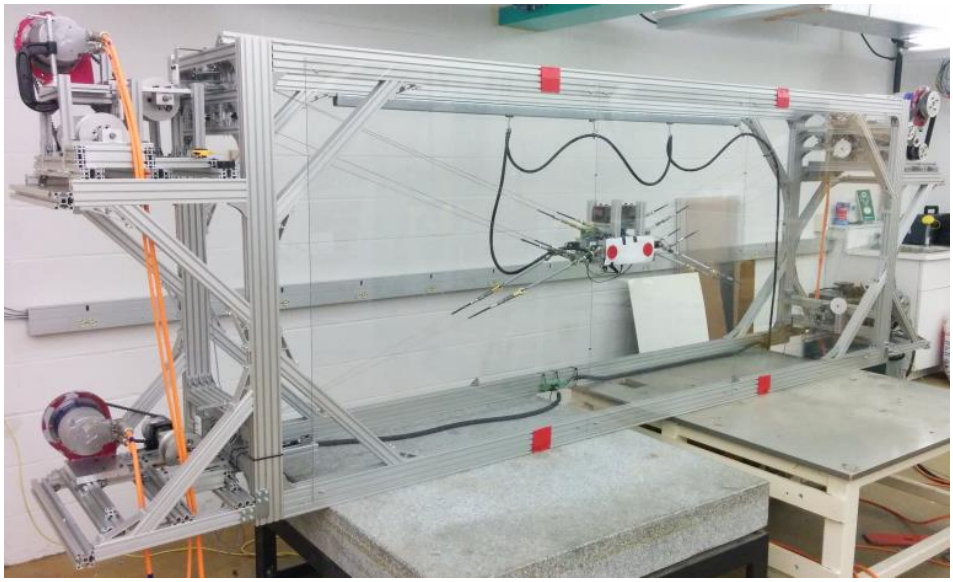

Figure 3-6: The prototype of planar warehousing KC-CDPR.

3.6.1 CDPR Configuration and Specifications

The cables' configuration of the warehousing robot is shown in Figure 3-7 and its dimensions are presented in Table 3-1. As Figure 3-7 illustrates, this robot uses 12 cables to provide a planar translational motion for the moving platform in *x*-*y* plane, where 8 cables (2 bunches of 4 cables) are driven by the top actuators and 4 cables (2 bunches of 2 cables) are driven by the bottom actuators.

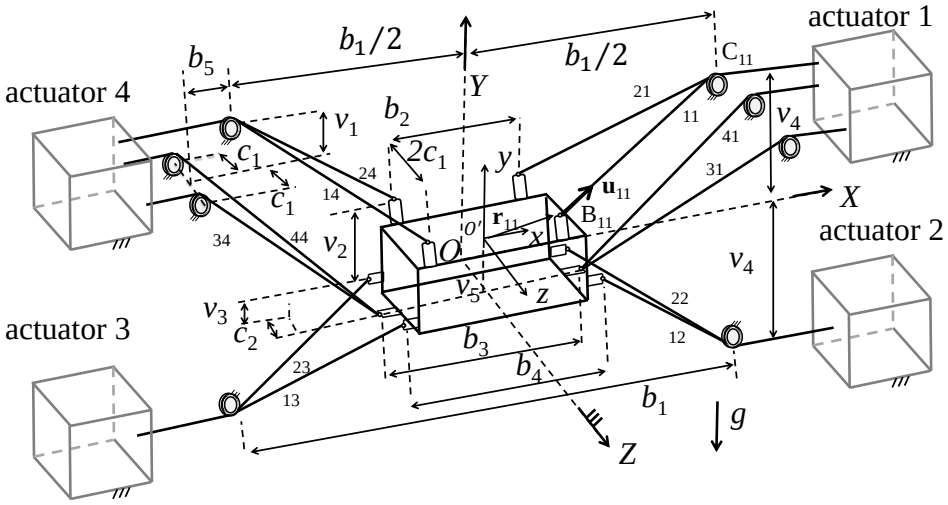

Figure 3-7: The warehousing KC-CDPR configuration.

In Figure 3-7, the coordinate system of *xyz* is attached to the moving platform centre of mass where the fixed coordinate system of *XYZ* is attached to the geometric centre of fixed frame. The moving platform and fixed frame, with respect to *x-y*, *y-z* and *X-Y*, *Y-Z* planes, are symmetric. Assuming equal lengths for all cables of each actuator, the illustrated configuration constrains four undesired DOFs of the moving platform. According to the illustrated configuration of cables, z, θ_x, θ_y, and θ_z are the constrained DOFs. In such conditions, the length of top cables can be controlled to provide the planar translational motion where the tension control of bottom cables can be used for stiffness maximization.

Table 3-1: Warehousing robot dimensions (in meters).

Dimension	Value	Dimension	Value	Dimension	Value
b_1	3	v_1	0.105	b_5	0.08
b_2	0.2050	v_2	0.059	c_1	0.065
b_3	0.3650	v_3	0.046	v_5	0.05
b_4	0.3450	v_4	0.5	c_2	0.095

The warehousing robot moving platform can carry an extra mass, illustrated in Figure 3-11, as payload. In addition, to provide a force feedback on the bottom cables, each one of these cables is connected to a linear spring that via a force sensor is connected to the moving platform. Table 3-2 represents the cables' mechanical properties, mass and inertia of the moving platform, the stiffness of bottom springs, and the limitation of cables' tension.

Table 3-2: Warehousing robot moving platform and cables properties.

Parameter	Description	Value
a	cross section area of the cables	2 mm^2
E	cables' young modulus of elasticity	55 GPa
K_S	bottom springs' stiffness	753 N/m
τ_{tmax}, τ_{bmax}, τ_{min}	top and bottom cables' maximum and cables' minimum tension	400, 150, 40N
m_{mp}, m_{pl}	moving platform and payload mass	8.8, 5.7 kg
I_{xx}, I_{yy}, I_{zz}	platform inertia entries	0.04, 0.16, 0.14 kg m^2
I_{xxpl}, I_{yypl}, $I_{zz\mathrm{pl}}$	platform & payload inertia entries	0.07, 0.18, 0.19 kg m^2

3.6.2 Tensions Redundancy

Based on the provided configuration in Figure 3-7 and (3-27), for a known static position of the moving platform, the tensions equation can be written as

$$\mathbf{\Omega}_{3\times1} = \bar{\mathbf{J}}'^{T}_{3\times4}\bar{\boldsymbol{\tau}}'_{4\times1} \tag{3-45}$$

where $\bar{\mathbf{J}}'$ is obtained form (3-28), $\boldsymbol{\tau}'=[\tau_1,\tau_2,\tau_3,\tau_4]^T$ and $\mathbf{\Omega}=[0,mg,0]^T$ is the external wrench. Regarding the dimension of $\bar{\mathbf{J}}'^{T}_{3\times4}$ in (3-45), we have one degree of redundancy in solution of $\boldsymbol{\tau}'$ which its redundant variable is denoted by α_1. Satisfying the allowable tension of cables, provides the feasible domain of α_1 as $[\alpha_{1\min}, \alpha_{1\max}]$.

Regarding the layout of the warehousing robot with a long projection of cables' length on the *x* and *y* axes in front of a short projection on *z* axis, we can expect a considerable flexibility in this direction. Thus, *z* direction is selected as the direction of stiffness maximization to find the optimum value of α_1. Accordingly, the optimization problem for finding optimum α_1 is written as

$$\begin{aligned} &\text{maximize}\, K_{trz}(\alpha_1) \\ &\text{over}\ \ \alpha_{1\min} \le \alpha_1 \le \alpha_{1\max} \end{aligned} \tag{3-46}$$

where $K_{trz}(\alpha_1)= \boldsymbol{\beta}_t^T\mathbf{K}_{tr}\boldsymbol{\beta}_t$ and $\boldsymbol{\beta}_t=[0,0,1]^T$. (3-46) provides α^*_1 as the optimum value of α_1. Having α^*_1, the initial length of top cables and the tension of bottom cables are achieved for every desired point. In addition, the stiffness matrix of the moving platform is obtained and used in vibration equations.

Having one degree of redundancy in (3-46), it can be shown that for the selected points of the workspace, the maximum value of K_{trz} are obtained in the maximum value of α_1. To show the optimum solution of a KC-CDPR with a higher degree of redundancy, a similar example with two degrees of redundancy is presented here. Figure 3-8 shows the CDPR configuration with an extra actuator.

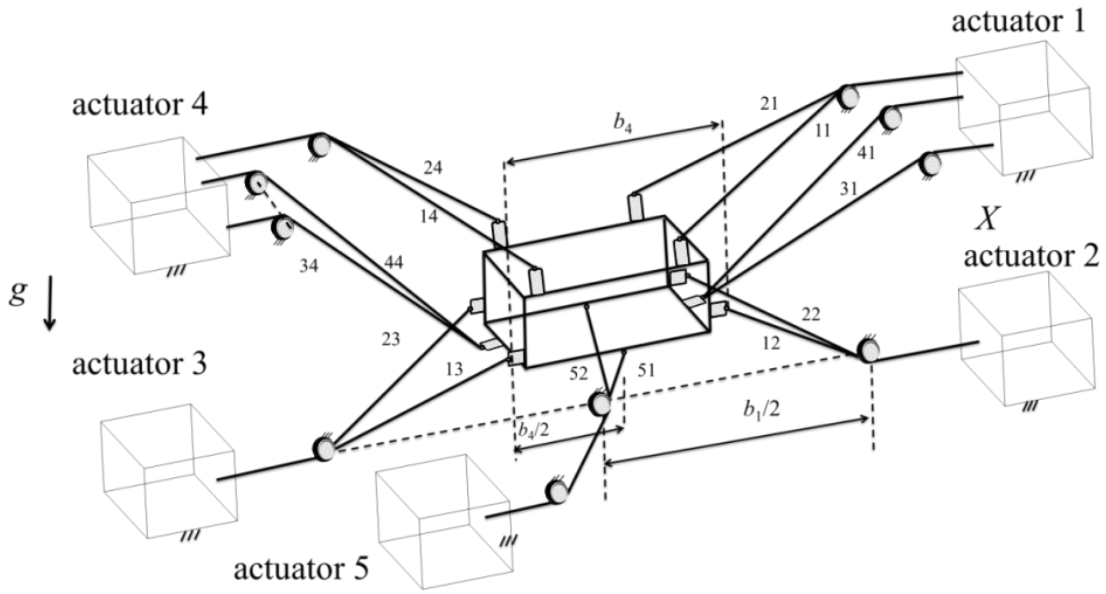

Figure 3-8: A planar CDPR with two degrees of redundancy.

In this example, arrangement of the cables and dimensions of the robot are the same and the only difference is in adding actuator 5, with illustrated connection points in Figure 3-8. Adding actuator 5 increases the tensions degree of redundancy form one to two. Accordingly, the solution of tensions and consequently stiffness matrix **K** are resulted as a function of α_1 and α_2. Accordingly, an optimization problem can be defined as

$$\begin{aligned} &\text{maximize } K_{trz}(\alpha_1,\alpha_2) \\ &\text{over } \boldsymbol{\alpha} \in \mathbb{R}^2 \\ &\text{subject to } \boldsymbol{\tau}_{\min} - \bar{\mathbf{J}}'^{T+}\boldsymbol{\Omega} \le \mathbf{H}\boldsymbol{\alpha} \le \boldsymbol{\tau}_{\max} - \bar{\mathbf{J}}'^{T+}\boldsymbol{\Omega} \end{aligned} \tag{3-47}$$

to maximize the moving platform's stiffness in *z* direction. Considering the same tension limitation for the bottom and top cables, for the static equilibrium conditions with zero payloads at $\mathbf{p}_5=[0.2,0.2]^T$, the feasible 2D polytope of $\boldsymbol{\tau}_{\min} - \bar{\mathbf{J}}'^{T+}\boldsymbol{\Omega} \le \mathbf{H}\boldsymbol{\alpha} \le \boldsymbol{\tau}_{\max} - \bar{\mathbf{J}}'^{T+}\boldsymbol{\Omega}$ is resulted as shown in Figure 3-9.

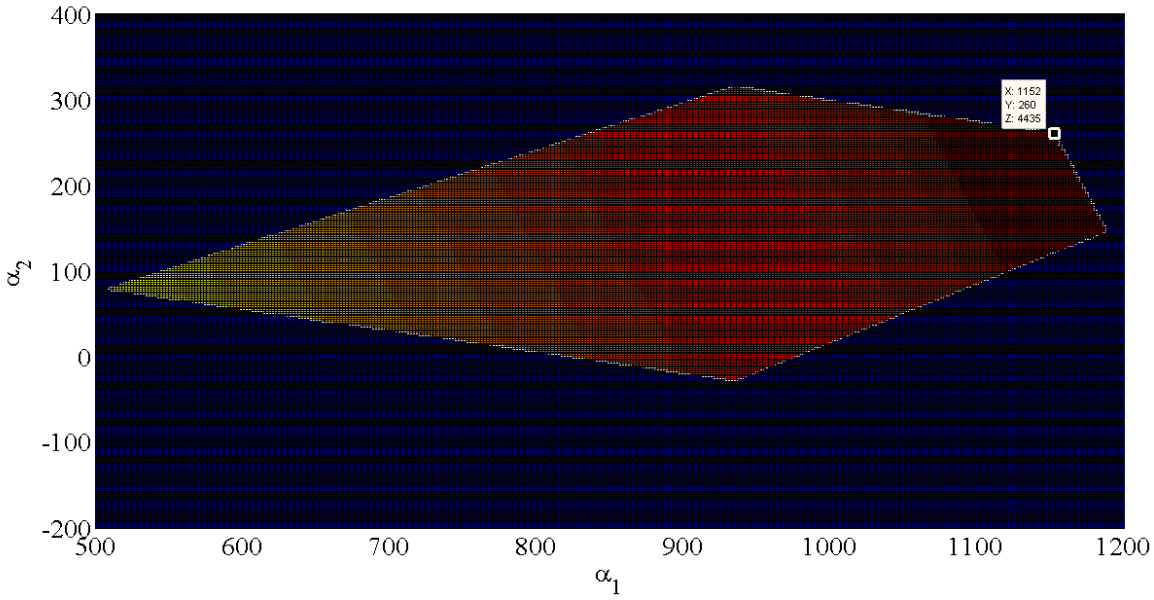

Figure 3-9: The feasible polytope of α_1 and α_2 at p_5.

The optimum values are resulted at $[\alpha^*_1,\alpha^*_2]$= [1154,260] which provides the maximum value of 4.435 kN/m for K_{trz}. According to the obtained optimized value, neither α^*_1, nor α^*_2 are taking their maximum or minimum values. Variation of K_{trz} over the feasible polytope is shown in Figure 3-10.

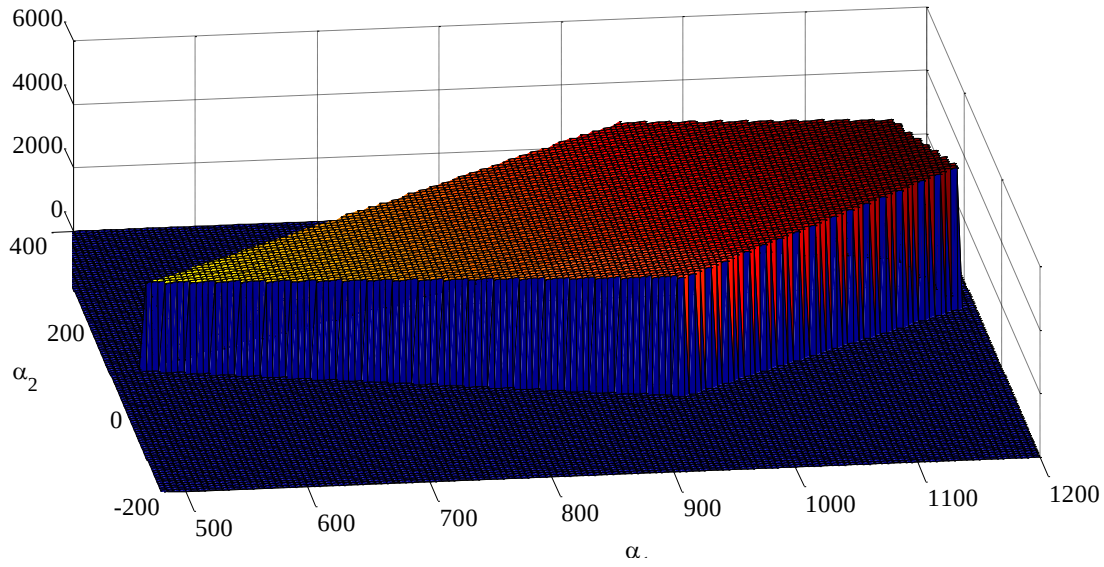

Figure 3-10: K_{trz} variation over the feasible 2D polygon of α_1 and α_2.

3.7 Experiments

3.7.1 Experimental Procedure

To validate the developed modelling approach, effects of kinematically constrained actuations, and optimization approach, three sets of experiments are designed and implemented. The first experiment evaluates the effects of optimized tensions on the moving platform's stiffness. The second experiment demonstrates the effectiveness of kinematically-constrained actuation method in vibration reduction and disturbance rejection of KC-CDPRs. Finally, the third experiment validates the vibration model of the KC-CDPRs.

In the first experiment, the moving platform is positioned in a desired position using top cables and by applying the optimal and non-optimal tension to the bottom cables, the stiffness of the platform in the optimized direction is studied and compared. In any desired position, using a Krypton RODYM® 6D position measurement system with 0.2 mm precision and four force sensors with 1 N precision shown in Figure 3-11, the moving platform position and bottom cables' tension are measured. To compare the effect of optimized α^*_1 on maximization of the robot stiffness, two other non-optimal values of α_1 in the feasible range of $[\alpha_{1\min}, \alpha_{1\max}]$ are used for the bottom cables' tension. Experiments are conducted for two payloads (zero and 5.7 kg) in 5 different poses, including the centre and four corners of a rectangle with a width of 0.8 m and a height of .4 m. Accordingly, $\mathbf{p}_0=[0,0]^T$, $\mathbf{p}_1=[0.4,-0.2]^T$, $\mathbf{p}_2=[0.4,0.2]^T$, $\mathbf{p}_3=[-0.4,0.2]^T$, and $\mathbf{p}_4=[-0.4,-0.2]^T$ are selected as the desired positions. Table 3-3 shows the total length of top cables in each position.

Table 3-3: The total length of top cables (in meters).

$\mathbf{p}_i$	$\mathbf{p}_0$	$\mathbf{p}_1$	$\mathbf{p}_2$	$\mathbf{p}_3$	$\mathbf{p}_4$
l_1	1.4702	1.1935	1.0309	1.8162	1.9132
l_4	1.4702	1.9132	1.8162	1.0309	1.1935

In addition to α^*_1, $\alpha_{1\min}$ and $\alpha_{1\mathrm{mid}}=(\alpha_{1\min}+\alpha_{1\max})/2$ are selected as non-optimal sets of bottom cables' tension. In the optimization process, the maximum time for calculation of α^*_1 using dual-simplex linear-programming algorithm [118] (implemented by the MATLAB function "linprog") was 0.01 seconds on a computer with Intel® Core™ i7-2600 3.4GHz processor and 8GB RAM. Table 3-4 and Table 3-5 provide α^*_1, $\alpha_{1\mathrm{mid}}$, $\alpha_{1\min}$ and their corresponding cables' tension for two case of zero and 5.7

payloads, respectively. Note that for the selected points of the workspace, α^*_1 is obtained as α_{1max}. Nevertheless, it is worth mentioning that this result cannot be extended to the other points of workspace, different $\boldsymbol{\beta}$ directions, or similar CDPRs.

Since direct measurement of stiffness is not possible, in order to evaluate the stiffness of the moving platform, an indirect approach has been used. As equation (3-17) indicates, free vibrations of the moving platform in all of its six DOFs is affected by the optimized stiffness matrix. Accordingly, the moving platform natural frequencies can be used as a comparison criterion.

In order to find a comparable natural frequency, a small perturbation is applied in *z* direction and the vibration signals of the moving platform are recorded. The same initial condition is considered in (3-17) and the vibration of the platform is simulated. For recording the desired signals, a six axis inertial measurement unit (IMU), illustrated in Figure 3-11, is used which records the translational accelerations and angular velocities of the moving platform.

Table 3-4: Optimal and non-optimal tensions for zero payloads (in Newton).

$\mathbf{p}_i$	$\mathbf{p}_0$	$\mathbf{p}_1$	$\mathbf{p}_2$	$\mathbf{p}_3$	$\mathbf{p}_4$
α^*_1	159.9	20	549.0	480.2	52.7
τ_1	121.2	64.3	237.9	233.5	62.1
τ_2	150.0	150.0	150.0	126.9	135.0
τ_3	150.0	135.0	126.9	150.0	150.0
τ_4	121.2	62.1	233.5	237.9	64.3
α_{1mid}	109.4	16.5	412.7	355.5	37.0
τ_1	89.6	52.2	179.7	178.7	52.4
τ_2	95.0	108.7	104.6	83.4	93.2
τ_3	95.0	93.2	83.4	104.6	108.7
τ_4	89.6	52.4	178.7	179.7	52.2
α_{1min}	59	12.9	276.3	230.8	21.4
τ_1	58.0	40.0	121.6	123.9	42.6
τ_2	40.0	67.4	59.2	40.0	51.4
τ_3	40.0	51.4	40.0	59.2	67.4
τ_4	58.0	42.6	123.9	121.6	40.0

Table 3-5: Optimal and non-optimal tensions for 5.7 Kg payloads (in Newton).

$\mathbf{p}_i$	$\mathbf{p}_0$	$\mathbf{p}_1$	$\mathbf{p}_2$	$\mathbf{p}_3$	$\mathbf{p}_4$
α^*_1	174.5	24.7	613.4	524.8	50.0
τ_1	144.1	77.5	267.7	267.8	79.6
τ_2	150.0	150.0	150.0	116.0	124.0
τ_3	150.0	124.0	116.0	150.0	150.0
τ_4	144.1	79.6	267.8	267.8	77.5
α_{1mid}	124.0	21.1	494.1	415.7	34.3
τ_1	112.6	65.3	216.9	220.0	69.8
τ_2	95.0	108.6	110.3	78.0	82.0
τ_3	95.0	82.0	78.0	110.3	108.6
τ_4	112.6	69.8	220.0	216.9	65.3
α_{1min}	73.6	17.6	374.9	306.6	18.6
τ_1	81.0	53.1	165.0	171.9	60.1
τ_2	40.0	67.1	70.6	40.0	40.0
τ_3	40.0	40.0	40.0	70.6	67.1
τ_4	81.0	60.1	171.9	166.0	53.1

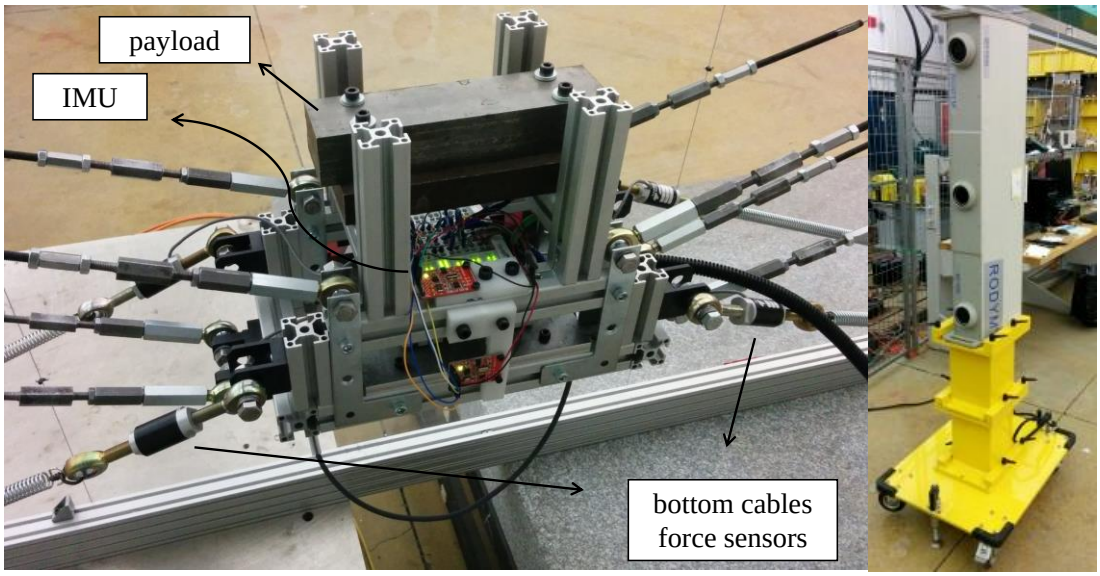

(a) (b)

Figure 3-11: Configuration of (a) the forces sensors, IMU and payload on the KC-CDPR moving platform and (b) the Krypton RODYM® measurement system camera.

In addition, to validate the model, the natural frequency of the platform in z direction f_{model} is also calculated and compared with the actual natural frequency of the platform f_{actual}. The error in the model and actual natural frequency of the platform in z direction is defined as

$$f_{\text{error}} = 100\frac{f_{\text{model}} - f_{\text{actual}}}{f_{\text{actual}}}. \tag{3-48}$$

In the second experiment, in order to show the effects of kinematically-constrained actuation method in restricting the rotational DOF of the moving platform, two different actuation methods are tested. For this goal, the circular trajectory of

$$\begin{aligned} x(t) &= x_0 + r_r \cos(\mathrm{f}(t/t_m) + 3\pi/2), \\ y(t) &= y_0 + r_r \sin(\mathrm{f}(t/t_m) + 3\pi/2), \\ \mathrm{f}(t/t_m) &= -40\pi(t/t_m)^7 + 140\pi(t/t_m)^6 - 168\pi(t/t_m)^5 + 70\pi(t/t_m)^4, \end{aligned} \tag{3-49}$$

is considered as the desired trajectory and a z-direction harmonic disturbance moment $\mathbf{m}_e$=1sin(10πt)$\mathbf{u}_z$ N.m. is applied on the moving platform, where, t, t_m=4 sec, [x_0, y_0] =[0,0] mm and r_r = 100 mm denote time, total motion time, centre and radius of the circle, respectively. In the considered motion, the initial and final values of jerk, acceleration, and velocity are zero. In this experiment, maximization of $K_{\theta z}$ is proposed to solve the tensions redundancy problem and the harmonic moment is made by a multi-axis reaction mechanism designed in [119]. To implement the experiment, first, the trajectory (3-49) is tracked by the robot with all 8 constraining top cables. Next, cables 41, 31, 34 and 44 are removed and the same experiment is repeated with only 4 constrained top cables. As Figure 3-12 indicates, in case of having only 4 constraining cables, the rotational stiffness of the moving platform is in the same order of that with common actuation of all 8 cables. However, as depicted in Figure 3-13, the stiffness of kinematically-constrained actuated platform is in a considerably higher order.

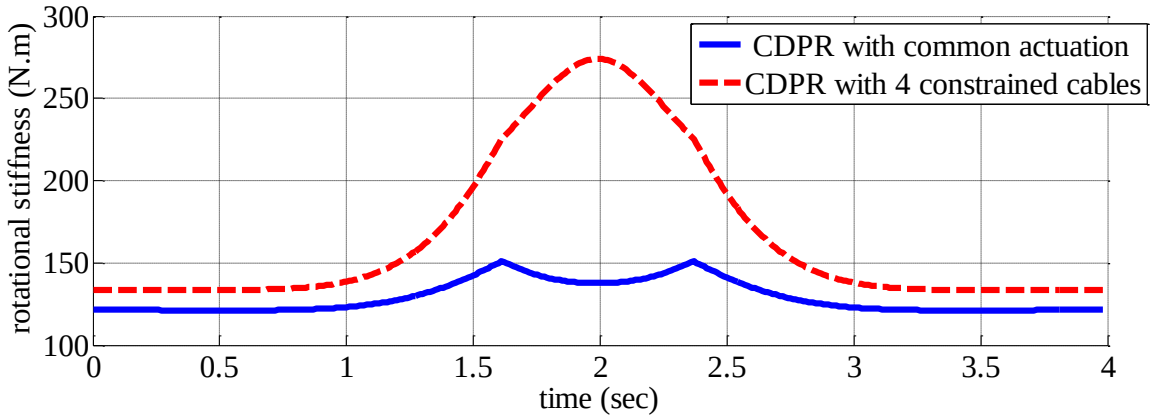

Figure 3-12: Moving platform $K_{\theta z}$ variation in common actuation and with 4 constrained cables.

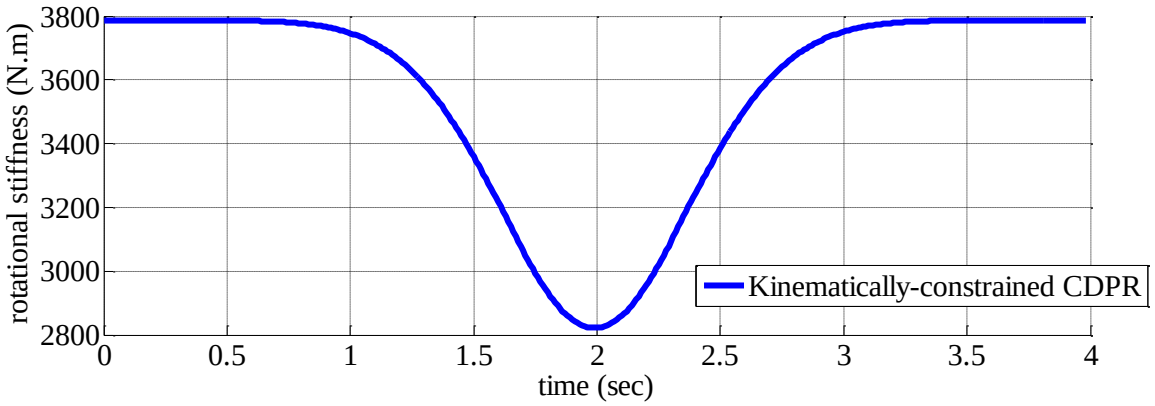

Figure 3-13: Kinematically-constrained moving platform $K_{\theta z}$ variation.

In the third set of experiments, in order to verify the developed vibration model in the planar directions, vibration of the moving platform in y and θ_z directions are tested. In these experiments, a harmonic external y-direction force as well as a harmonic z-direction moment with different frequencies are applied on the moving platform in different positions where the vibration signals of the moving platform are recorded. Based on the recorded inputs and vibration signals, corresponding Bode plots are obtained and used to find the natural frequency of the system in forced vibration in y and θ_z directions. The experimental natural frequencies are compared with the corresponding model natural frequencies and the results are discussed. Figure 3-14 shows the recorded y-direction acceleration of the moving platform in $\mathbf{p}_0$ as an example.

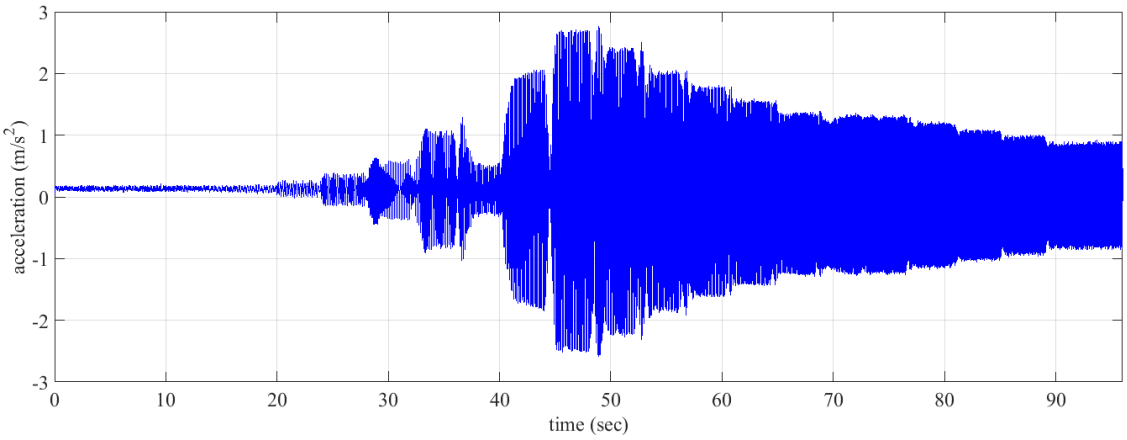

Figure 3-14: *y*-direction vibration signal at $\mathbf{p}_0$ used for Bode plotting.

3.7.2 Experiment Results

Table 3-7 provides the actual and model natural frequencies of the moving platform for zero and 5.7 kg payloads in the first experiment. The corresponding natural frequency errors are also shown in these tables. As seen in the tables and as expected, the optimal cables' tension result in maximum natural frequency or in fact maximum stiffness in the *z* direction. This is true in all the platform positions and also for different payloads.

Table 3-6: Actual and model natural frequencies for zero payloads (in Hz).

$\mathbf{p}_i$		$\mathbf{p}_0$	$\mathbf{p}_1$	$\mathbf{p}_2$	$\mathbf{p}_3$	$\mathbf{p}_4$
α^*_1	f_{model}	2.55	2.50	3.33	3.33	2.50
	f_{actual}	2.4	2.62	3.23	3.17	2.67
	$f_{\text{error (\%)}}$	+6.5	-4.5	+3.3	+5.1	-6.3
$\alpha_{1\text{mid}}$	f_{model}	2.36	2.39	3.12	3.12	2.39
	f_{actual}	2.20	2.53	3.04	3.01	2.58
	$f_{\text{error (\%)}}$	+7.3	-5.4	+2.7	+4.2	-7.1
$\alpha_{1\text{min}}$	f_{model}	2.16	2.27	2.9	2.9	2.27
	f_{actual}	1.99	2.44	2.77	2.79	2.47
	$f_{\text{error (\%)}}$	+8.6	-6.8	+4.4	+3.7	-8.2

Table 3-7: Actual and model natural frequencies for 5.7 kg payloads (in Hz).

$\mathbf{p}_i$		$\mathbf{p}_0$	$\mathbf{p}_1$	$\mathbf{p}_2$	$\mathbf{p}_3$	$\mathbf{p}_4$
α^*_1	f_{model}	2.05	1.98	2.66	2.66	1.98
	f_{actual}	1.98	2.11	2.53	2.48	2.13

	$f_{error\ (\%)}$	+3.3	-6.2	+5.2	+7.1	-6.9
α_{1mid}	f_{model}	1.89	1.9	2.51	2.51	1.9
	f_{actual}	1.78	2.07	2.41	2.36	2.05
	$f_{error\ (\%)}$	+6.6	-8.2	+4.2	+6.6	-7.3
α_{1min}	f_{model}	1.74	1.81	2.36	2.36	1.81
	f_{actual}	1.63	1.95	2.19	2.15	2.01
	$f_{error\ (\%)}$	+7.1	-7.3	+8.1	+9.7	-9.6

The accuracy of the model could also be inferred from the error in the actual and calculated natural frequency of the platform in *z* direction. The maximum error in frequency for zero and 5.7 kg payloads are 8.6 and 9.7%, respectively. Such errors considering the complexity of the experimental setup and its pulley system is acceptable. The error in the model could be reduced further by including more details of the cable collector system; however, the optimization system developed in this thesis is independent from such model improvements.

Figure 3-15 shows recorded acceleration of the platform in *z* direction at position $\mathbf{p}_0$. Taking the Fourier transform of the signal, the dominant frequency will be considered as the natural frequency of the platform in *z* direction. It is worth mentioning that the damping ratio of the illustrated vibration signal is 0.05 which results in 0.2 percent error in calculation of the moving platform natural frequency. We have similar results for the damping ratio of other selected points of workspace showing that the cables' damping can be ignored.

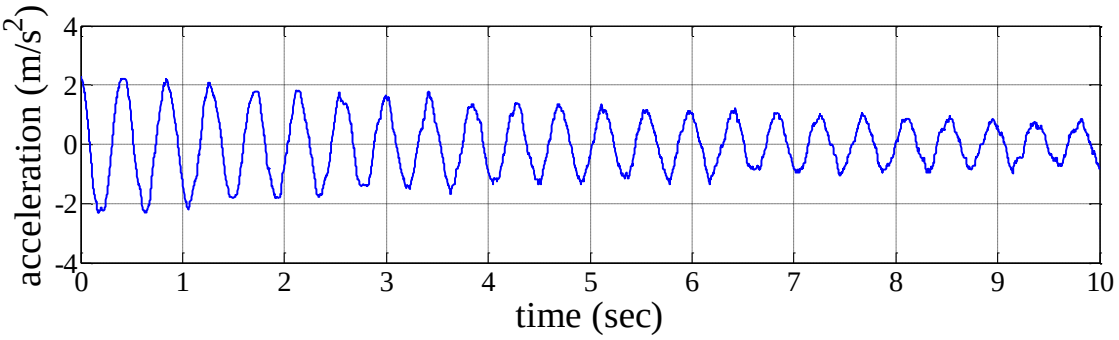

Figure 3-15: *z*-direction acceleration signal of moving platform at $\mathbf{p}_0$.

Figure 3-16 compares the rotational angular velocity of the moving platform in the second experiment. As this figures demonstrates, for the robot with only 4 constrained cables, the moving platform undesired rotational vibration is significantly considerable than the kinematically-

constrained actuated robot. Root-mean-square deviations of depicted signals are obtained as 8.02 and 0.79 which proves the considerable effects of kinematically-constrained actuation method on disturbance rejection and vibration limitation of the CDPR.

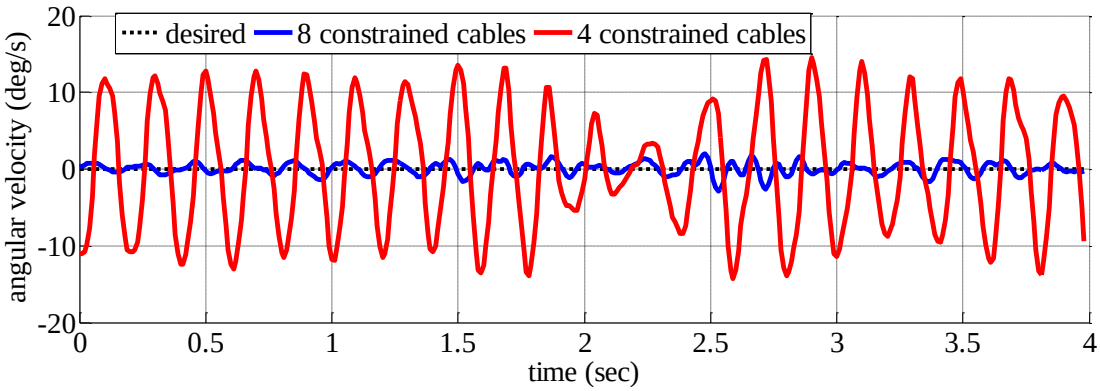

Figure 3-16: *z*-direction angular velocity in the second experiment.

Based on the recorded inputs of the reaction actuators and vibration signals of the IMU, corresponding Bode plots are obtained and used to find the natural frequency of the system in y and θ_z directions. As an example, the Bode plot of y-direction vibrations are presented in Figure 3-17. As this figure illustrates, the moving platform has a natural frequency of 9.23 Hz which is close to the first natural frequency of the model 10.02 Hz at $\mathbf{p}_0$. Similarly, natural frequency of the system has been obtained for other points and presented in Table 3-8.

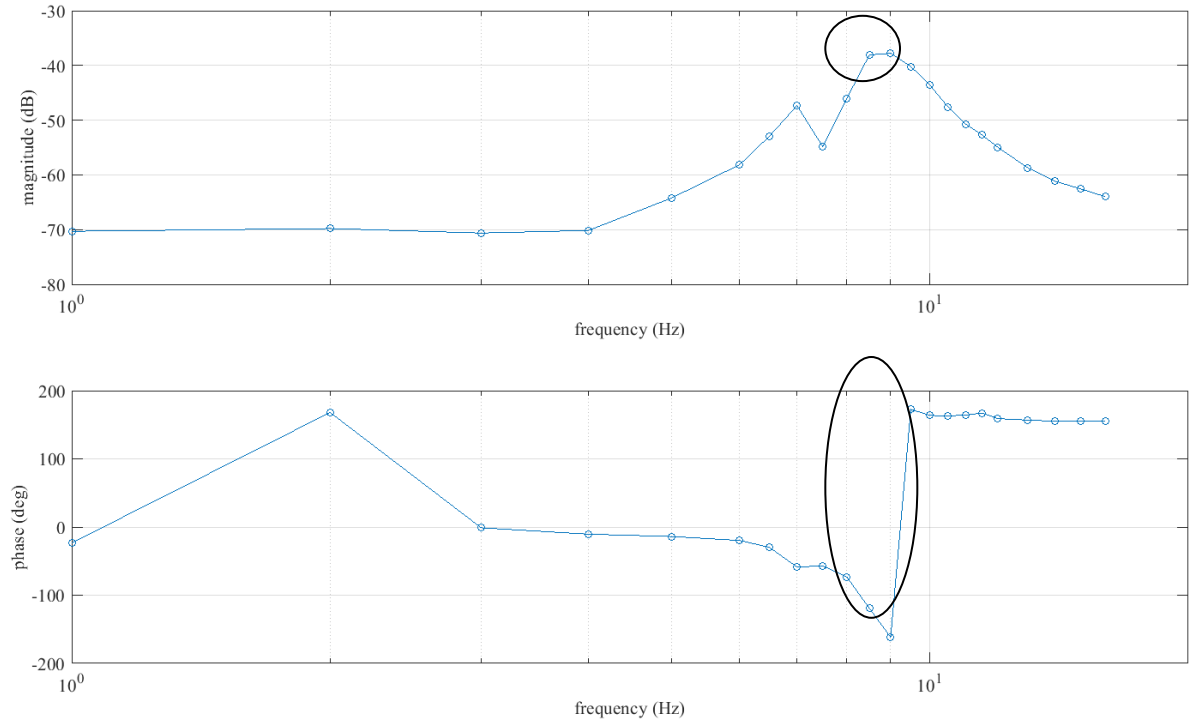

Figure 3-17: Bode plot of the platform vibrations in *y* direction.

Table 3-8: Actual and model natural frequencies for 5.7 kg payloads (in Hz).

$\mathbf{p}_i$		$\mathbf{p}_0$	$\mathbf{p}_1$	$\mathbf{p}_2$	$\mathbf{p}_3$	$\mathbf{p}_4$
x (m)		0	0.4	0.4	-0.4	-0.4
y (m)		0	-0.2	0.2	0.2	-0.2
excitation in y direction	f_{model}	10.02	12.96	6.49	6.49	12.96
	f_{actual}	9.23	11.04	7.56	7.32	10.67
	$f_{error\ (\%)}$	8.6	17.4	-14.15	-11.341	21.46
excitation in θ_z direction	f_{model}	15.32	15.08	16.65	16.65	15.08
	f_{actual}	12.68	13.26	14.22	13.87	12.98
	$f_{error\ (\%)}$	20.82	13.73	17.10	20.04	16.18

As the results of Table 3-8 demonstrate, the natural frequency of the developed model can estimate the natural frequency of the system in the planar directions with a maximum error of 21.46 percent which by considering the complexity of the experimental setup and its pulley system is acceptable.

3.8 Conclusion

A general dynamic model of the flexible redundant KC-CDPRs was developed and the effects of cables' kinematic constraints and redundant tensions on the stiffness of CDPRs were studied. By the goal of perturbation minimization, maximization of the stiffness of moving platform in a desired direction was proposed as a linear objective function to address the redundancy problem of the cables' tension. The proposed approach has been developed generally and used in modeling and stiffness maximization of a planar redundant warehousing robot as a case study. Experimental evaluation of natural frequency of the moving platform for optimized and non-optimized tensions and also different payloads has demonstrated validity of the proposed approach. Agreement between the theoretical and experimental results confirms the validity of the developed model and effectiveness of kinematically-constrained auction method in stiffness improvement of CDPRs.

Chapter 4: Robust Control Design

4.1 Introduction

In this chapter, the developed linear parametric varying (LPV) dynamic model is based for control design of CDPRs. The new dynamic model not only lets us to investigate the disturbance effects on the vibration of the moving platform in different directions along the motion but also enables us to use a wide class of well-established robust and optimal vibration control techniques for LPV systems. Accordingly, we not only benefit from minimization of the disturbance effects on the trajectory-tracking performance, but also receive an advantage form the simplicity of design and implementation of such controllers. The significance of this new approach becomes more apparent in control design of redundant KC-CDPRs. Based on the developed model, the effect of the kinematically-constrained actuation method on limiting the moving platform's undesired vibrations can be analyzed and the controller can be simplified to counteract the vibrations of platform in flexible DOFs only.

Accordingly, LPV−H∞ control design techniques are used for the development of vibration controller to optimally attenuate the effect of external disturbances on the robot's trajectory-tracking performance. Considering the effects of kinematically-constrained actuation method in eliminating the CDPRs' undesired DOFs and limiting undesired vibrations in other DOFs, the developed general approach is simplified for redundant KC-CDPRs and examined in motion control of a planar KC-CDPR. Experimental results not only confirm the effectiveness of the proposed modeling and control approach, but also demonstrate the potency of the kinematically-constrained actuation method in eliminating undesired DOFs as well as modeling and control design simplification.

The rest of this chapter is structured as follows: Section 4.2 provides the preliminary definitions and theorems which are used in the control design part. Section 4.3 develops the LPV control structure and simplifies it for redundant KC-CDPRs. Section 4.4 uses the developed approach for trajectory-tracking control of the planar warehousing KC-CDPR as a case study and presents the experimental procedures and results. Finally, Section 4.5 discusses the conclusions.

The following sections of this chapter are based on previously published works of "Kinematically-Constrained Redundant Cable-Driven Parallel Robots: Modeling, Redundancy Analysis, and Stiffness Optimization, IEEE/ASME Transactions on Mechatronics, 2017" [116] and "Vibration Decoupled Modeling and Robust Control of Redundant Cable-Driven Parallel Robots IEEE/ASME Transactions

on Mechatronics, 2018" [117] by "Hamed Jamshidifar et al." and are reproduced with permission, from IEEE. Accordingly, the copyright of the following sections is owned by IEEE. This thesis author specific contribution to these paper is to: "prepare all the graphics and results, prepare the final manuscript. These papers are co-authored by Dr. Amir Khajepour and Dr. Baris Fidan as supervisors. Also, Mitch Rushton, in assisting with experimental setup and testing, and Saeid Khosravani, in control design analysis. In reference to IEEE copyrighted material which is used with permission in this thesis, the IEEE does not endorse any of university/educational entity's name goes here's products or services. Internal or personal use of this material is permitted.

4.2 Preliminaries

Before presenting the control design approach for CDPRs and KC-CDPRs, some basic definitions and theorems are provided in this section. It is worth mentioning that this section has been written based on the reference book [120]. Accordingly, some of the proofs are not provided in this chapter and referred to [120].

Definition 4.1: A linear dynamic system whose mathematical description is not varying by time is named linear-time-invariant (LTI).

Theorem 4.1: The *n*-dimensional LTI system

$$\begin{aligned} &\dot{\mathbf{x}}(t) = \mathbf{A}\dot{\mathbf{x}}(t), t \geq 0 \\ &\mathbf{x}(0) = \mathbf{x}_0, \end{aligned} \tag{4-1}$$

where $\mathbf{A}$ is a constant matrix, t denotes time, $\mathbf{x}$ denotes the vector of states and $\mathbf{x}_0$ is the initial conditions of the states, is globally asymptotically stable if there exist a positive definite matrix $\mathbf{P}$ such that the Lyapunov inequality

$$\mathbf{A}^T\mathbf{P} + \mathbf{P}\mathbf{A} < 0 \tag{4-2}$$

holds.

Proof: Consider the positive Lyapunov function

$$V = \mathbf{x}^T\mathbf{P}\mathbf{x} \tag{4-3}$$

with the time derivative of

$$\dot{V} = \dot{\mathbf{x}}^T\mathbf{P}\mathbf{x} + \mathbf{x}^T\mathbf{P}\dot{\mathbf{x}} \tag{4-4}$$

where replacing from (4-2) gives

$$\dot{V} = \mathbf{x}^T(\mathbf{A}^T\mathbf{P} + \mathbf{P}\mathbf{A})\mathbf{x} \tag{4-5}$$

which is negative unless at $\mathbf{x}$=0 which based on the Lyapunov theorem means global asymptotic stability of the system (4-1)■.

Definition 4.2: A linear dynamic system whose mathematical description is a function of varying parameters, where the parameters are bounded and their values are in a known set, is named linear-parameter-varying (LPV). The known set is usually considered as a compact and convex polytope.

A LPV system can be written in the general form of

$$\begin{aligned}&\dot{\mathbf{x}}(t)=\mathbf{A}(\boldsymbol{\rho}(t))\mathbf{x}(t)+\mathbf{E}(\boldsymbol{\rho}(t))\mathbf{w}_e(t),\ t\geq 0,\\&\mathbf{z}(t)=\mathbf{C}(\boldsymbol{\rho}(t))\mathbf{x}(t)+\mathbf{F}(\boldsymbol{\rho}(t))\mathbf{w}_e(t),\\&\mathbf{x}(0)=\mathbf{x}_0\end{aligned} \tag{4-6}$$

where $\boldsymbol{\rho}$ denotes the vector of varying parameters, $\mathbf{w}_e$ denotes the external disturbance and $\mathbf{z}$ is the output of the system.

Definition 4.3: The LPV system

$$\begin{aligned}&\dot{\mathbf{x}}(t)=\mathbf{A}(\boldsymbol{\rho}(t))\mathbf{x}(t),\ t\geq 0,\\&\mathbf{x}(0)=\mathbf{x}_0\end{aligned} \tag{4-7}$$

is said to be quadratically stable if the positive definite quadratic form

$$V(\mathbf{x})=\mathbf{x}^T\mathbf{P}_0\mathbf{x},\mathbf{P}_0>0 \tag{4-8}$$

is a Lyapanouv funtion for (4-7). V in (4-8) is often refered to as common Lyapunov function or parametric-independent Lyapanouv function.

Definition 4.4: The LPV system is said to be robustly stable if the positive definitie quadratic form

$$V(\mathbf{x},\boldsymbol{\rho})=\mathbf{x}^T\mathbf{P}(\boldsymbol{\rho})\mathbf{x},\mathbf{P}(\boldsymbol{\rho})>0 \tag{4-9}$$

is a Lyapunov function for it, where V in this case is often referred to as a parameter-dependent Lyapunov function.

Proposition 4.1: Consider the time-varying parameter vector $\boldsymbol{\rho}$ and assume the system is robustly stable, then the spectrum of $\mathbf{A}(\boldsymbol{\rho})$ is bounded away from the imaginary axis for all $\boldsymbol{\rho}$. Moreover, the faster the parameters are, the farther the eigenvalues from imaginary axis.

Proof: Differentiating the Lyapunov function (4-9), we have

$$\dot{V}=\mathbf{x}^T\left[\mathbf{A}(\boldsymbol{\rho})^T\mathbf{P}(\boldsymbol{\rho})+\mathbf{P}(\boldsymbol{\rho})\mathbf{A}(\boldsymbol{\rho})+\sum_{i=1}^{N}\dot{\rho}_i\frac{\partial\mathbf{P}(\boldsymbol{\rho})}{\partial\rho_i}\right]\mathbf{x} \tag{4-10}$$

where $\boldsymbol{\rho}$ and $\dot{\boldsymbol{\rho}}$ are bounded and in two known sets. Having the robust stability conditions for the system means there exists $\mathbf{P}(\boldsymbol{\rho})$ such that, above expression, is negative for all $\boldsymbol{\rho}$ and $\dot{\boldsymbol{\rho}}$. Let us denote the eigenvector associated with eigenvalue $\eta_i(\boldsymbol{\rho})$ of $\mathbf{A}(\boldsymbol{\rho})$ by $\boldsymbol{\eta}_i(\boldsymbol{\rho})$, then we have

$$\boldsymbol{\eta}_i(\boldsymbol{\rho})^T \left[\mathbf{A}(\boldsymbol{\rho})^T \mathbf{P}(\boldsymbol{\rho}) + \mathbf{P}(\boldsymbol{\rho})\mathbf{A}(\boldsymbol{\rho}) + \sum_{k=1}^{N} \dot{\rho}_k \frac{\partial \mathbf{P}(\boldsymbol{\rho})}{\partial \rho_k} \right] \boldsymbol{\eta}_i(\boldsymbol{\rho}) < 0 \tag{4-11}$$

for all $\boldsymbol{\rho}$ and $\dot{\boldsymbol{\rho}}$ which implies

$$\text{real}(\eta_{\text{i}}(\boldsymbol{\rho})) < -\sum_{\text{i}=1}^{\text{N}} \dot{\rho}_{\text{k}} \frac{\boldsymbol{\eta}_{\text{i}}(\boldsymbol{\rho})^{\text{T}} \frac{\partial \mathbf{P}(\boldsymbol{\rho})}{\partial \rho_{\text{k}}} \boldsymbol{\eta}_{\text{i}}(\boldsymbol{\rho})}{2\boldsymbol{\eta}_{\text{i}}(\boldsymbol{\rho})^{\text{T}} \mathbf{P}(\boldsymbol{\rho}) \boldsymbol{\eta}_{\text{i}}(\boldsymbol{\rho})} . \tag{4-12}$$

Since $\boldsymbol{\eta}_i(\boldsymbol{\rho})^T \mathbf{P}(\boldsymbol{\rho})\boldsymbol{\eta}_i(\boldsymbol{\rho}) > 0$ and $\boldsymbol{\eta}_i(\boldsymbol{\rho})^T \frac{\partial \mathbf{P}(\boldsymbol{\rho})}{\partial \rho_k} \boldsymbol{\eta}_i(\boldsymbol{\rho})$ can be both negative and positive over time, therefore, for all values of $\boldsymbol{\rho}$ and $\dot{\boldsymbol{\rho}}$ the real part of η_i needs to be negative and according to (4-12), the faster the parameters are the father eigenvalues from the imaginary axis ■.

Defnition 4: consider the mapping $\varsigma : \mathbb{R}_{\geq 0} \to \mathbb{C}^n$, then the L_2-norm of ς is defined as

$$\|\varsigma\|_{L_2} = \sqrt{\int_0^\infty \varsigma(s)^T \varsigma(s) ds} . \tag{4-13}$$

The space of signals mapping $\mathbb{R}_{\geq 0}$ to $\mathbb{C}^n$ with finite L_2-norm is denoted by $L_2(\mathbb{R}_{\geq 0}, \mathbb{C}^n)$ which for simplicity is denoted by L_2.

Definition 4.5: Consider Π as a bounded operator from L_2 to L_2. The L_2-gain of Π is defined as

$$\|\Pi\|_{L_2 - L_2} = \sup_{\|\varsigma\|_{L_2}=1} \left\{ \|\Pi\varsigma\|_{L_2} \right\} . \tag{4-14}$$

Definition 4.6: The H_∞-norm of transfer function **G** is defined by

$$\|\mathbf{G}\|_{H_\infty} = \sup_{\varpi \in \mathbb{R}} \bar{\sigma}\{\mathbf{G}(s)\}, s = j\varpi . \tag{4-15}$$

where $\bar{\sigma}(.)$ denotes the maximum singular value of **G**.

Lemma 4.1 (Bounded-Real Lemma): Consider the LTI sytem

$$\begin{aligned} \dot{\mathbf{x}} &= \mathbf{A}\mathbf{x} + \mathbf{B}\mathbf{u}, \\ \mathbf{z} &= \mathbf{C}\mathbf{x} + \mathbf{D}\mathbf{u} \end{aligned} \tag{4-16}$$

and the transfer function

$$\mathbf{G}(s) = \mathbf{C}(s\mathbf{I} - \mathbf{A})^{-1}\mathbf{B} + \mathbf{D} \tag{4-17}$$

between **u** and **z**, then, the following statements are equivalent:

1- The H_∞-norm of **G** is smaller than $\gamma > 0$.
2- There exists a positive definite matrix **P** such that the LMI

$$\begin{bmatrix} \mathbf{A}^T\mathbf{P}+\mathbf{PA} & \mathbf{PB} & \mathbf{C} \\ * & -\gamma\mathbf{I} & \mathbf{D}^T \\ * & * & -\gamma\mathbf{I} \end{bmatrix} < 0 \tag{4-18}$$

holds, where * stand for the transpose of symmetric entries.

Proof: Proof of Lemma 4.1 is provided in [120].

4.3 Control Design

4.3.1 LPV Gain-Scheduling Robust Control Design

Tools for analyzing the LPV systems gain-scheduling control approach are inherited from robust control theory where the main difference between the common robust control design and the LPV robust control design is based on the knowledge of us from the system. In the robust control design some parameters of the system are unknown and our knowledge is usually limited to their upper and lower bounds, where in the LPV framework those parameters are assumed to be known or measurable. Therefore, the parameters can be used in the control law to improve the performance of the controller. Accordingly, considering the LVP system

$$\begin{aligned} \dot{\mathbf{x}}(t) &= \mathbf{A}(\boldsymbol{\rho}(t))\mathbf{x}(t) + \mathbf{B}(\boldsymbol{\rho}(t))\mathbf{u}, \\ \mathbf{z}(t) &= \mathbf{C}(\boldsymbol{\rho}(t))\mathbf{x} \end{aligned} \tag{4-19}$$

the gain scheduled control law can be considered as

$$u(t) = \mathbf{K}_G(\boldsymbol{\rho}(t))\mathbf{x}(t) \tag{4-20}$$

where the controller gain matrix $\mathbf{K}_G$ is a function of parameters. Considering the generic parameter dependent LPV system

$$\begin{aligned} \dot{\mathbf{x}}(t) &= \mathbf{A}(\boldsymbol{\rho}(t))\mathbf{x}(t) + \mathbf{B}(\boldsymbol{\rho}(t))\mathbf{u} + \mathbf{E}(\boldsymbol{\rho}(t))\mathbf{w}_e, \\ \mathbf{z}(t) &= \mathbf{C}(\boldsymbol{\rho}(t))\mathbf{x} + \mathbf{D}(\boldsymbol{\rho}(t))\mathbf{u} + \mathbf{F}(\boldsymbol{\rho}(t))\mathbf{w}_e \end{aligned} \tag{4-21}$$

we have the following theorem for the robust stabilization of the system using gain scheduled state feedback. It is worth mentioning that Theorem 4.1 is the same as Theorem 3.3.6 in [120] where the proof is provide based on [120].

Theorem 4.2: The LPV system (4-21), with the control law $\mathbf{u}(t)=\mathbf{K}_G(\boldsymbol{\rho}(t))\mathbf{x}(t)$ is robustly stabilizable if there exists a differentiable positive definite matrix function $\boldsymbol{\Gamma}(\boldsymbol{\rho}(t))$, a matrix function $\boldsymbol{\Psi}(\boldsymbol{\rho}(t))$, and positive scalar γ such that the linear matrix inequality (LMI)

$$\begin{bmatrix} \boldsymbol{\Xi}(\boldsymbol{\rho},\mathbf{v}) & \mathbf{E}(\boldsymbol{\rho}) & \left[\mathbf{C}(\boldsymbol{\rho})\boldsymbol{\Gamma}(\boldsymbol{\rho})+D(\boldsymbol{\rho})\boldsymbol{\Gamma}(\boldsymbol{\rho})\right]^T \\ * & -\gamma\mathbf{I} & F(\boldsymbol{\rho})^T \\ * & * & -\gamma\mathbf{I} \end{bmatrix} < 0 \tag{4-22}$$

holds for all admissible $\boldsymbol{\rho}$ and $\left|\dot{\rho}_i\right| \le v_i$ where

$$\mathbf{K}_g(\boldsymbol{\rho})=\boldsymbol{\Psi}(\boldsymbol{\rho})\boldsymbol{\Gamma}(\boldsymbol{\rho})^{-1}, \boldsymbol{\Xi}=\mathbf{A}(\boldsymbol{\rho})\boldsymbol{\Gamma}(\boldsymbol{\rho})+\boldsymbol{\Gamma}^T(\boldsymbol{\rho})\mathbf{A}^T(\boldsymbol{\rho})+\mathbf{B}\boldsymbol{\Psi}(\boldsymbol{\rho})+\boldsymbol{\Psi}^T(\boldsymbol{\rho})\mathbf{B}^T-\sum_{i=1}^{N} v_i \frac{\partial\boldsymbol{\Gamma}(\boldsymbol{\rho})}{\partial\rho_i}, \tag{4-23}$$

v_i is the maximum variation rate of ρ_i and $*$ stands for the transpose of symmetric entries. Moreover, the L_2-gain of the transfer $\mathbf{w}_e \rightarrow \mathbf{z}$ of the closed-loop system is less than γ.

Proof: Considering the control law $\mathbf{u}(t)=\mathbf{K}_G(\boldsymbol{\rho}(t))\mathbf{x}(t)$, the closed-loop LPV system is obtained as

$$\begin{aligned} \dot{\mathbf{x}} &= (\mathbf{A}(\boldsymbol{\rho})+\mathbf{B}(\boldsymbol{\rho})\mathbf{K}_G(\boldsymbol{\rho}))\mathbf{x}+\mathbf{E}(\boldsymbol{\rho})\mathbf{w}_e, \\ \mathbf{z} &= (\mathbf{C}(\boldsymbol{\rho})+\mathbf{D}(\boldsymbol{\rho})\mathbf{K}_G(\boldsymbol{\rho}))\mathbf{x}+\mathbf{F}(\boldsymbol{\rho})\mathbf{w}_e \end{aligned} \tag{4-24}$$

which by substituting in Lemma 4.1, gives

$$\begin{bmatrix} \Upsilon(\boldsymbol{\rho})+\partial\mathbf{P}(\boldsymbol{\rho}) & \mathbf{P}(\boldsymbol{\rho})\mathbf{E}(\boldsymbol{\rho}) & \left[\mathbf{C}(\boldsymbol{\rho})+D(\boldsymbol{\rho})\mathbf{K}_G(\boldsymbol{\rho})\right]^T \\ * & -\gamma\mathbf{I} & F(\boldsymbol{\rho})^T \\ * & * & -\gamma\mathbf{I} \end{bmatrix} < 0 \tag{4-25}$$

where $\Upsilon(\boldsymbol{\rho})=\mathrm{He}[\mathbf{P}(\boldsymbol{\rho})\mathbf{A}(\boldsymbol{\rho})+\mathbf{P}(\boldsymbol{\rho})\mathbf{B}(\boldsymbol{\rho})\mathbf{K}_G(\boldsymbol{\rho})]$, $\partial\mathbf{P}(\boldsymbol{\rho})=\sum_{i=1}^{N} v_i \frac{\partial\boldsymbol{\Gamma}(\boldsymbol{\rho})}{\partial\rho_i}$. Using the fact that for a nonsingular and differentiable matrix Q(t), we have

$$Q^{-1}(t)\frac{dQ(t)}{dt}Q^{-1}(t)=-\frac{d}{dt}[Q^{-1}(t)] \tag{4-26}$$

and by performing a conjugate transformation with $diag(\boldsymbol{\Gamma}(\boldsymbol{\rho}), \mathbf{I}, \mathbf{I})$, one can get to $\boldsymbol{\Psi}(\boldsymbol{\rho})= \mathbf{K}_G(\boldsymbol{\rho})\boldsymbol{\Gamma}(\boldsymbol{\rho})$ where $\boldsymbol{\Gamma}(\boldsymbol{\rho})=\mathbf{P}^{-1}(\boldsymbol{\rho})$ ■.

4.3.2 Control Design for Commonly-Actuated CDPRs

Based on the developed LPV model in Chapter 3, by providing $\bar{\mathbf{x}}$ and $\bar{\boldsymbol{\tau}}$, $\mathbf{K}$ is resulted as a function of them which is time-varying but available for measurement. Hence, (3-17) can be considered as a

linear parametric varying (LPV) dynamic system that can be transformed to the standard state-space form

$$\begin{aligned}
&\dot{\mathbf{x}}_{\delta s}(t) = \mathbf{A}(\boldsymbol{\rho}(t))\mathbf{x}_{\delta s}(t) + \mathbf{B}\mathbf{u}_{\delta s}(t) + \mathbf{E}\boldsymbol{\omega}_e(t),\\
&\mathbf{z}_{\delta s} = \mathbf{C}\mathbf{x}_{\delta s}(t),\\
&\mathbf{A} = \begin{bmatrix} 0 & \mathbf{I} \\ -\mathbf{M}^{-1}\mathbf{K} & -\mathbf{M}^{-1}\mathbf{Q} \end{bmatrix}, \mathbf{B} = \mathbf{E} = \begin{bmatrix} 0 \\ \mathbf{I} \end{bmatrix}, \mathbf{C} = \mathbf{I},\\
&\mathbf{u}_{\delta s} = -\mathbf{M}^{-1}\mathbf{u}_{\delta}, \boldsymbol{\omega}_e(t) = -\mathbf{M}^{-1}\mathbf{w}_e,
\end{aligned} \tag{4-27}$$

where $\mathbf{x}_{\delta s} = [\mathbf{x}_{\delta}^T, \dot{\mathbf{x}}_{\delta}^T]^T$ is the state vector of system, $\mathbf{z}_{\delta s}$ denotes the system output, $\boldsymbol{\omega}_e$ is the external disturbance vector and $\boldsymbol{\rho}$ is an N-dimensional vector which includes all the variable entries of $\mathbf{A}$. It is worth mentioning that in the developed formulation, the control action $\mathbf{u}_{\delta}$ is considered to be provided by all cables of the redundant CDPR, where $\mathbf{u}_{\delta}$ can be provided by a smaller number of cables as long as the controllability of the system is held. Consequently, we can have a simpler control structure which can be implemented more easily. This idea has been used in control design of KC-CDPRs which is discussed in the following.

To control an LPV system, various approaches have been proposed in the literature, see [120], [121] and the references therein. In classical gain-scheduling controller design, one needs to design several linear time invariant (LTI) controllers for fixed values of scheduling parameters. The salient disadvantage is that guarantying the stability of the switching LTI controllers is not easy and also the parameters' rate of changes is not included in the design. Alternatively, using the LPV framework, stability of the system and effect of the parameters' rate of variation can be analyzed systematically [122]. The theorem below, which is similar to Theorem 4.2, provides a method to design a robust controller for system (4-27).

Theorem 4.3: Consider the LPV system (4-27) and small arbitrary positive constants ε_1 and ε_2. If there exist a differentiable positive definite matrix function $\boldsymbol{\Gamma}(\boldsymbol{\rho}(t))$, a matrix function $\boldsymbol{\Psi}(\boldsymbol{\rho}(t))$, and positive scalar γ such that the linear matrix inequality (LMI)

$$\begin{bmatrix} \mathbf{\Xi} & \mathbf{E} & \mathbf{\Gamma}^T\mathbf{C}^T \\ * & -\gamma\mathbf{I} & 0 \\ * & * & -\gamma\mathbf{I} \end{bmatrix} < -\varepsilon_1\mathbf{I}, \mathbf{\Gamma} > \varepsilon_2\mathbf{I} \tag{4-28}$$

holds for all admissible $\boldsymbol{\rho}$ and $|\dot{\rho}_i| \le v_i$ where

$$\mathbf{\Xi} = \mathbf{A}(\boldsymbol{\rho})\mathbf{\Gamma}(\boldsymbol{\rho}) + \mathbf{\Gamma}^T(\boldsymbol{\rho})\mathbf{A}^T(\boldsymbol{\rho}) + \mathbf{B}\mathbf{\Psi}(\boldsymbol{\rho}) + \mathbf{\Psi}^T(\boldsymbol{\rho})\mathbf{B}^T - \sum_{i=1}^{N} v_i \frac{\partial \mathbf{\Gamma}(\boldsymbol{\rho})}{\partial \rho_i} \tag{4-29}$$

v_i is the maximum variation rate of ρ_i and $*$ stands for the transpose of symmetric entries, then:

(i) The LPV system (4-27) is robustly stabilizable by the control law

$$\mathbf{u}_{\delta s}(t) = \mathbf{K}_G(\boldsymbol{\rho}(t))\mathbf{x}_{\delta s},$$
$$\mathbf{K}_{\delta s}(\boldsymbol{\rho}) = \mathbf{\Psi}(\boldsymbol{\rho})\mathbf{\Gamma}(\boldsymbol{\rho})^{-1} \tag{4-30}$$

(ii) The controller (4-30) guarantees that the L_2-gain of the transfer function from $\boldsymbol{\omega}_e$ to $\mathbf{z}_{\delta s}$ in the closed loop system is less than the positive scalar γ.

Proof: Using Lemma 4.1 one can write the following inequality for the closed loop system

$$\begin{bmatrix} \mathbf{\Xi}' & \mathbf{PE} & \mathbf{C}^T \\ * & -\gamma\mathbf{I} & 0 \\ * & * & -\gamma\mathbf{I} \end{bmatrix} < 0 \tag{4-31}$$

where

$$\mathbf{\Xi}' = \mathbf{P}(\boldsymbol{\rho})\mathbf{A}(\boldsymbol{\rho}) + \mathbf{A}^T(\boldsymbol{\rho})\mathbf{P}^T(\boldsymbol{\rho}) + \mathbf{P}(\boldsymbol{\rho})\mathbf{B}(\boldsymbol{\rho})\mathbf{K}_G(\boldsymbol{\rho}) + \mathbf{K}_G^T(\boldsymbol{\rho})\mathbf{B}^T(\boldsymbol{\rho})\mathbf{P}^T(\boldsymbol{\rho}) + \sum_{i=1}^{N} v_i \frac{\partial \mathbf{P}(\boldsymbol{\rho})}{\partial \rho_i}. \tag{4-32}$$

Applying a congruence transformation with *diag*($\mathbf{\Gamma}(\boldsymbol{\rho})$, **I**, **I**), one get to $\mathbf{\Psi}(\boldsymbol{\rho})=\mathbf{K}_G(\boldsymbol{\rho})\mathbf{\Gamma}(\boldsymbol{\rho})$ where $\mathbf{\Gamma}(\boldsymbol{\rho})=\mathbf{P}^{-1}(\boldsymbol{\rho})$. Theorem 4.3 is a special case of Theorem 4.2. Hence, the result directly follows ■.

Remark.1: It is well known that LMIs are not strictly convex and different solvers may result in different gains, however, corresponding attenuation levels of γ will be quite close. Given that the minimization is to seek an infimum for γ, some solvers can lead to extremely large values for the design matrices. To address this issue, the LMI

$$\begin{bmatrix} \xi_3 \begin{bmatrix} \xi_1 & 0 \\ 0 & \xi_2 \end{bmatrix} & \mathbf{\Psi}^T \\ * & \xi_3\mathbf{I} \end{bmatrix} > \varepsilon_3\mathbf{I} \tag{4-33}$$

is considered to restrict the size of matrix $\mathbf{\Psi}$ to constrain the gains of the controller, where ε_3 is a small arbitrary positive constant and the positive scalars of ξ_1, ξ_2 and ξ_3 are free variables to shape the

controller gains properly [123]. This method is effective in practice; however, it adds another constraint in the admissible set of which makes the analysis more conservative. Another method to avoid the numerical difficulty is revising the objective function to make the solver to minimize $(\gamma+\varepsilon_0 \text{trace}(\boldsymbol{\Psi}(\boldsymbol{\rho}_m)\boldsymbol{\Psi}(\boldsymbol{\rho}_m)^T))$ where ε_0 is a positive scalar and $\boldsymbol{\rho}_m$ is the average value vector of the scheduling parameters. It is worth mentioning that the number of gridding points to solve the resulted LMIs depends on the convergence of defined constants in $\boldsymbol{\Psi}(\boldsymbol{\rho})$ and $\boldsymbol{\Gamma}(\boldsymbol{\rho})$ as well as the variation of γ. Accordingly, in order to solve each LMI, the number of gridding points is increased gradually to have an acceptable convergence for the defined constants where we have a small variation in γ. Based on Theorem 4.3 and Remark.1, we propose use of the control law (4-30), where $\boldsymbol{\Psi}$ is selected to satisfy the LMIs (4-28) and (4-33), for motion control of CDPRs. Block diagram of the proposed LPV control scheme is shown in Figure 4-1.

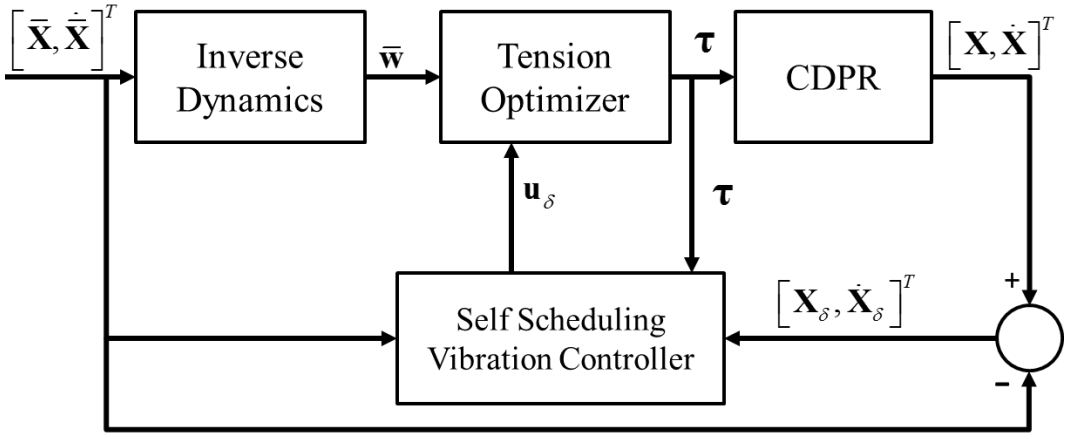

Figure 4-1: Control block diagram of the LPV control scheme for redundant CDPRs.

4.3.3 Control Re-Design for KC-CDPRs

By proper arrangement of enough number of constraint cables in KC-CDPRs, the platform's undesired DOFs can be highly restricted such that we can assume that the platforms vibration in some DOFs are negligible. By removing the less vibrating coordinates, the control structure can be simplified. Accordingly, instead of using all cables to provide the control signal $\boldsymbol{\tau}_\delta$, holding the controllability conditions, we use enough number of cables in control design of KC-CDPRs. Based on the proposed approach, the overall control block diagram of KC-CDPRs is resulted as shown in Figure 4-2.

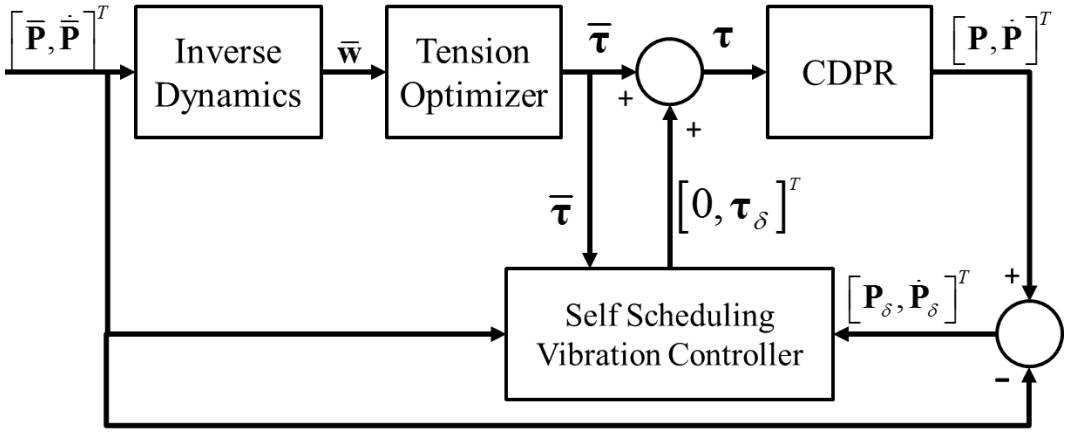

Figure 4-2: Block diagram of the re-designed control scheme for KC-CDPRs.

It is worth to mention that it is simpler to apply $\boldsymbol{\tau}_\delta$ using the single-cable actuators. Accordingly, to implement the controller command $\boldsymbol{\tau}$, the non-stretched length of multiple cables are found based on their nominal tensions and controlled by their spool system and the tension of vibration controller cables is controlled by their actuators.

4.4 Real-Time Implementation on the Warehousing Robot

To show the details of proposed modeling and control approach and demonstrate its effectiveness, the planar KC-CDPR is studied.

4.4.1 Planar KC-CDPR Stiffness Analysis

In order to give an insight into the effects of kinematically-constrained actuation method on the stiffness of the moving platform, a numerical stiffness analysis is provided in this section. Considering static equilibrium conditions, the stiffness of the platform are compared for two cases of KC-CDPR and the commonly actuated CDPR of Figure 4-3 over a workspace of $-1\text{m} \leq x \leq +1\text{m}$ and $-0.4\text{m} \leq y \leq +0.4\text{m}$. Table 4-1 compares the platform's stiffness in all directions.

Table 4-1: Comparison of directional stiffness in the planar CDPR and KC-CDPR.

Commonly Actuated CDPR Directional Stiffness			
Stiffness	Average	minimum	maximum
k_x	142 kN/m	60.7 kN/m	316.3 kN/m
k_y	35.1 kN/m	3.0 kN/m	109.8 kN/m
k_z	1.33 kN/m	0.6 kN/m	2.6 kN/m
$k_{\theta x}$	1.87 Nm	0.27 Nm	5.2 Nm
$k_{\theta y}$	230.7 Nm	144.3 Nm	519.0 Nm
$k_{\theta z}$	436.2 Nm	169.8 Nm	100.4 Nm
KC-CDPR Directional Stiffness			
Stiffness	Average	minimum	maximum
k_x	561.2 kN/m	239.5 kN/m	1223 kN/m
k_y	135 kN/m	4.1 kN/m	431.6 kN/m
k_z	2.5 kN/m	1.46 kN/m	3.94 kN/m
$k_{\theta x}$	163 Nm	21.92 Nm	343.9 Nm
$k_{\theta y}$	1543 Nm	839 Nm	2127 Nm
$k_{\theta z}$	5318 Nm	2095 Nm	11849 Nm
KC-CDPR Directional Stiffness Ratio			
Stiffness	Average	minimum	maximum
k_x	3.9	3.9	3.9
k_y	3.9	1.4	3.9
k_z	1.9	2.4	1.5
$k_{\theta x}$	87.2	81.2	66.1
$k_{\theta y}$	6.7	5.8	4.1
$k_{\theta z}$	12.2	12.3	118.5

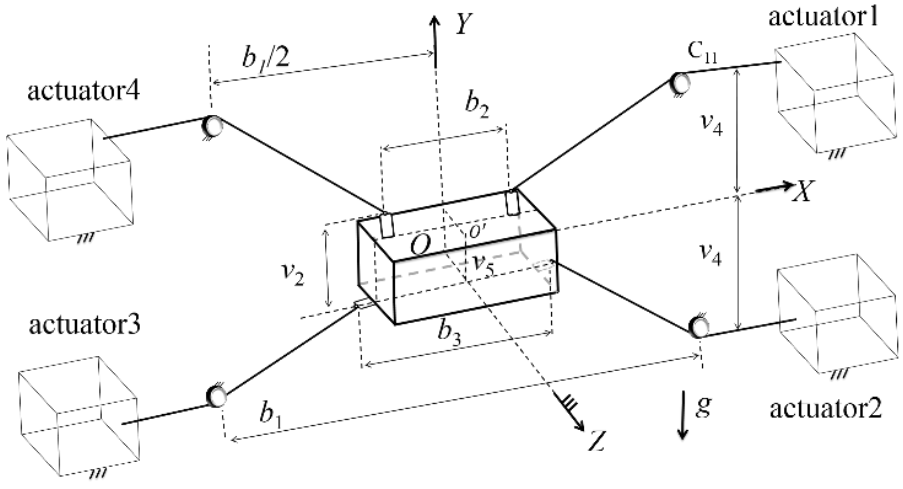

Figure 4-3: Configuration of the warehousing CDPR with common arrangment of cables and no series elastic actuator.

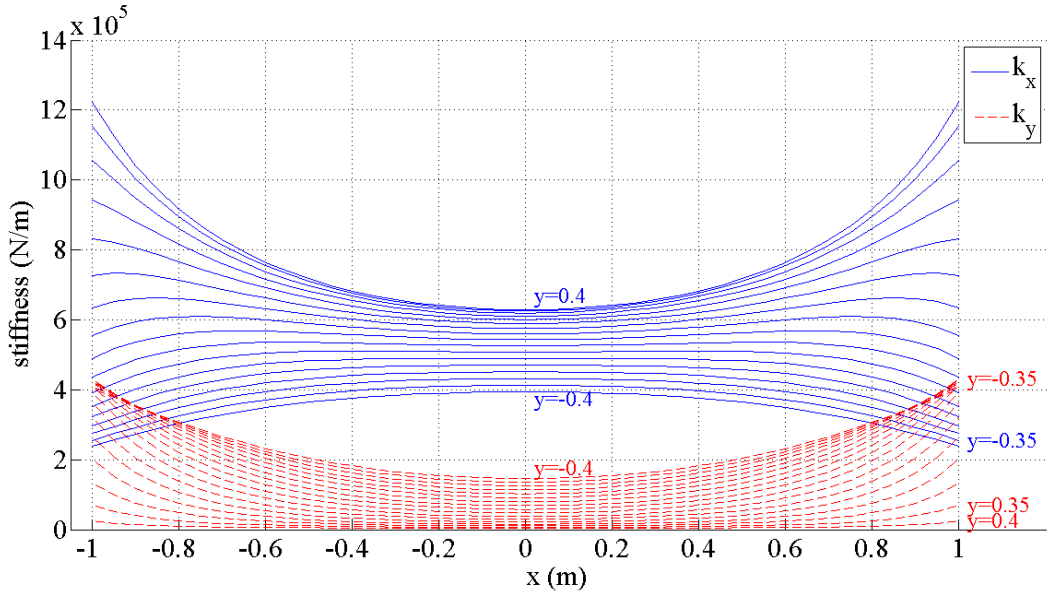

Figure 4-4: Comparison of k_y and k_x over the workspace.

As the results of Table 4-1 demonstrate, by adding two cables on each one of the top actuators, the moving platform's stiffness in both θ_z and x directions have been increased considerably. Comparing the corresponding values, we have 290% and 1220% increment in the average value of k_x and $k_{\theta z}$ and 290% and 1230% improvement in the minimum values of k_x and $k_{\theta z}$, respectively. However, because of the vertical alignment of the top cables in the middle of the workspace, especially in the top-middle points of the workspace, we have a small stiffness improvement in this direction. Moreover, by comparing k_x and k_y values in the KC-CDPR, as illustrated in Figure 4-4, we can see for a large portion of the workspace, as selected in Figure 4-5 and illustrated in Figure 4-6, k_y has very small values.

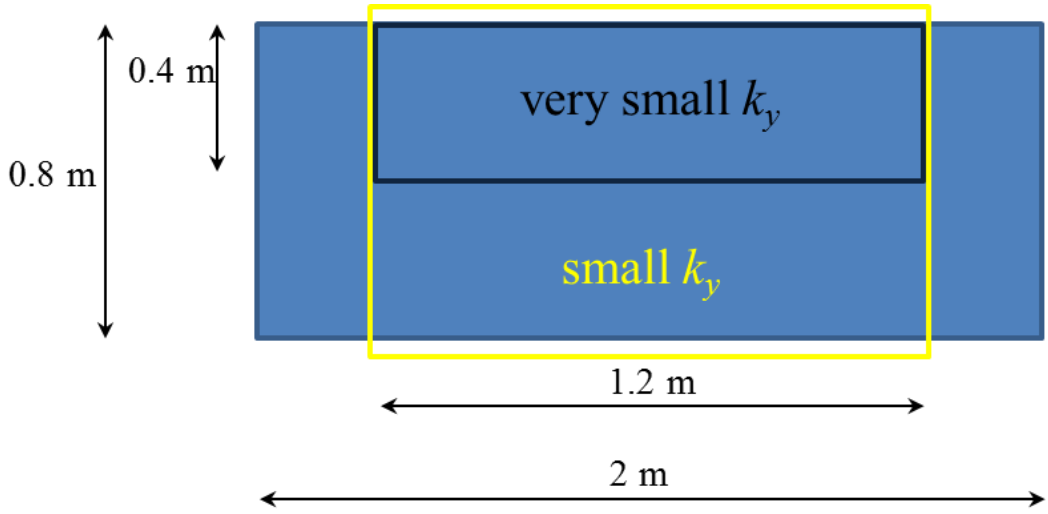

Figure 4-5: Selected parts of the workspace with small values for k_y.

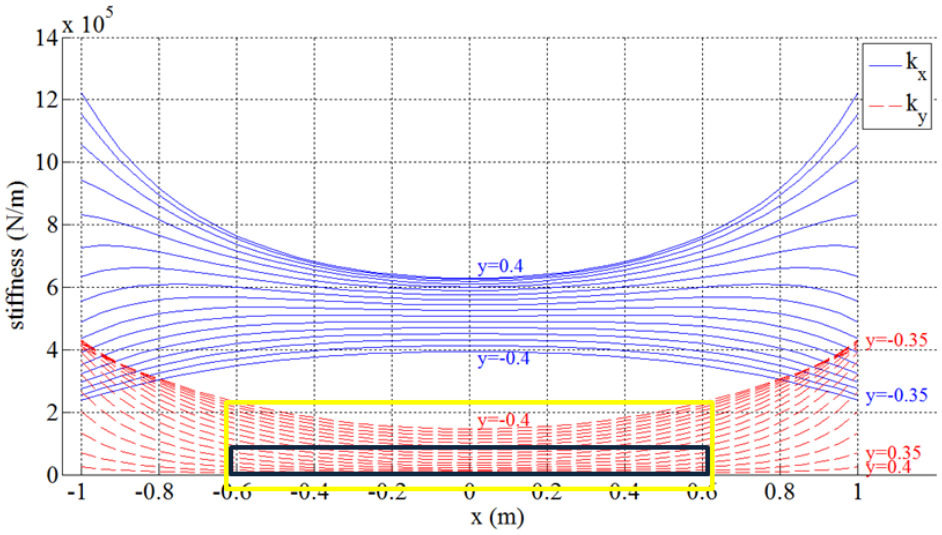

Figure 4-6: Corresponding k_y values for the selected parts of the workspace.

It can be shown that by adding the number of cables we can increase k_x and $k_{\theta z}$ even more to reach a desired level, however, k_y still remains low. Accordingly, the moving platform flexibility in x and θ_z directions can be neglected. Therefore, the vibration equation of the moving platform is considered as

$$m_{\text{mp}}\ddot{y}_{\delta} + k_y y_{\delta} = u_{\delta y} \tag{4-34}$$

where m_{mp} and k_y denote the mass and stiffness of moving platform and $u_{\delta y}$ is the required control action provided by the bottom cables. Rewriting (4-34) in the state-space form, we obtain

$$\dot{\mathbf{x}}_{\delta s}(t) = \mathbf{A}(\boldsymbol{\rho}(t))\mathbf{x}_{\delta s}(t) + \mathbf{B}\mathbf{u}_{\delta s}(t) + \mathbf{E}\omega_e(t),$$
$$\mathbf{z}_{\delta s} = \mathbf{x}_{\delta s}(t), \mathbf{A} = \begin{bmatrix} 0 & 1 \\ -\rho & 0 \end{bmatrix}, \mathbf{B} = \mathbf{E} = \begin{bmatrix} 0 \\ 1 \end{bmatrix}, \tag{4-35}$$

where $\mathbf{x}_{\delta s} = [y_\delta, \dot{y}_\delta]^T$ denotes the position and the velocity, $\mathbf{z}_{\delta s}$ is the system output, $\mathbf{u}_{\delta s} = \mathbf{u}_\delta / m_{\text{mp}}$ is the control action, ω_e is the external disturbance and $\rho = k_y / m_{\text{mp}}$ is the time- varying parameter which depends on the moving platform's stiffness and mass. Using the LPV presentation one can design the controller considering the varying parameter ρ in addition to the system outputs to stabilize the system and improve the performance. As (4-35) indicates, ρ is the single variable parameter of this system. Accordingly, variation of both k_y and m_{mp} can be considered in design of the controller. Given that the robot has a limited workspace and defined motions the known range of k_y and its variation rate are available. Regarding the known range of m_{mp} and k_y, a variation range of [290, 43200] is obtained for ρ.

4.4.2 Planar KC-CDPR Control Design

This section is concerned with the design of a robust LPV controller to minimize the L_2-gain from the disturbance ω_e to the output $\mathbf{z}_{\delta s}$ for the closed-loop system, preserving the internal stability. The design is based on the framework explained in Section 4.3. For the uncontrolled system (29), there is a complex pair of eigenvalues with no damping. This results in undesired vibrations that are directly related to the varying parameter of ρ. Therefore, the objective is to obtain robust dynamic performance for all variations of ρ in the operating workspace. Applying Theorem 4.3, the synthesis LMIs given in (4-30) and (4-33) are solved off-line for the given range. The gridding method is used to convert the infinite set of LMIs to numerically traceable finite LMIs. It is assumed that the relation of design matrices and scheduling parameter are the affines of $\Gamma(\rho) = \Gamma_0 + \Gamma_1\rho + \Gamma_2\rho^2$ and $\Psi(\rho) = \Psi_0 + \Psi_1\rho + \Psi_2\rho^2$. MOSEK solver is used along with YALMIP in MATLAB to solve the LMIs over the given range for ρ and $|v| \leq 60$. Accordingly, the number of gridding points for the considered range of ρ is obtained as 5000.

The obtained self-scheduling controller gains are depicted in Figure 4-7 where the magnitude of both gains decrease as ρ is increasing. It means that as the moving platform getting stiffer the system will be more stable and the controller gains can be reduced consequently and vice versa. Note that this is the phenomenon that is captured by the LPV design. The LTI controller on the other hand cannot

consider such a variation and results in a high-gain controller which is not appropriate in all conditions.

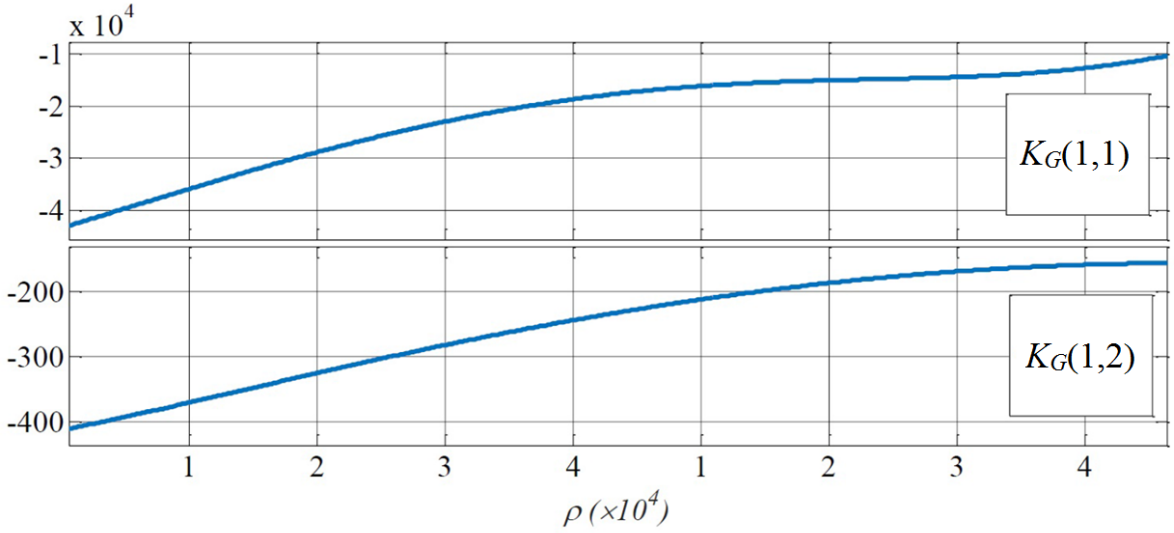

Figure 4-7: LPV controller gains versus ρ.

In order to show the benefits of the designed LPV controller, Figure 4-8 and Figure 4-9 compare the frequency response of both transfer functions from ω_e to the position and velocity with the LPV and LTI (PD) controller as well as the controller off case. In these figures, Bode plot of these cases are depicted for different values of ρ while the LTI controller remains fixed and the LPV controller gains are changing respectively. The LTI-controller is a fixed PD controller that is fine-tuned in the experiments and its gains are found as $\mathbf{K}_{PD}$=[30000,100]. It can be seen that for the controller-off and LTI-controller cases, the system bandwidth is changing with variation of ρ while the bandwidth remains relatively unchanged when the LPV controller is in the loop. It can also be seen that the LPV design outperforms the LTI-controller as ρ varies in a large domain. The time domain comparison of the designed controller is reported in the next section.

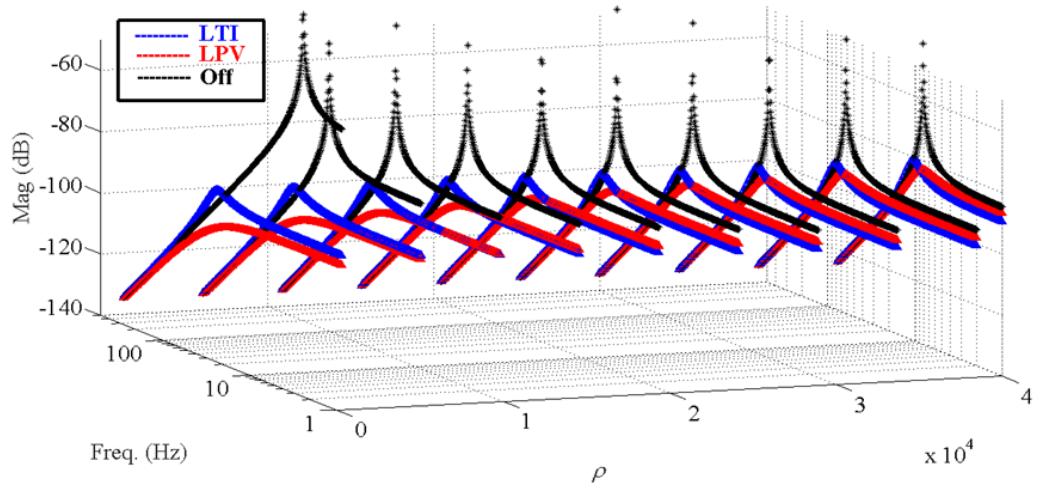

Figure 4-8: Frequency response of transfer function from ω_e to y_δ.

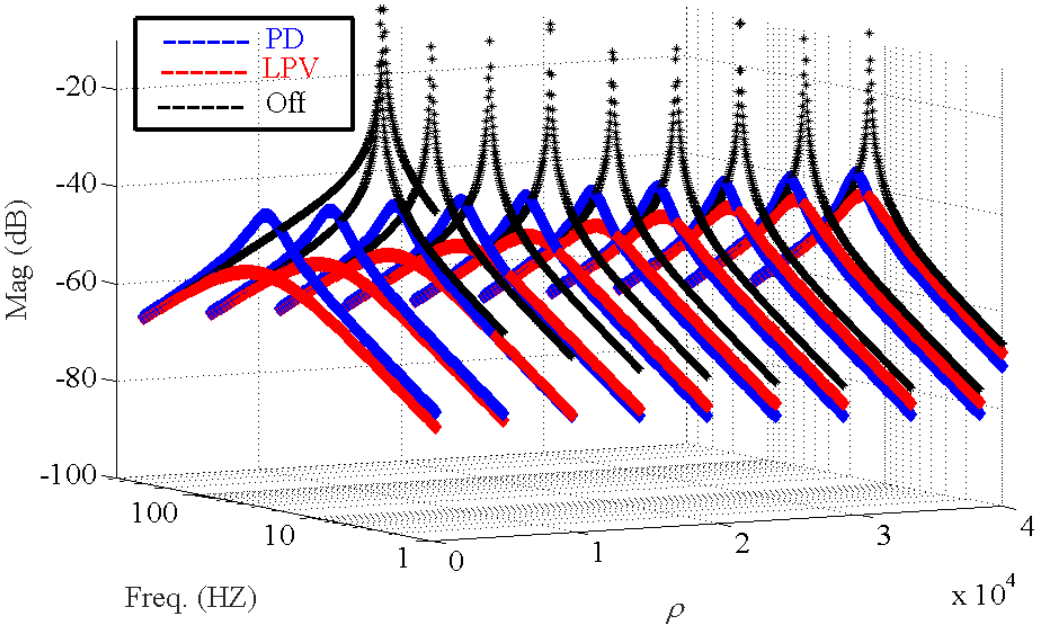

Figure 4-9: Frequency response of transfer function from ω_e to y_δ.

In order to investigate the effects of the developed control approach on vibration suppression of two DOFs of the moving platform, vibration control of the moving platform in both y and θ_z directions are tested. Accordingly, in an approximated model, the effects of stiffness coupling between these DOFs are assumed to be negligible and the vibration equations of the system are considered as

$$m_{\mathrm{mp}}\ddot{y}_{\delta} + k_y y_{\delta} = u_{\delta y},$$
$$I_{\mathrm{cmzz}}\ddot{\theta}_{z\delta} + k_{\theta z}\theta_{z\delta} = u_{\delta\theta z} \tag{4-36}$$

where I_{mpzz} is the platform's inertia, and $k_{\theta z}$ and $u_{\theta z}$ denote the rotational stiffness of the moving platform and vibration control signal in z direction. Neglecting the coupled stiffness, we use the presented approach to control the moving platform's vibrations in both y and θ_z directions, which consider

$$\rho_{\theta z} = \frac{k_{\theta z}}{I_{\mathrm{mpzz}}} \tag{4-37}$$

as the measurable varying parameter corresponding to θ_z direction.

4.5 Experiments Design

In order to evaluate the designed controller, its performance is examined in different parts of the workspace. In the first experiment, we have selected a circular trajectory that covers top right points of the workspace where k_y is small. In the second experiment, a similar circular trajectory covers the bottom right part of the workspace where k_y has bigger values. To form a circular motion with zero initial and final values for jerk, acceleration, and velocity, the coordinates of the selected circular trajectory are selected as

$$x(t) = x_0 + r_r \cos(f(t/t_m) + 3\pi/2),$$
$$y(t) = y_0 + r_r \sin(f(t/t_m) + 3\pi/2), \tag{4-38}$$
$$f(t/t_m) = -40\pi(t/t_m)^7 + 140\pi(t/t_m)^6 - 168\pi(t/t_m)^5 + 70\pi(t/t_m)^4$$

where $[x_0, y_0]$, r_r and tm denote the center of circle, its radius and motion time which for these experiments are selected as $[x_0, y_0] = [100, \pm 100]$ mm, $r_r = 100$ mm and $t_m = 8$ seconds. In order to examine the robustness and performance of the designed controller to disturbances, a scenario has been considered in which the KC-CDPRs end-effector reaction with its environment causes a harmonic disturbance force which is amplifying the undesired vibration of the moving platform during its motion. Accordingly, using a multi-reaction system designed in [119], a harmonic y-direction disturbance force, with a frequency of 4 Hz and the maximum amplitude of 20 N in the time intervals of [2.8-3.8] sec and [4.8-5.8] sec, is applied on the moving platform. In order to evaluate the performance of the designed controller in the top-middle part of the workspace, where k_y has significantly small values, the defined trajectory is selected to be tracked where $[x_0, y_0] = [0, 150]$ mm, t_m=8 sec and r_r=100 mm, and the disturbance force has the same conditions. In each motion, the performance of the proposed controller is compared with the tuned PD controller as well as a robust

sliding mode controller designed based on the developed approach of [124] considering the variation of the KC-CDPR's stiffness and mass. In addition to top and bottom motions, the performance of the designed controller is also evaluated for a known variation of payload in the third and fourth experiments. With a payload of 5.7 Kg, these experiments repeat the same trajectories of the first and second experiments.

In order to test the trajectory-tracking performance of the robot, when the vibration of the platform are controlled in two directions, a rectangular trajectory at the center of workspace with 0.4 m width and 0.2 m height is considered where the acceleration of the moving platform during motion is held continuous. Total time of the motion is considered as 15 and 5 seconds to provide a slow and fast motion, where the experiments have been done with and without the payload.

For solving the tensions redundancy problem, k_y has been maximized as a linear objective function of tensions using linear programing approach. In order to provide the states signals, a 3D camera system or an Inertial Measurement Unit (IMU) could be used. Regarding the application of the robot to work in the warehousing environments, where there is not enough space for the camera to see the moving platform, an IMU is used. The raw data of the IMU are noisy and drifted. Accordingly, the *y*-direction velocity and position signals are obtained by applying appropriate drift removing, filtering and integration techniques, discussed in [125]–[127], on *y*-direction acceleration signal. For real-time implementation of the designed controllers, Beckhoff TwinCAT software is used. The codes are developed in MATLAB-Simulink, where its integration with TwinCAT lets us to translate the codes into TwinCAT which with a minimum sample-time of 250 microseconds can be executed on the robot. In each experiment, using a Krypton RODYM 6D position measurement system, with precision of 0.2 mm and 0.1 degree, the motion of the moving platform is recorded. To provide *y*-direction acceleration signal and measurement of other accelerations and angular velocities, a six axis IMU is utilized. Figure 4-10 shows the details of measurement systems and moving platform

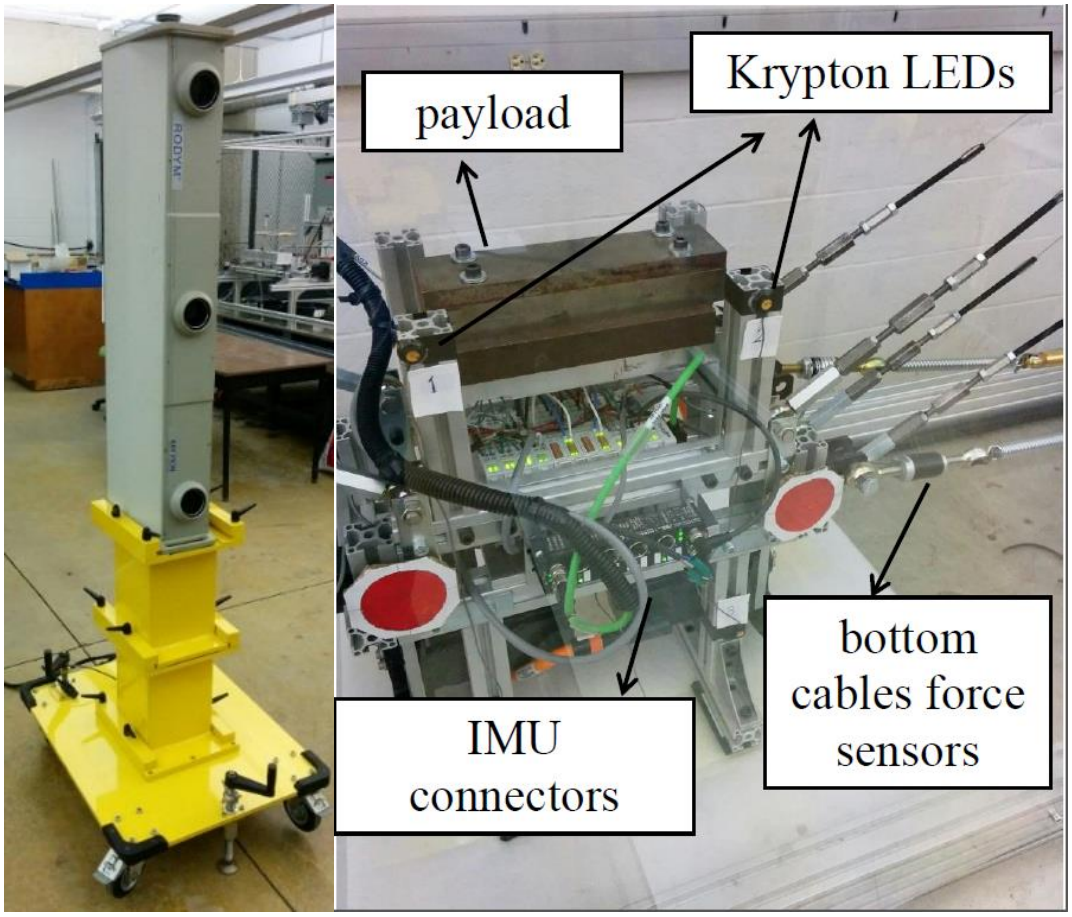

Figure 4-10: (a) Krypton RODYM camera, (b) Moving platform details.

4.6 Results and Discussion

4.6.1 Circular motion

To compare the performance of the proposed controllers, translational trajectories, angles, angular velocities and accelerations of the moving platform are recorded in each experiment. For example in top motion with zero payloads, the moving platform's trajectory and acceleration signals of y and x directions are illustrated in Figure 4-11, Figure 4-12 and Figure 4-13, respectively. The tension of cables connected to actuators 2 and 3 are also illustrated in Figure 4-14 and Figure 4-15. To show the effect of kinematic constraints in limiting θ_z-direction vibrations, the angular velocity of the moving platform is shown in Figure 4-16. Based on the provided plots, as expected, y-direction acceleration signal shows the most considerable errors. Accordingly, this signal is selected for performance comparison of different methods in the designed experiments. In order to compare the y-direction

acceleration error signals, root-mean- square deviation (RMSD) of these signals are represented in Table 4-2 and Table 4-3. In order to demonstrate the small effects of the disturbance force on the vibration of the moving platform in *x* direction, root-mean square deviation of the moving platform's acceleration signals in this direction are presented in Table 4-4.

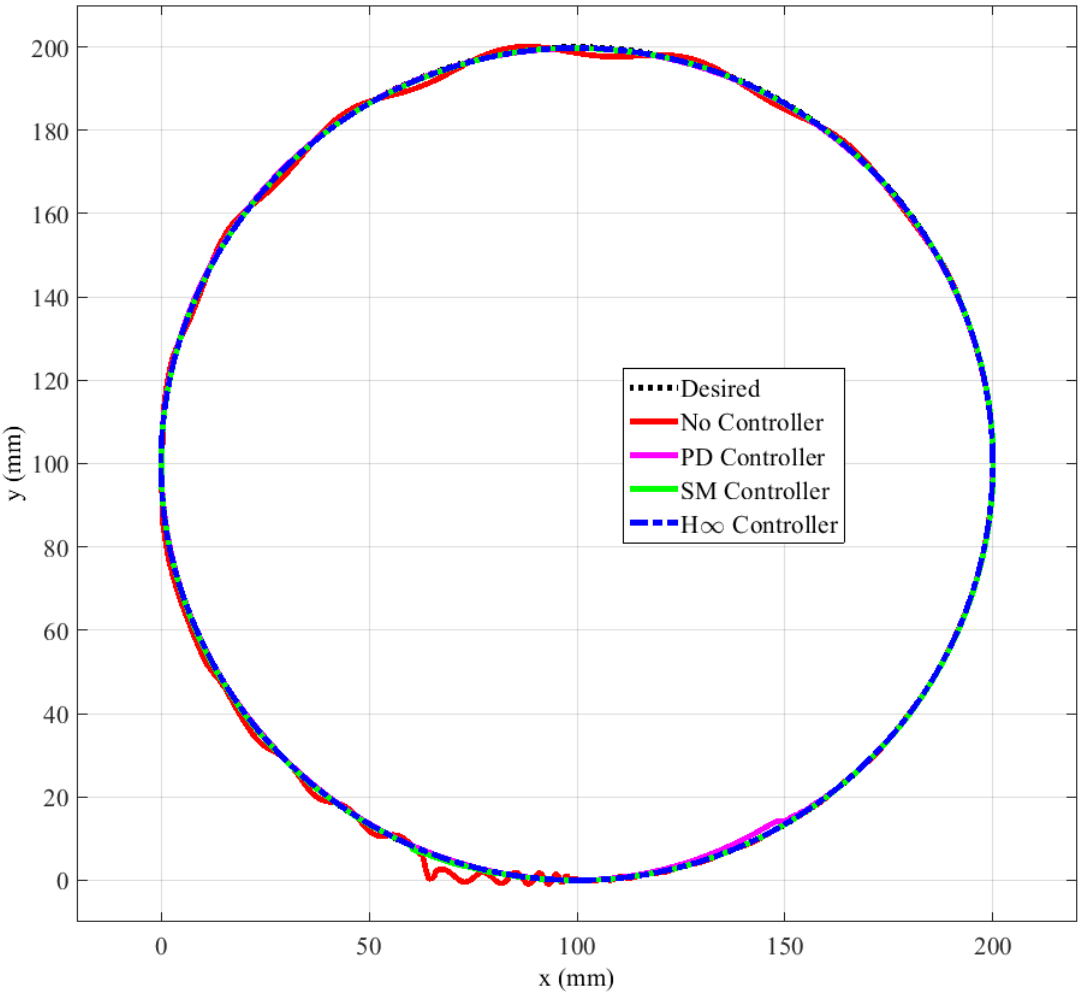

Figure 4-11: Trajectory of the moving platform in top motion without payload.

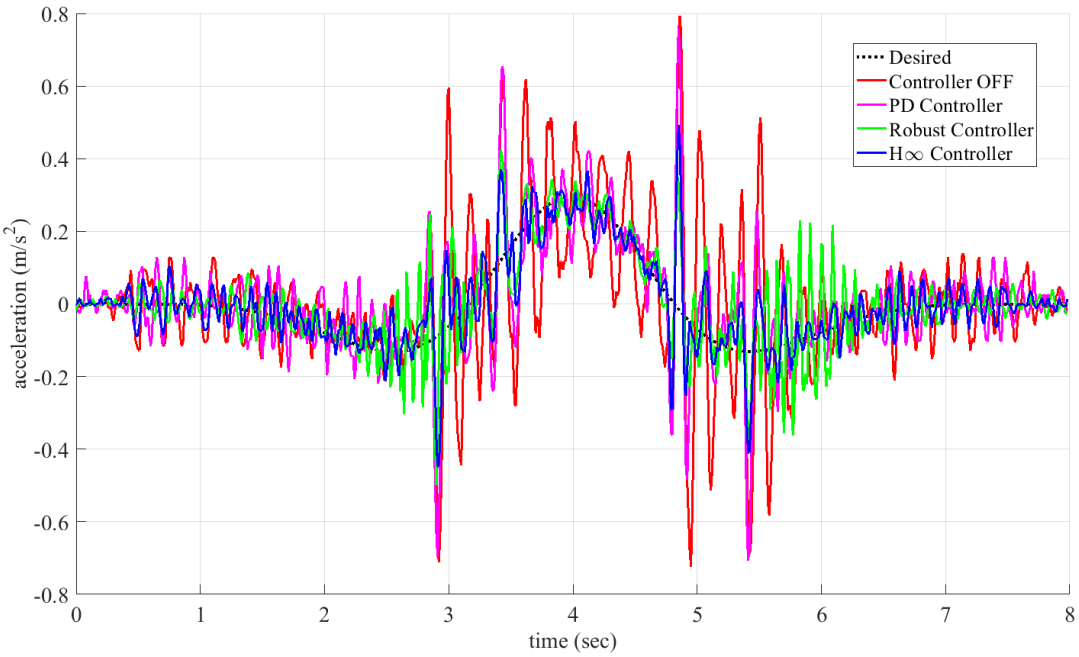

Figure 4-12: *y*-direction acceleration in top motion without payload.

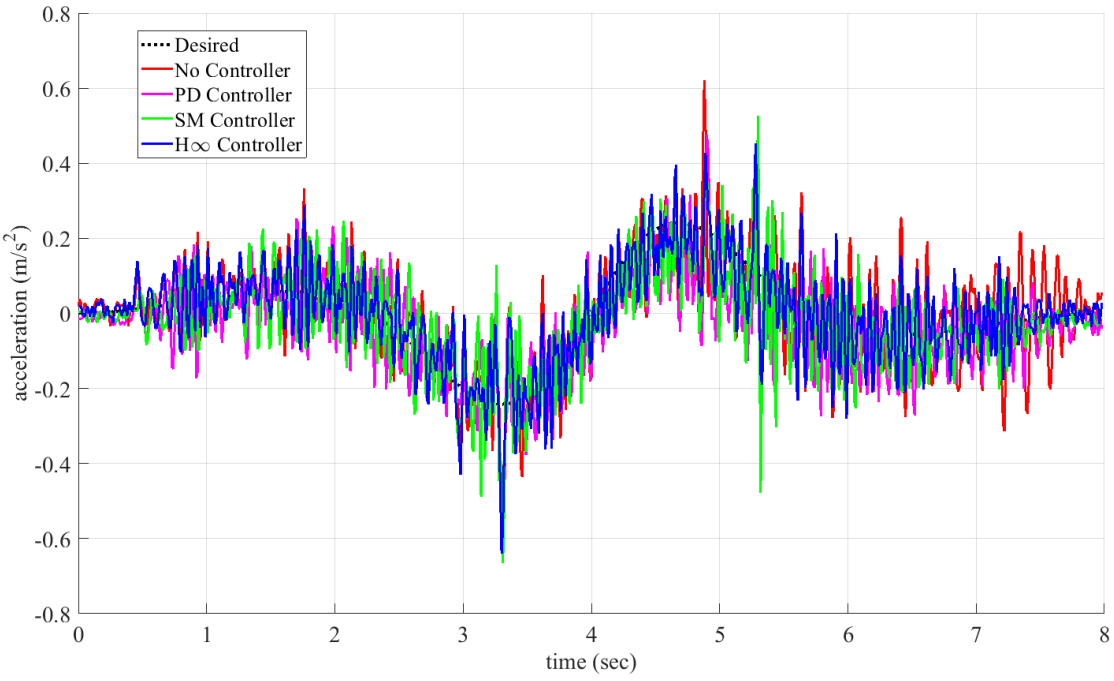

Figure 4-13: *x*-direction acceleration in top motion without payload.

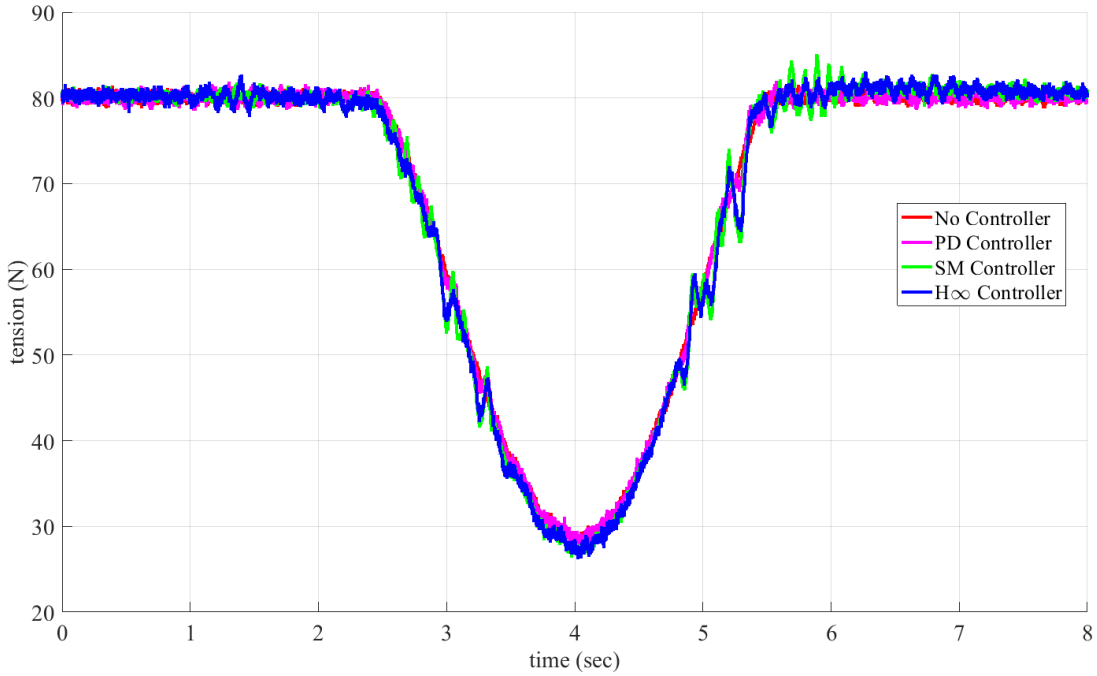

Figure 4-14: Average tension of cables of actuation unit 2.

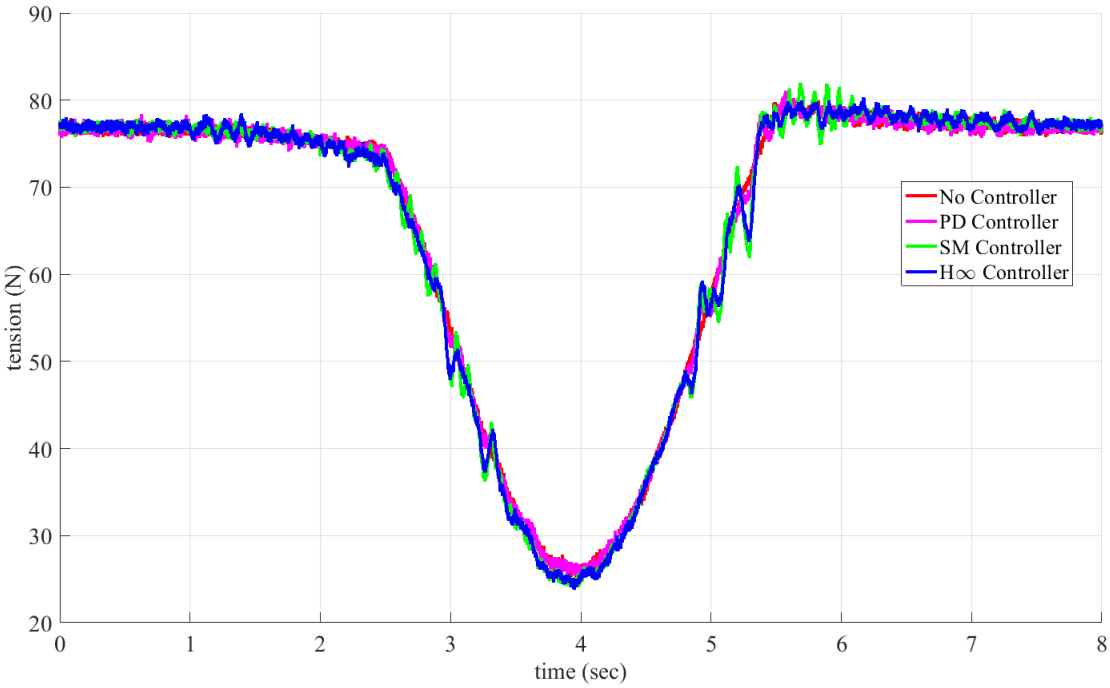

Figure 4-15: Average tension of cables of actuation unit 3.

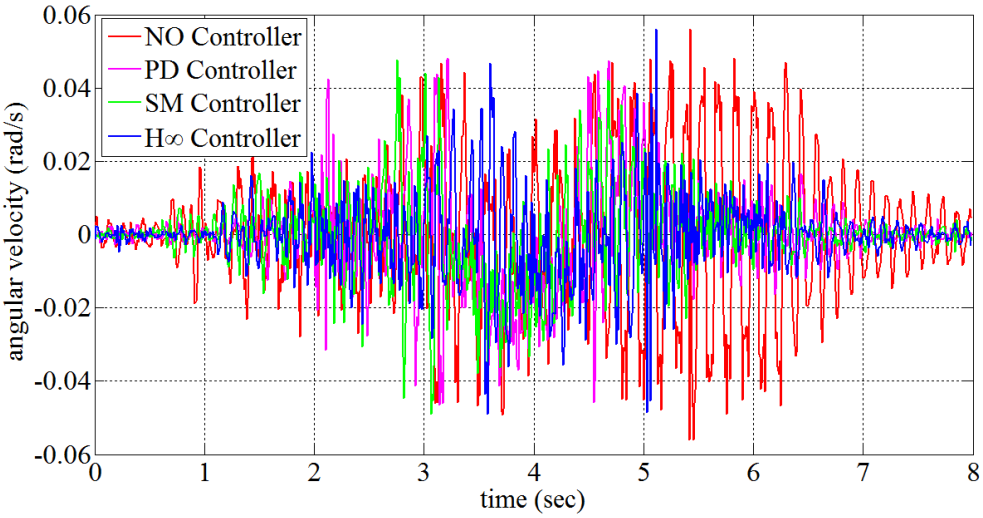

Figure 4-16: θz-direction angular velocity in top motion without payload.

Considering the results in Table 4-2 and Table 4-3, we can conclude that the designed LPV controller has a considerable improvement in comparison with the well-tuned PD controller. In addition, performance of the LPV approach is comparable with the sliding mode control approach of [124]. Compared to the sliding mode approach, the effectiveness of the LPV approach in minimization of the undesired vibrations can be seen in the positions that the KC-CDPR is suffering from a low stiffness. As the results of Table 4-3 show, the vibration of the moving platform in tracking the top-middle trajectory is more considerable where the designed controller shows a better performance improvement compared with both the well-tuned PD and the sliding mode controllers. Adding the payload reduces the performance of the PD controller which has not considered such variation in the design process where the performance of the LPV and the robust sliding mode control are not affected considerably.

Table 4-2: *y*-direction acceleration error RMSD for top and bottom circular motions.

Top Motion (No Payload)				
Controller	Off	PD	SM	LPV-H_∞
RMSD	0.71	0.19	0.10	0.08
Bottom Motion (No Payload)				
Controller	Off	PD	SM	LPV-H_∞
RMSD	0.18	0.12	0.08	0.07
Top Motion (With Payload)				
Controller	Off	PD	SM	LPV-H_∞
RMSD	1.2	0.41	0.18	0.15
Bottom Motion (With Payload)				
Controller	Off	PD	SM	LPV-H_∞
RMSD	0.2	0.16	0.11	0.09

Table 4-3: *y*-direction acceleration error RMSD for top-middle circular motions.

Top-Middle Motion (No Payload)				
Controller	Off	PD	SM	LPV-H_∞
RMSD	1.5	0.64	0.23	0.17
Top-Middle Motion (With Payload)				
Controller	Off	PD	SM	LPV-H_∞
RMSD	2.3	1.6	0.41	0.28

Table 4-4: *x*-direction acceleration error RMSD for top and bottom circular motions.

Top Motion (No Payload)				
Controller	Off	PD	SM	LPV-H_∞
RMSD	0.1	0.08	0.07	0.06
Bottom Motion (No Payload)				
Controller	Off	PD	SM	LPV-H_∞
RMSD	0.13	0.10	0.07	0.06
Top Motion (With Payload)				
Controller	Off	PD	SM	LPV-H_∞
RMSD	0.15	0.13	0.11	0.09
Bottom Motion (With Payload)				
Controller	Off	PD	SM	LPV-H_∞
RMSD	0.17	0.15	0.12	0.1

In addition to control algorithm comparisons, the role of kinematic constraints in vibration elimination of θ_z and x directions are examined and confirmed. To show this role, Figure 4-16 and Figure 4-13 are provided as two samples. As these figures indicate, we have very small values for the errors of x-direction acceleration as well as z-direction angular velocity, where we have similar results in other experiments. As the results of Table 4-4 demonstrate, the disturbance force has a small effect on the vibration of the moving platform in x direction. It can be shown that by adding the number of cables, we can increase k_x to reduce x-direction vibrations into a desired level.

4.6.2 Rectangular Motion

To compare the trajectory-tracking performance when the vibrations are controlled in both y and θ_z directions, two sets of motion are experimented and corresponding translational acceleration and angular velocity of the platform are recorded and compared. As an example, for the motions with no payload, such results are illustrated in Figure 4-17 and Figure 4-19. In order to quantify the comparisons, root-mean-square-deviation of the recorded signals are compared in Table 4-5.

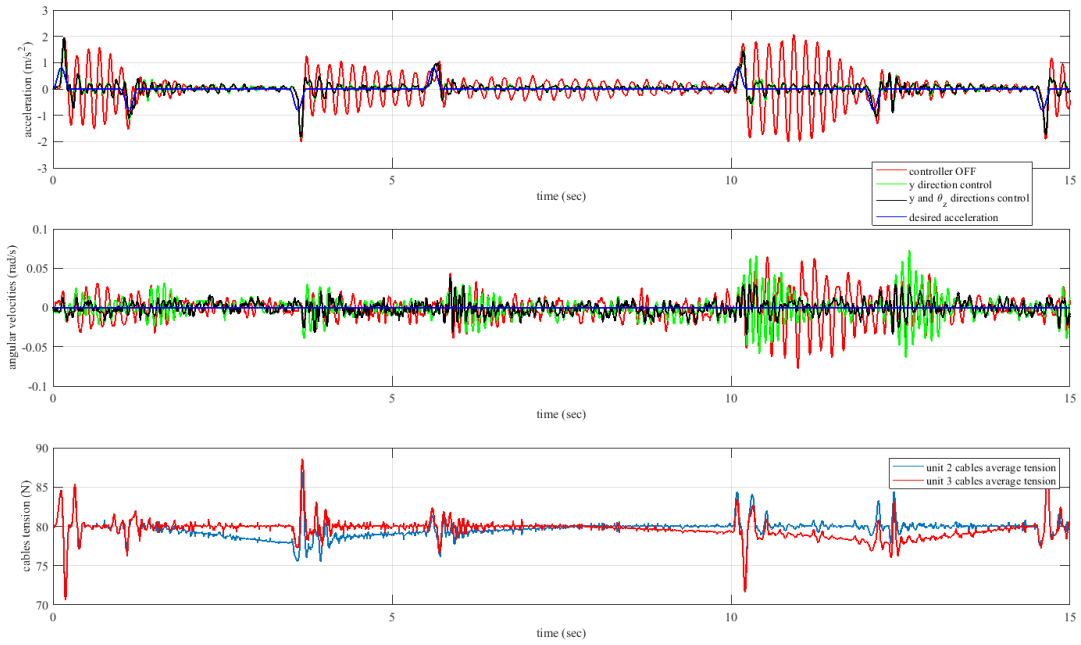

Figure 4-17: Vibration signals and control inputs in slow rectangular motion without payload.

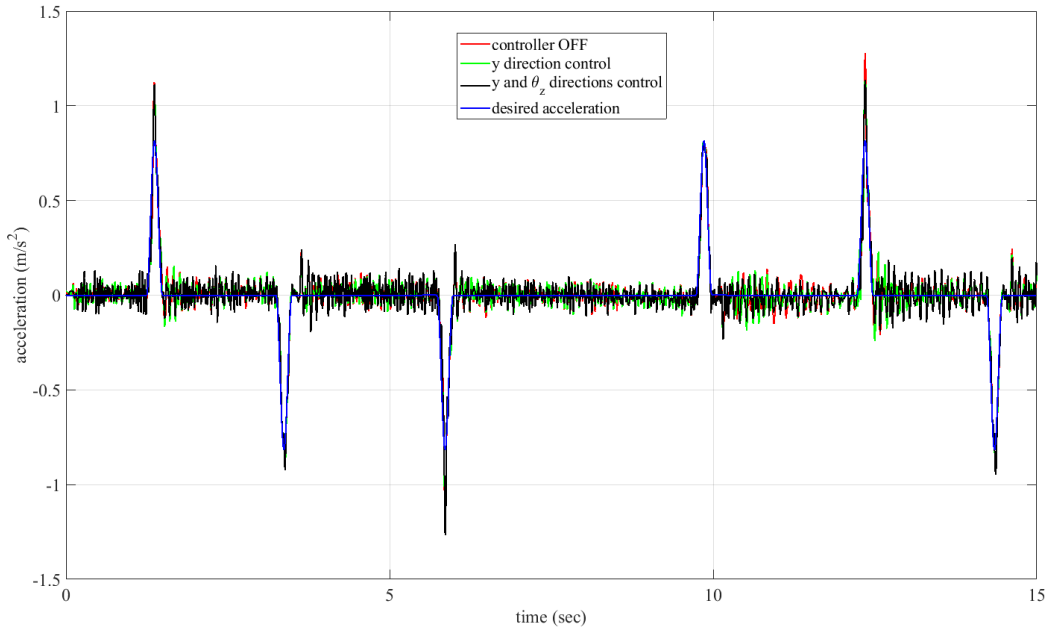

Figure 4-18: *x*-direction vibration signals in slow rectangular motion without payload.

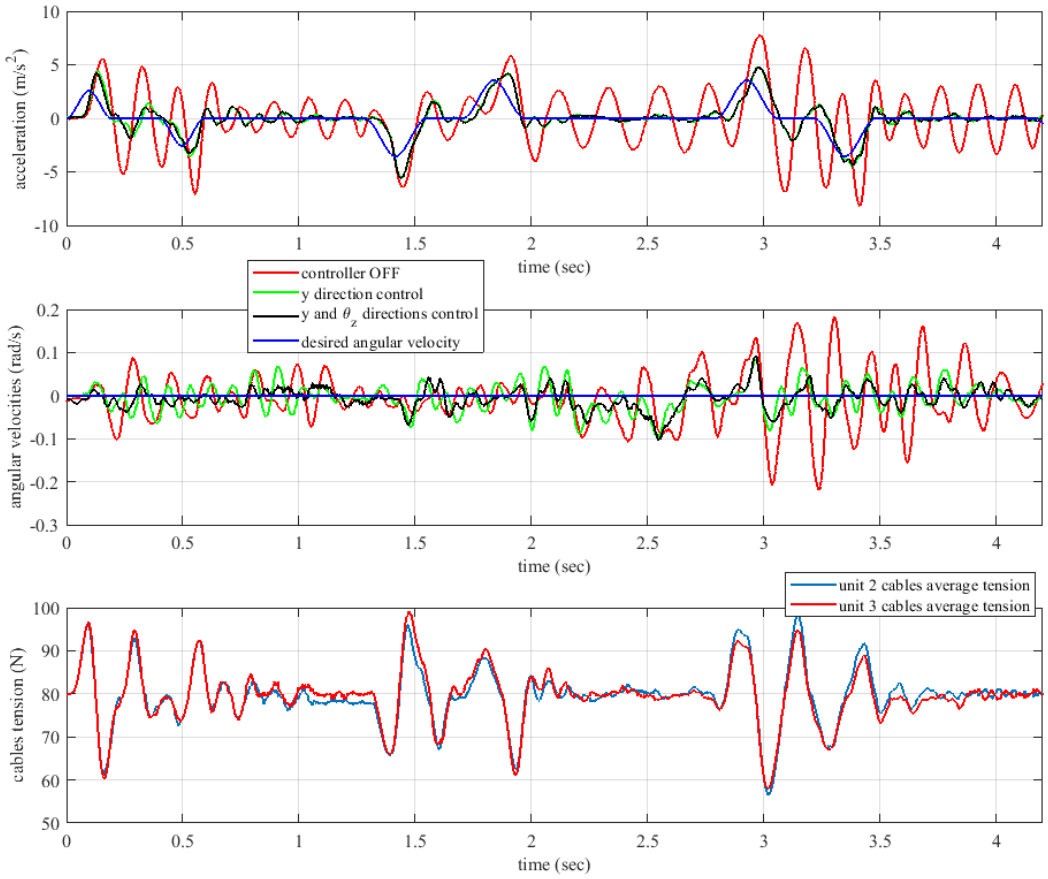

Figure 4-19: Vibration signals and control inputs in fast rectangular motion without payload.

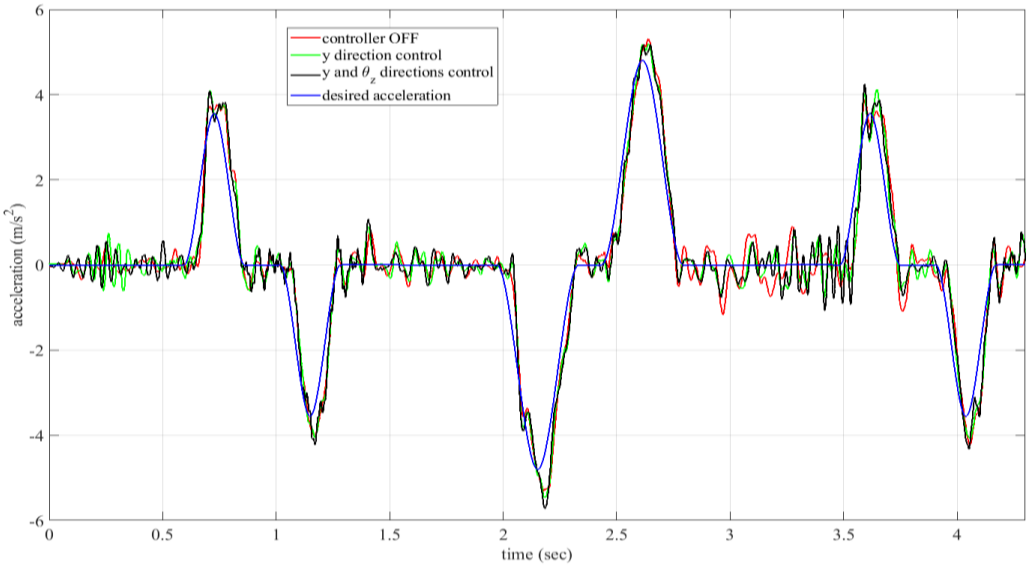

Figure 4-20: *x*-direction vibration signals in fast rectangular motion without payload.

Table 4-5: RMSD of the rectangular motions.

Slow Motion (No Payload)			
Controller	Off	y direction	y and θ_z directions
$\ddot{y}_\delta$	0.565	0.200	0.203
$\dot{\theta}_{z\delta}$	0.0166	0.0138	0.0083
Fast Motion (No Payload)			
Controller	Off	y direction	y and θ_z directions
$\ddot{y}_\delta$	2.612	0.912	0.900
$\dot{\theta}_{z\delta}$	0.0618	0.0311	0.0245
Slow Motion (With Payload)			
Controller	Off	y direction	y and θ_z directions
$\ddot{y}_\delta$	2.362	0.360	0.236
$\dot{\theta}_{z\delta}$	0.0478	0.0307	0.0199
Fast Motion (With Payload)			
Controller	Off	y direction	y and θ_z directions
$\ddot{y}_\delta$	1.9377	1.253	0.8263
$\dot{\theta}_{z\delta}$	0.0577	0.0430	0.0303

As the results of Table 4-5 indicate, suppressing the moving platforms vibrations in two DOFs provide a better trajectory-tracking performance for the KC-CDPRs where based on the results of Figure 4-18 and Figure 4-20 the vibration of the moving platform in x direction is negligible.

4.7 Conclusion

In order to investigate the effects of KC-CDPRs' end-effector disturbances on the trajectory-tracking performance of such robots and to minimize the moving platform undesired vibrations during its

motion, based on decoupling of nominal dynamics and vibration dynamics terms, a new modeling and robust control approach was developed and examined experimentally. In addition, the impact of kinematically-constrained cables arrangements in eliminating CDPRs undesired DOFs and simplification of control design were shown. In the modeling, the desired motion and undesired vibration equations were decoupled to calculate the nominal and vibration control tension of cables. The moving platform's vibration dynamics was modeled as an LPV system. Accordingly, LPV-H∞ control approach was used to suppress the undesired effect of external disturbance on the platform's trajectory-tracking performance. The developed modeling and control approach were simplified for KC-CDPRs and validated by implementing on a planar robot. Experimental results demonstrate the effectiveness and simplicity of implementation of the developed robust controller for different motions and payloads in the presence of external disturbances. Moreover, the effects of kinematically-constrained actuation method on improvements of the CDPRs' stiffness, elimination of undesired DOFs and simplification of control design were validated.

Chapter 5: Stiffness-Based Trajectory-Planning

5.1 Introduction

In order to find the optimum geometry of the trajectories which are connecting two certain points as the start and stop points of motion, this chapter investigates the stiffness-based trajectory-planning problem of KC-CDPRs. In addition, a time-optimal zero-to-zero continuous-jerk motion is designed to track such trajectories.

In the first part of this chapter, instead of considering a predetermined geometry for the trajectory between the start and stop points, the concept of stiffness-based trajectory-planning is proposed which is used to find the geometry of an optimal trajectory which guarantees minimum average perturbations for the moving platform under external disturbance.

Based on the vibration decoupled model of the moving platform developed in Chapter 3, the structural stiffness matrix of the moving platform is derived as a function of the desired trajectory. Having the start and stop points of the rest-to-rest motion, a set of smooth trajectories are considered as the feasible trajectories. Given the trajectory dependent formulation of the stiffness matrix and the external disturbance direction, a methodology is developed to find the unique smooth trajectory that minimizes the perturbation effects of the external disturbance on the moving platform along the motion. Minimizing the perturbation during the motion reduces undesired vibration of the moving platform and hence improves the performance of KC-CDPRs and reduces the maintenance cost in the long term. Such optimization is more effective in KC-CDPRs whose end-effectors generate disturbance forces/moments that stimulate undesired platform vibrations.

After finding the geometry of the stiffness-optimum trajectory, in the second part of this chapter, a new time-optimal zero-to-zero continuous-jerk motion is proposed to track such trajectory. The proposed motion keeps the continuity of the platforms' velocity, acceleration and jerk where considers the limitations of cables' velocity, acceleration and tension.

Considering the inverse kinematics of a KC-CDPR with pure translational motion, a 7^{th}-order polynomial function of time is proposed. Satisfying the initial and final conditions of motion and cables' velocity, acceleration and tension limitations provides a unique time-optimal zero-to-zero continuous-jerk motion for the platform.

To clarify the concept of stiffness-based trajectory-planning, consider the 3D KC-CDPR illustrated in Figure 5-1, used for pick-&-place applications. Vertical motions in this KC-CDPR with different payloads can apply an uncertain vertical force on the moving platform, stimulating vertical vibrations.

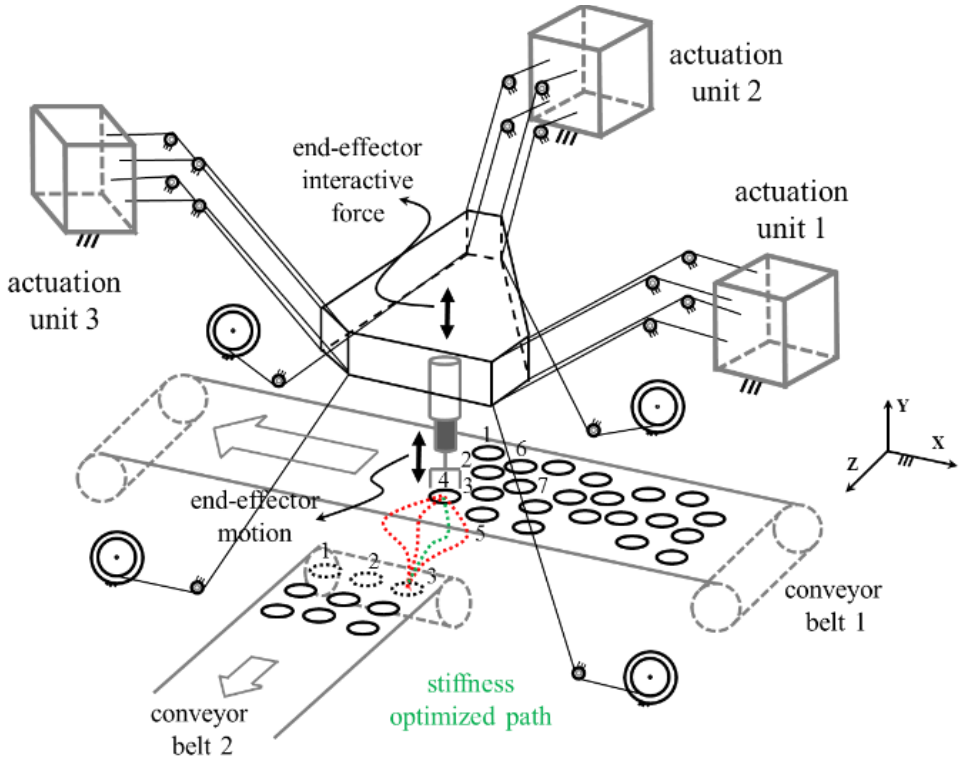

Figure 5-1: A KC-CDPR with constant external disturbance for pick-&-place applications.

In order to accomplish pick-&-place motions, the moving platform has infinite smooth trajectory options between two determined points. Here, we consider the platform's perturbation amplitude in a certain pre-defined direction as the quantitative selection criterion to be minimized. Accordingly, a stiffness-optimum trajectory is obtained.

Having the geometry of the stiffness-optimum trajectory, we need to design a motion to track it. In such case, designing a zero-to-zero continuous-jerk motion can reduces the stimulating effects of jerk non-continuity which can result in undesired vibrations. Finding the minimum time for such motion make such KC-CDPR more time efficient.

The chapter is organized as follows: Section 6.2 studies directional perturbations for different scenarios of the disturbance forces/moments, and derives the corresponding stiffness-based objective functions. Section 6.3 studies trajectory-planning for stiffness optimization that is formulated in two

forms; maximizing the average stiffness and maximizing the minimum stiffness in the selected trajectory. Section 6.4 proposes an algorithm to solve the optimization problem for the two formulations. Section 6.5 investigate the problem of zero-to-zero continuous-jerk motion design and provides numerical and experimental results to demonstrate the effectiveness of the proposed algorithms. Section 6.6 concludes the chapter.

5.2 KC-CDPRs' Structural Perturbations

In order to investigate the effects of external disturbances on the perturbation of the moving platform, structural stiffness matrix of the moving platform is reviewed in this section. It was shown in chapter 3 that the moving platform's stiffness matrix **K** consists of two parts; structural stiffness $\mathbf{K}_k$ due to the inherent stiffness of the cables, and the tensional stiffness $\mathbf{K}_\tau$, due to cables' tension. $\mathbf{K}_k$ is a function of the moving platform coordinates only, and forms the dominant part of the stiffness matrix and is used to select stiffness-optimum trajectory in rest-to-rest motions. $\mathbf{K}_k$ can be partitioned as

$$\mathbf{K}_{k\,6\times6}(\bar{\mathbf{X}}) = \begin{bmatrix} \mathbf{K}_{ktr\,3\times3} & \mathbf{K}_{ktrro\,3\times3} \\ \mathbf{K}_{krotr\,3\times3} & \mathbf{K}_{kro\,3\times3} \end{bmatrix}, \tag{5-1}$$

where $\mathbf{K}_{ktr}$, $\mathbf{K}_{kro}$, are the translational and rotational parts and $\mathbf{K}_{ktrro}$ and $\mathbf{K}_{krotr}$ are the combined parts of $\mathbf{K}_k$. Considering $\mathbf{w}_e=[\mathbf{f}_e{}^T,\mathbf{m}_e{}^T]^T$ as the disturbance wrench and $\mathbf{K}_k$ as the dominant part of **K**,

$$\mathbf{x}_\delta(\bar{\mathbf{x}}) = \mathbf{K}_k^{-1}(\bar{\mathbf{x}})\mathbf{w}_e(\bar{\mathbf{x}}) \tag{5-2}$$

is obtained as the moving platform's perturbation vector with translational and rotational perturbation components. Accordingly, all possible scenarios are considered and corresponding objective functions are formulated in the following.

5.2.1 Translational Perturbation due to Disturbance Force

Lemma 6.1: Consider application of an arbitrary (pure force) disturbance wrench vector $\mathbf{w}_e=[\mathbf{f}_e{}^T,0^T]^T$, on the KC-CDPR, generating translational perturbation with magnitude $p_{\delta\beta t}$ in an arbitrary direction of unit vector $\boldsymbol{\beta}_t=[\beta_{tx}, \beta_{ty}, \beta_{tz}]^T$. For this case, maximizing the translational structural stiffness

$$K_{ktr\beta t}(\bar{\mathbf{x}}) = \boldsymbol{\beta}_t^T \mathbf{K}_{ktr} \boldsymbol{\beta}_t \tag{5-3}$$

of the moving platform in $\boldsymbol{\beta}_t$ direction minimizes $p_{\delta\beta t}$.

Proof: Considering $f_{e\beta t}$ and $p_{\delta\beta t}$ as the magnitude of external force and translational perturbation in $\boldsymbol{\beta}_t$ direction,

$$K_{ktr\beta t} = \frac{f_{e\beta t}}{p_{\delta\beta t}} \tag{5-4}$$

is defined as the translational stiffness in $\boldsymbol{\beta}_t$ direction. Based on (5-4), for a given external force $f_{e\beta t}$, the maximum value of $K_{ktr\beta t}$ provides the minimum perturbation $p_{\delta\beta t}$. Accordingly, to complete the proof it is only required to show (5-3). Considering $\mathbf{f}_e$ as the disturbance force vector and $\mathbf{p}_\delta$ as the linear perturbation vector, we have

$$\mathbf{f}_e = \mathbf{K}_{ktrans}\mathbf{p}_\delta\,, \tag{5-5}$$

then, to provide $p_{\delta\beta t}$ in $\boldsymbol{\beta}_t$ direction,

$$\mathbf{f}_{e\beta t} = \mathbf{K}_{ktr}\boldsymbol{\beta}_t\, p_{\delta\beta t} \tag{5-6}$$

is required to be applied on the moving platform. Projecting $\mathbf{f}_{e\beta t}$ in $\boldsymbol{\beta}_t$ direction gives the magnitude of $f_{e\beta t}$ as

$$f_{e\beta t} = \boldsymbol{\beta}_t^T\mathbf{f}_{e\beta t}\,. \tag{5-7}$$

Based on the definition of $K_{ktr\beta t}$ in (5-4), substituting (5-6) in (5-7) gives (5-3) ■.

5.2.2 Rotational Perturbation due to Disturbance Moment

Lemma 6.2: Consider application of an arbitrary (pure moment) disturbance wrench vector $\mathbf{w}_e=[0^T,\mathbf{m}_e{}^T]^T$ on the KC-CDPR, generating rotational perturbation with magnitude $\theta_{\delta\beta\theta}$ in an arbitrary direction of unit vector $\boldsymbol{\beta}_\theta=[\beta_{\theta x},\beta_{\theta y},\beta_{\theta z}]^T$. For this case, maximizing the rotational structural stiffness

$$K_{kro\beta\theta}(\bar{\mathbf{x}}) = \boldsymbol{\beta}_\theta^T\mathbf{K}_{krot}\boldsymbol{\beta}_\theta \tag{5-8}$$

of the moving platform in $\boldsymbol{\beta}_\theta$ direction minimizes $\theta_{\delta\beta\theta}$.

Proof: Proof of Lemma 6.2 is similar to the proof of Lemma 6.1 and due to space limitations is not replicated ■.

5.3 Trajectory-planning Algorithms

Considering the start and stop points of $\mathbf{p}_0$ and $\mathbf{p}_1$ in Figure 5-2, the smooth parameterized trajectory $\bar{\mathbf{x}}(\mu)$ connecting $\mathbf{p}_0$ and $\mathbf{p}_1$, where μ denotes the trajectory parameter, the structural stiffness matrix of the platform is obtained as a function of $\bar{\mathbf{x}}(\mu)$ where depending on the external disturbance and the sensitive direction of the moving platform, one of the objective functions of **Error! Reference ource not found.** can be used for trajectory-planning.

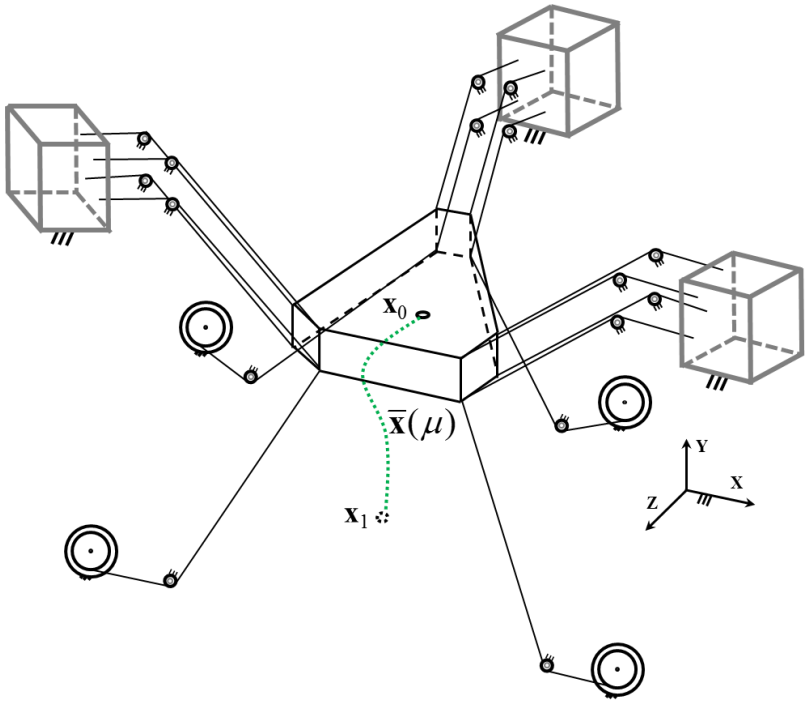

Figure 5-2: Rest-to-rest trajectory-planning for KC-CDPRs.

In order to provide multiple options for the smooth connecting trajectories between $\mathbf{x}_0$ and $\mathbf{x}_1$, the *N*th-order polynomial

$$\bar{\mathbf{x}}(\mu)=\sum_{k=0}^{N}\mathbf{a}_k\mu^k, 0\le\mu\le 1 \tag{5-9}$$

is considered as a generic solution, where $\mathbf{a}_i$s denote 6-dimensional constant multipliers that satisfy the initial and final conditions

$$\bar{\mathbf{x}}(0)=\mathbf{x}_0, \bar{\mathbf{x}}(1)=\mathbf{x}_1. \tag{5-10}$$

In addition to (5-10), in order to provide a limited domain for selected trajectories, one can add

$$\bar{\mathbf{x}}_{\min}\le\bar{\mathbf{x}}(\mu)\le\bar{\mathbf{x}}_{\max}, 0\le\mu\le 1 \tag{5-11}$$

as the boundary constraints.

Based on (5-9), each objective function of **Error! Reference source not found.** is obtained as a function of $\mathbf{a}_i$s and μ. By considering a limited number of points for $0\le\mu\le 1$ and one of the objective functions of **Error! Reference source not found.**, optimal $\mathbf{a}_i$s can be found. To clarify the details of uch approach, two of such objectives are explained in the following cases where their corresponding optimization algorithms are developed.

5.3.1 Minimizing the Maximum Perturbation

Let us consider a disturbance force $\mathbf{f}_e$ with known direction but uncertain magnitude. In this section, we study finding the trajectory for this case that maximize the minimum stiffness of the moving platform in the known direction of the disturbance force. In this case, based on Lemma 6.1, we guarantee that the platform's maximum perturbation magnitude is minimized if the trajectory solves the optimization problem

$$\begin{aligned}
&\text{maximize} \left\{ \begin{array}{c} \min K_{ktr\beta t}(\mathbf{a}_0, \mathbf{a}_1, ..., \mathbf{a}_N) \\ \text{over } 0 \le \mu \le 1 \end{array} \right\} \\
&\text{over } \mathbf{a}_i \in \mathbb{R}^6, \\
&\text{subject to } \bar{\mathbf{x}}(0) = \mathbf{x}_0, \bar{\mathbf{x}}(1) = \mathbf{x}_1, \bar{\mathbf{x}}_{\min} \le \bar{\mathbf{x}}(\mu) \le \bar{\mathbf{x}}_{\max}, \text{where } \bar{\mathbf{x}}(\mu) = \sum_{k=0}^{N} \mathbf{a}_k \mu^k, 0 \le \mu \le 1.
\end{aligned} \tag{5-12}$$

Maximizing the minimum stiffness can be a good choice for KC-CDPRs which are suffering from considerably lower stiffness in a certain direction. In such cases, system uncertainty can stimulate the platform's vibration easily and selecting a trajectory with maximum stiffness in that direction can improve the performance of KC-CDPR.

5.3.2 Minimizing the Average Perturbation

Consider a KC-CDPR with a disturbance force $\mathbf{f}_e$ in a known direction but uncertain magnitude. In this case, we study finding the trajectory that maximize the average stiffness of the moving platform in the known direction of the disturbance force. In this case, based on Lemma 6.1, we guarantee that the platform's average perturbation magnitude is minimized if the trajectory solves the optimization problem

$$\begin{aligned}
&\text{maximize} \left\{ \begin{array}{c} \text{average}\{K_{ktr\beta t}(\mathbf{a}_0, \mathbf{a}_1, ..., \mathbf{a}_N, \mu)\} \\ \text{over} 0 \le \mu \le 1 \end{array} \right\} \\
&\text{over } \mathbf{a}_i \in \mathbb{R}^6, i = 0,1,...,N \\
&\text{subject to } \bar{\mathbf{x}}(0) = \mathbf{x}_0, \bar{\mathbf{x}}(1) = \mathbf{x}_1, \bar{\mathbf{x}}_{\min} \le \bar{\mathbf{x}}(\mu) \le \bar{\mathbf{x}}_{\max}, \text{where } \bar{\mathbf{x}}(\mu) = \sum_{k=0}^{N} \mathbf{a}_k \mu^k \text{ and } 0 \le \mu \le 1.
\end{aligned} \tag{5-13}$$

Regarding the nonlinearity of the obtained objective functions, different Nonlinear Programming (NP) techniques can be used to solve the defined optimization problems. Here the a sequential quadratic programming and the interior-point convex optimization techniques [128] (implemented by the MATLAB functions "fminimax" and "fmincon") are used for solving (5-12) and (5-13) on a computer with Intel® Core™ i7-2600 3.4GHz processor and 8GB RAM.

5.4 Time-Optimal Zero-to-Zero Continuous-Jerk Motion Design

After finding the geometry of the stiffness-optimum trajectory, a motion needs to be designed to track such trajectory. In this section, we focus on a motion with a zero-to-zero continuous-jerk which keeps the continuity of the velocity and acceleration along the trajectory and considers the limitations of cables' velocity, acceleration and tension. Finding the minimum required time for such motion is studied in the following.

Based on the developed kinematic model in Chapter 3, considering a pure translational motion for the moving platform, we have

$$\dot{l}_i = -\mathbf{u}_i^T \dot{\mathbf{p}} \tag{5-14}$$

as the linear velocity of cable *i*, where differentiating both sides of (5-14) with respect to time gives

$$\ddot{l}_i = -\mathbf{u}_i^T \ddot{\mathbf{p}} \tag{5-15}$$

as the acceleration of such cable.

Considering (5-9) as the stiffness-optimum trajectory of the moving platform, the translational coordinates of the moving platform is obtained as

$$\bar{\mathbf{p}}(\mu) = \sum_{k=0}^{N} \mathbf{a}'_k \mu^k,\ 0 \le \mu \le 1. \tag{5-16}$$

where $\mathbf{a}'_i$ denotes vector $\mathbf{a}_i$ with only its three first entries. Denoting the total motion time with t_m and considering μ as a function of time t, (5-16) can be written as

$$\bar{\mathbf{p}}(t) = \sum_{k=0}^{N} \mathbf{a}'_k \mu^k(t) \tag{5-17}$$

where

$$\mu(0) = 0, \mu(t_m) = 1. \tag{5-18}$$

Considering zero value for the jerk, acceleration, and velocity of the moving platform at the start and stop points of the motion, we have

$$\dot{\bar{\mathbf{p}}}(0) = \dot{\bar{\mathbf{p}}}(t_m) = 0,\ \ddot{\bar{\mathbf{p}}}(0) = \ddot{\bar{\mathbf{p}}}(t_m) = 0, \dddot{\bar{\mathbf{p}}}(0) = \dddot{\bar{\mathbf{p}}}(t_m) = 0. \tag{5-19}$$

Substituting (5-17) in (5-19) gives

$$\dot{\mu}(0) = \dot{\mu}(t_m) = 0, \ddot{\mu}(0) = \ddot{\mu}(t_m) = 0, \dddot{\mu}(0) = \dddot{\mu}(t_m) = 0 \tag{5-20}$$

which beside (5-18) provides 8 initial/final conditions for $\mu(t)$. In order to provide a solution for $\mu(t)$ to satisfy such conditions, different continuous function of time can be proposed. In this study, we propose a 7th-order polynomial

$$\mu(t) = c_7 t^7 + c_6 t^6 + c_5 t^5 + c_4 t^4 + c_3 t^3 + c_2 t^2 + c_1 t^1 + c_0 \tag{5-21}$$

with 8 unknown multipliers c_is. Replying from (5-21) in (5-18) and (5-20), provides the unique solution of

$$\mu(t) = -20(\frac{t}{t_m})^7 + 70(\frac{t}{t_m})^6 - 84(\frac{t}{t_m})^5 + 35(\frac{t}{t_m})^4. \tag{5-22}$$

Let us replace t/t_m with λ, then we have

$$\begin{aligned}
&\mu(\lambda) = -20\lambda^7 + 70\lambda^6 - 84\lambda^5 + 35\lambda^4, \\
&\dot{\mu}(\lambda) = \frac{\partial \mu}{\partial \lambda}\dot{\lambda} = \frac{1}{t_m}(-140\lambda^6 + 420\lambda^5 \text{-} 420\lambda^4 \text{+} 140\lambda^3), \\
&\ddot{\mu}(\lambda) = \frac{\partial^2 \mu}{\partial \lambda^2}\dot{\lambda}^2 = \frac{1}{t_m^2}(-840\lambda^5 + 2100\lambda^4 \text{-} 1680\lambda^3 \text{+} 420\lambda^2),\ 0 \le \lambda \le 1.
\end{aligned} \tag{5-23}$$

Denoting the maximum acceleration and velocity of the cables are denoted by $\dot{l}_{\max}$ and $\ddot{l}_{\max}$, based on (5-14) and (5-15), we have

$$\begin{aligned}
&\left|\mathbf{u}_i^T \dot{\bar{\mathbf{p}}}\right| \le \dot{l}_{\max}, \\
&\left|\mathbf{u}_i^T \ddot{\bar{\mathbf{p}}}\right| \le \ddot{l}_{\max}.
\end{aligned} \tag{5-24}$$

as limitations of velocity/acceleration for each cable. Replacing from (5-17) in (5-24) we have

$$\begin{aligned}
&\left|\mathbf{u}_i^T (\frac{\partial \bar{\mathbf{p}}}{\partial \mu})\frac{\partial \mu}{\partial \lambda}\dot{\lambda}\right| \le \dot{l}_{\max}, \\
&\left|\mathbf{u}_i^T ((\frac{\partial^2 \bar{\mathbf{p}}}{\partial \mu^2})(\frac{\partial \mu}{\partial \lambda}\dot{\lambda})^2 + (\frac{\partial \bar{\mathbf{p}}}{\partial \mu})\frac{\partial^2 \mu}{\partial \lambda^2}\dot{\lambda}^2)\right| \le \ddot{l}_{\max}
\end{aligned} \tag{5-25}$$

which, based on (5-23), gives

$$\begin{aligned}
&\left|\frac{1}{t_m}\right|\left|\mathbf{u}_i^T (\frac{\partial \bar{\mathbf{p}}}{\partial \mu})(-140\lambda^6 + 420\lambda^5 \text{-} 420\lambda^4 \text{+} 140\lambda^3)\right| \le \dot{l}_{\max}, \\
&\left|\frac{1}{t_m^2}\right|\left|\mathbf{u}_i^T ((\frac{\partial^2 \bar{\mathbf{p}}}{\partial \mu^2})(-140\lambda^6 + 420\lambda^5 \text{-} 420\lambda^4 \text{+} 140\lambda^3)^2 + (\frac{\partial \bar{\mathbf{p}}}{\partial \mu})(-840\lambda^5 + 2100\lambda^4 \text{-} 1680\lambda^3 \text{+} 420\lambda^2))\right| \le \ddot{l}_{\max}
\end{aligned} \tag{5-26}$$

and can be written as

$$t_m \geq \max(t_{vi}, t_{ai}), i \in \{1,2,..,n\} \tag{5-27}$$

where

$$t_{vi}(\lambda) = \frac{\left| \mathbf{u}_i^T (\frac{\partial \bar{\mathbf{p}}}{\partial \mu})(-140\lambda^6 + 420\lambda^5 - 420\lambda^4 + 140\lambda^3) \right|}{\dot{l}_{\max}},$$

$$t_{ai}(\lambda) = \sqrt{\frac{\left| \mathbf{u}_i^T ((\frac{\partial^2 \bar{\mathbf{p}}}{\partial \mu^2})(-140\lambda^6 + 420\lambda^5 - 420\lambda^4 + 140\lambda^3)^2 + (\frac{\partial \bar{\mathbf{p}}}{\partial \mu})(-840\lambda^5 + 2100\lambda^4 - 1680\lambda^3 + 420\lambda^2)) \right|}{\ddot{l}_{\max}}}. \tag{5-28}$$

Based on (3-27), by considering a pure translational motion for the moving platform, we have

$$\mathbf{M}_m \begin{bmatrix} \ddot{\bar{\mathbf{p}}}^T & 0^T \end{bmatrix}^T = \bar{\mathbf{J}}'^T \bar{\boldsymbol{\tau}}' \tag{5-29}$$

which based on (5-17), can be written as

$$\mathbf{M}_m \frac{1}{t_m^2} \begin{bmatrix} ((\frac{\partial^2 \bar{\mathbf{p}}}{\partial \mu^2})(\frac{\partial \mu}{\partial \lambda})^2 + (\frac{\partial \bar{\mathbf{p}}}{\partial \mu})\frac{\partial^2 \mu}{\partial \lambda^2})^T & 0^T \end{bmatrix}^T = \bar{\mathbf{J}}'^T \bar{\boldsymbol{\tau}}'. \tag{5-30}$$

Considering $\bar{\mathbf{p}} = \begin{bmatrix} \bar{x}, \bar{y}, \bar{z} \end{bmatrix}$ and $\mathbf{M}_m = m_{mp}\mathbf{I}$, (5-30) gives

$$\begin{aligned}
&\frac{m_{mp}}{t_m^2}((\frac{\partial^2 \bar{x}}{\partial \mu^2})(\frac{\partial \mu}{\partial \lambda})^2 + (\frac{\partial \bar{x}}{\partial \mu})\frac{\partial^2 \mu}{\partial \lambda^2}) = J_{11}'^T \bar{\tau}_1' + J_{12}'^T \bar{\tau}_2' + \cdots + J_{1n}'^T \bar{\tau}_n', \\
&\frac{m_{mp}}{t_m^2}((\frac{\partial^2 \bar{y}}{\partial \mu^2})(\frac{\partial \mu}{\partial \lambda})^2 + (\frac{\partial \bar{y}}{\partial \mu})\frac{\partial^2 \mu}{\partial \lambda^2}) = -m_{mp} g + J_{21}'^T \bar{\tau}_1' + J_{22}'^T \bar{\tau}_2' + \cdots + J_{2n}'^T \bar{\tau}_n', \\
&\frac{m_{mp}}{t_m^2}((\frac{\partial^2 \bar{z}}{\partial \mu^2})(\frac{\partial \mu}{\partial \lambda})^2 + (\frac{\partial \bar{z}}{\partial \mu})\frac{\partial^2 \mu}{\partial \lambda^2}) = J_{31}'^T \bar{\tau}_1' + J_{32}'^T \bar{\tau}_2' + \cdots + J_{3n}'^T \bar{\tau}_n',
\end{aligned} \tag{5-31}$$

where $J'^T ij$ denotes the entry of row i and column j of $\bar{\mathbf{J}}'^T$.

Let us consider the cables' tension allowable interval as $0 \leq \boldsymbol{\tau}_{\min} \leq \bar{\boldsymbol{\tau}}' \leq \boldsymbol{\tau}_{\max}$, where $\boldsymbol{\tau}_{\min}=[\tau_{1\min},\tau_{2\min},\ldots,\tau_{n\min}]^T$ and $\boldsymbol{\tau}_{\max}=[\tau_{1\max},\tau_{2\max},\ldots,\tau_{n\max}]^T$ denote the vectors of cables' minimum and maximum allowable tensions. Based on (5-31), it can be shown that the conservative value of

$$t_m \geq \max(t_{mx}, t_{my}, t_{mz}), \tag{5-32}$$

where

$$\frac{1}{t_{mx}}=\left(\sup_{\boldsymbol{\tau}_{\min}\le\bar{\boldsymbol{\tau}}'\le\boldsymbol{\tau}_{\max}}\left\{\frac{J_{11}'^{T}\bar{\tau}_1+J_{12}'^{T}\bar{\tau}_2+\cdots+J_{1n}'^{T}\bar{\tau}_n}{m_{mp}((\frac{\partial^2\bar{x}}{\partial\mu^2})(\frac{\partial\mu}{\partial\lambda})^2+(\frac{\partial\bar{x}}{\partial\mu})\frac{\partial^2\mu}{\partial\lambda^2})}\right\}\right)^{\frac{1}{2}},$$

$$\frac{1}{t_{my}}=\left(\sup_{\boldsymbol{\tau}_{\min}\le\bar{\boldsymbol{\tau}}'\le\boldsymbol{\tau}_{\max}}\left\{\frac{-m_{mp}g+J_{21}'^{T}\bar{\tau}_1+J_{22}'^{T}\bar{\tau}_2+\cdots+J_{2n}'^{T}\bar{\tau}_n}{m_{mp}((\frac{\partial^2\bar{y}}{\partial\mu^2})(\frac{\partial\mu}{\partial\lambda})^2+(\frac{\partial\bar{y}}{\partial\mu})\frac{\partial^2\mu}{\partial\lambda^2})}\right\}\right)^{\frac{1}{2}}, \qquad (5\text{-}33)$$

$$\frac{1}{t_{mz}}=\left(\sup_{\boldsymbol{\tau}_{\min}\le\bar{\boldsymbol{\tau}}'\le\boldsymbol{\tau}_{\max}}\left\{\frac{J_{31}'^{T}\bar{\tau}_1+J_{32}'^{T}\bar{\tau}_2+\cdots+J_{3n}'^{T}\bar{\tau}_n}{m_{mp}((\frac{\partial^2\bar{z}}{\partial\mu^2})(\frac{\partial\mu}{\partial\lambda})^2+(\frac{\partial\bar{z}}{\partial\mu})\frac{\partial^2\mu}{\partial\lambda^2})}\right\}\right)^{\frac{1}{2}},$$

satisfies $0\le\boldsymbol{\tau}_{\min}\le\bar{\boldsymbol{\tau}}'\le\boldsymbol{\tau}_{\max}$.

Having $\bar{\mathbf{p}}$ as a function of μ, and μ as a function of λ, all parts in inequalities of (5-27) and (5-32) are obtained as a function of λ. Then by considering $0\le\lambda\le1$, the minimum value of t_m is obtained. Having the minimum value of t_m , $\bar{\mathbf{p}}$ is obtained as a function of time.

5.5 Examples

In this section, the details of stiffness-based trajectory-planning methodology, proposed in Section 5.3, and time-optimal zero-to-zero continuous-jerk motion design, studied in Section 5.4, are investigated through four examples.

Example 6.1: Based on the warehousing robot configuration presented in Figure 5-3, consider $\mathbf{p_0}$=[-0.4,-0.2]^{T}m and $\mathbf{p_1}$=[0.4, 0.2]^{T}m as the start and stop points of the motion, where maximization of the average translational stiffness of the moving platform in *y* direction is required. It is also required to compare the average stiffness of the stiffness-optimum trajectory with other options, including the trajectory with minimum average stiffens and the straight line.

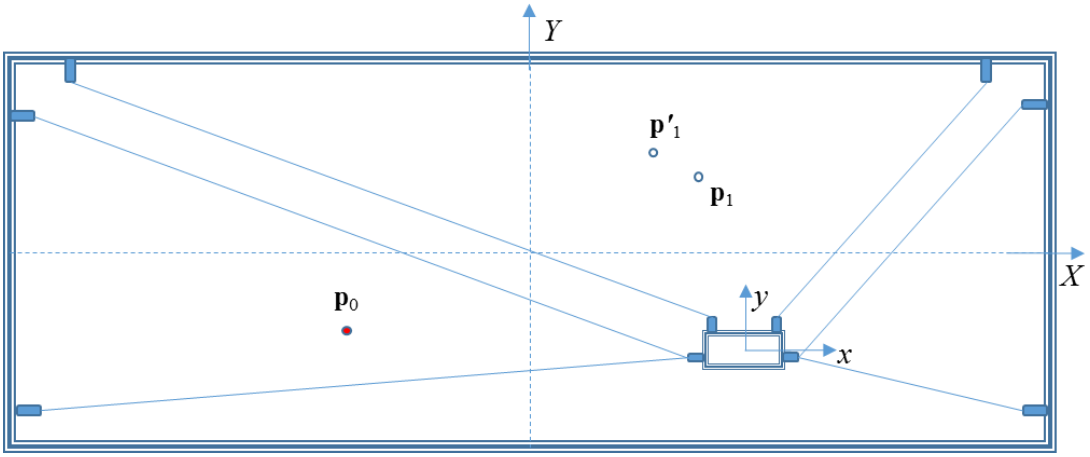

Figure 5-3: Desired start and stop points of the moving platform.

Considering a fifth order polynomial for the desired trajectory of the moving platform, and [-0.4, 0.4]m and [-0.2, 0.2]m as the allowable interval of x and y, we have

$$\begin{aligned} &x(\mu) = a_{10} + a_{11}\mu \\ &y(\mu) = a_{20} + a_{21}\mu + a_{20}\mu^2 + a_{21}\mu^3 + a_{20}\mu^4 + a_{21}\mu^5 \\ &\text{subject to } x(0) = -0.4, x(1) = +0.4, y(0) = -0.2, y(1) = +0.2, \\ &-0.4 \le x(\mu) \le +0.4, -0.2 \le y(\mu) \le +0.2, 0 \le \mu \le 1 \end{aligned} \tag{5-34}$$

where by replacing x and y in $\mathbf{K}$, the optimization task (5-12) is reformulated as

$$\begin{aligned} &\text{maximize} \left\{ \begin{array}{c} \text{average}\{K_{ktry}(\mathbf{a}_0, \mathbf{a}_1, ..., \mathbf{a}_N, \mu)\} \\ \text{over } 0 \le \mu \le 1 \end{array} \right\} \\ &\text{over } \mathbf{a}_i \in \mathbb{R}^2 \end{aligned} \tag{5-35}$$

subject to (5-34). In order to solve (5-35), a 40 point evenly distributed grid is considered for μ, where by using interior-point convex optimization technique the solution of

$$\begin{aligned} &x(\mu) = -0.4 + 0.8\mu,\ 0 \le \mu \le 1 \\ &y(\mu) = \text{-}0.1831 + 0.0423x \text{-} 0.9457x^2 \text{-} 2.3642x^3 + 13.0617x^4 + 32.6541x^5 \end{aligned} \tag{5-36}$$

is obtained with 5 iterations in 0.25 seconds. Along the obtained trajectory, y-direction average stiffness is 104.0 kN/m which is comparable with the trajectory

$$\begin{aligned} &x(\mu) = -0.4 + 0.8\mu, 0 \le \mu \le 1 \\ &y(\mu) = 0.1831 + 0.0423x + 0.9457x^2 \text{-} 2.3642x^3 \text{-} 13.0617x^4 + 32.6541x^5 \end{aligned} \tag{5-37}$$

with the minimum average stiffness of 32.3 kN/m. It is worth mentioning the average *y*-direction stiffness along the straight pass

$$x(\mu) = -0.4 + 0.8\mu, 0 \le \mu \le 1$$
$$y(\mu) = +.5x, \tag{5-38}$$

is 66.3 kN/m. Figure 5-4 illustrate the designed trajectories and compare their average *y*-direction stiffness.

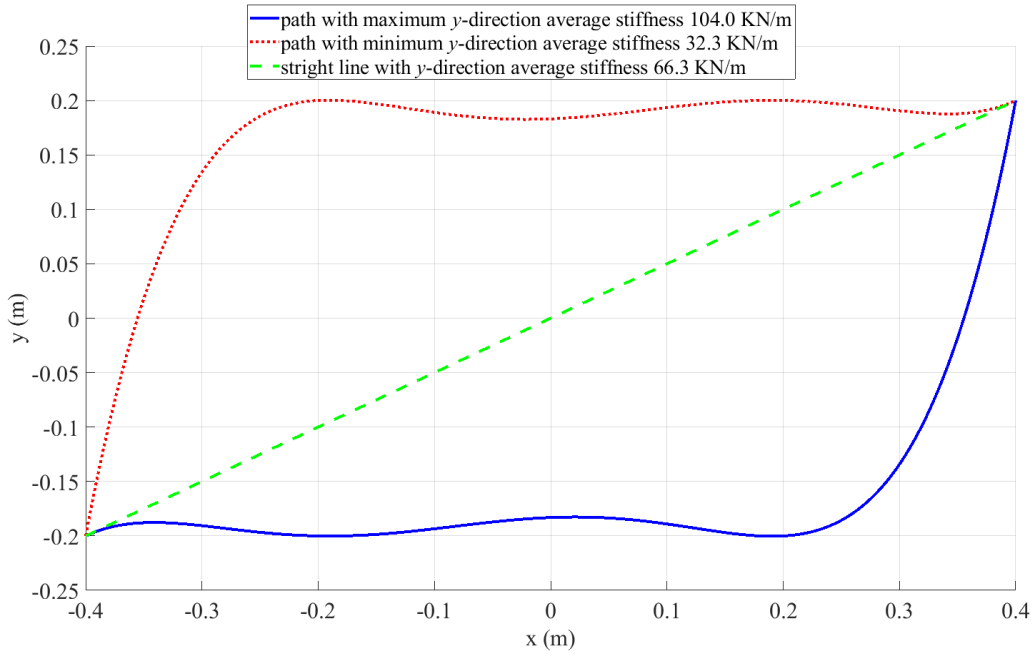

Figure 5-4: Trajectories with the maximum and minimum average structural stiffness in *y* direction.

Example 6.2: In this example, in order to demonstrate the effectiveness of the proposed trajectory-planning effects on vibration reduction of the moving platform, rest-to-rest motion of the warehousing robot through the obtained trajectories of Example 6.1 are tested. The acceleration signal of the moving platform in *y* direction is recorded and compared. In order to provide a zero-to-zero continuous-jerk motion for the moving platform, we consider

$$\mu(t) = -20\left(\frac{t}{t_m}\right)^7 + 70\left(\frac{t}{t_m}\right)^6 - 84\left(\frac{t}{t_m}\right)^5 + 35\left(\frac{t}{t_m}\right)^4 \tag{5-39}$$

where t_m is considered as 4 seconds. Desired *y*-direction acceleration of the moving platform along selected trajectories are illustrated in Figure 5-5 where the acceleration deviations are presented in Figure 5-6. Root-mean-square-deviation of the recorded vibration signals are obtained as 0.08 and 0.03 m/s^2. As Figure 5-5 illustrates, the maximum absolute value of accelerations are close where the deviation of the acceleration signals are considerably different. Similar experiments provide similar results which demonstrate the effectiveness of proposed trajectory-planning in vibration reduction of the moving platform in rest-to-rest motions.

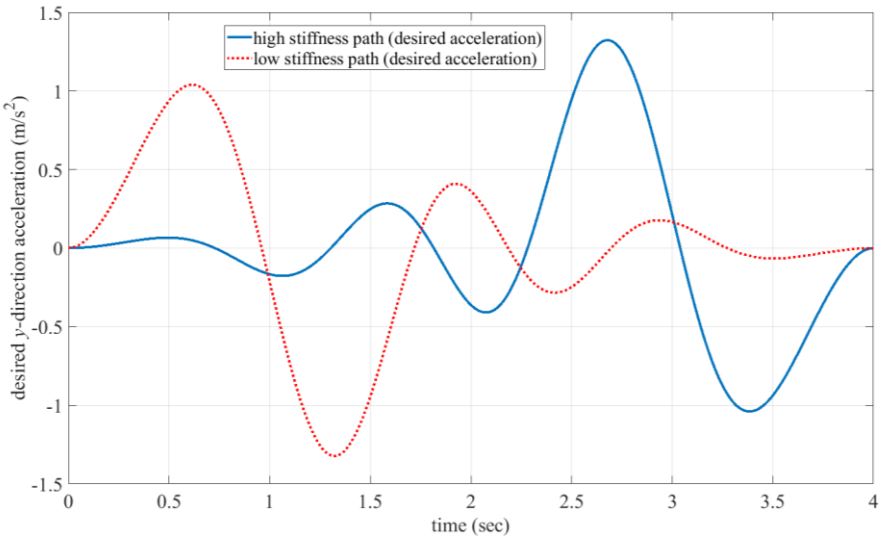

Figure 5-5: Desired *y*-direction acceleration of the moving platform in selected motions.

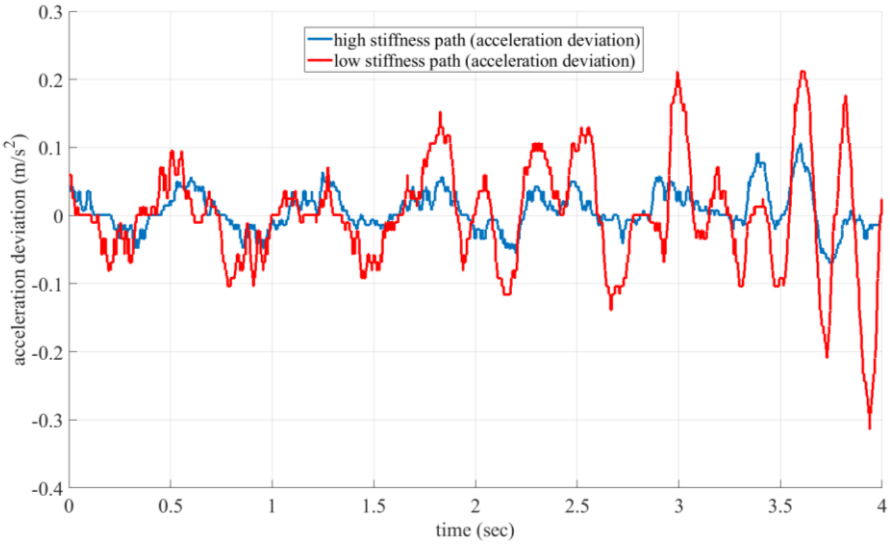

Figure 5-6: *y*-direction acceleration deviation in selected motions.

Example 6.3: Consider the conditions of Example 6.2, where we have two options for the stop point including $\mathbf{p}_1$=[0.4, 0.2]^{T}m and $\mathbf{p}'_1$=[0.3,0.25]^{T}m. In this case, the optimum average y-direction stiffness of the trajectory to reach the second destinations needs to be obtained and compared with that of first destination. In addition comparing such average stiffness with the straight line trajectories is required.

The average y-direction stiffness of the platform in the trajectory

$$\begin{aligned} &x(\mu) = a_{10} + a_{11}\mu \\ &y(\mu) = a_{20} + a_{21}\mu + a_{20}\mu^2 + a_{21}\mu^3 + a_{20}\mu^4 + a_{21}\mu^5 \\ &\text{subject to } x(0) = -0.4, x(1) = +0.3, y(0) = -0.2, y(1) = +0.2, \\ &-0.4 \le x(\mu) \le +0.3, -0.2 \le y(\mu) \le +0.25, 0 \le \mu \le 1 \end{aligned} \tag{5-40}$$

to the second destination is maximized through

$$\begin{aligned} &\text{maximize} \left\{ \begin{array}{c} \text{average}\{K_{ktry}(\mathbf{a}_0, \mathbf{a}_1, ..., \mathbf{a}_N, \mu)\} \\ \text{over } 0 \le \mu \le 1 \end{array} \right\} \\ &\text{over } \mathbf{a}_i \in \mathbb{R}^2 \end{aligned} \tag{5-41}$$

subject to (5-40). In order to solve (5-41) a grid with 35 points is considered for μ, where by using interior-point convex optimization technique the solution of

$$\begin{aligned} &x(\mu) = -0.4 + 0.7\mu,\ 0 \le \mu \le 1 \\ &y(\mu) = \text{-}0.1855\text{-}0.0912x\text{-}1.3187x^2 + 2.9945x^3 + 41.2088x^4 + 68.6813x^5 \end{aligned} \tag{5-42}$$

is obtained with 5 iterations in 0.2 seconds. The average stiffness along the trajectory to reach to the second destination is 101.3 kN/m which is less than that of the first trajectory. Accordingly, to have a larger average stiffness in y direction, $\mathbf{p}_1$=[0.4,0.2]^{T}m is selected as the optimum destination. Trajectories (5-36) and (5-42) are illustrated in Figure 5-7 where their average y-direction stiffness are compared with corresponding straight lined between start and stop points.

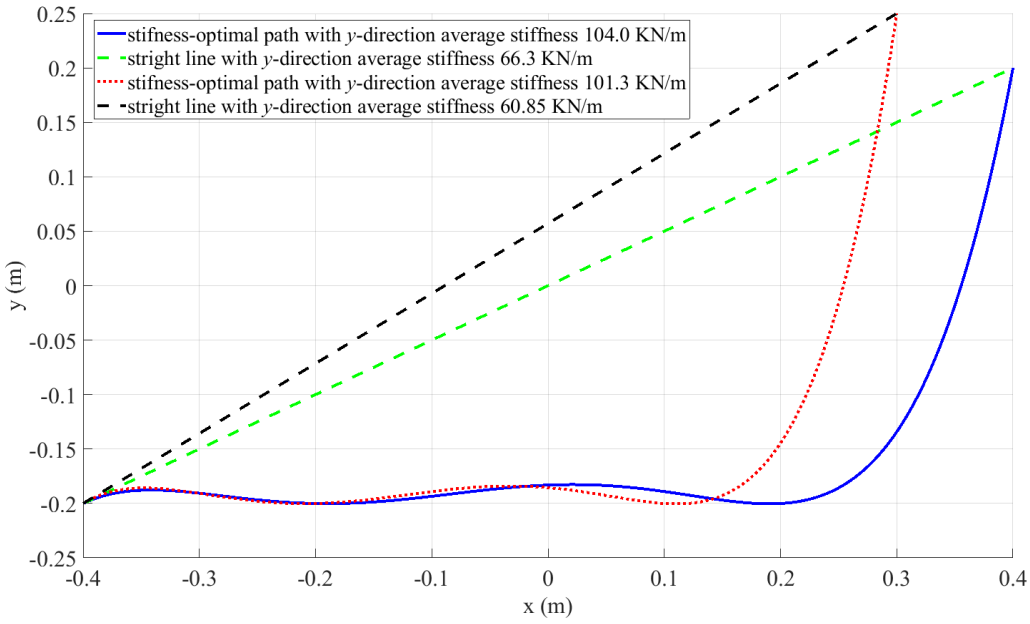

Figure 5-7: Optional trajectories with different average structural stiffness in *y* direction.

It is worth mentioning that in case of having different choices for the start point, more options with various structural stiffnesses are available where the proposed approach can be used to select the best option among them.

Example 6.4: In this example, the minimum motion time along the stiffness-optimum and the straight line trajectories, illustrated trajectories in Figure 5-4, are compared. The maximum velocity and acceleration of the cables are considered as 1.4 m/s and 7 m/s^2, where the maximum tension of top and bottom cables are 400N and 80N and the minimum tension of all cables is 40 N.

Based on the proposed approach in Section 5.4, by checking inequalities of (5-27) and (5-32), the minimum feasible value of t_m is obtained as 1.3461 seconds along the stiffness-optimum trajectory where minimum feasible t_m along the straight trajectory is obtained as 2.6622 seconds.

Figure 5-8 illustrates the minimum t_m for each value of λ, to satisfy each inequality in (5-27) and (5-32), where in such motion, the minimum value of t_m is limited by the maximum acceleration of actuator 4. Considering t_m=1.3461 sec, the position, velocity, acceleration and jerk of the moving platform along the stiffness-optimum trajectory are obtained which are presented in Figure 5-9 to Figure 5-12. Accordingly, the velocity and acceleration of the cables are obtained and illustrated in Figure 5-13 and Figure 5-14, where Figure 5-15 shows the cables' tension along such trajectory.

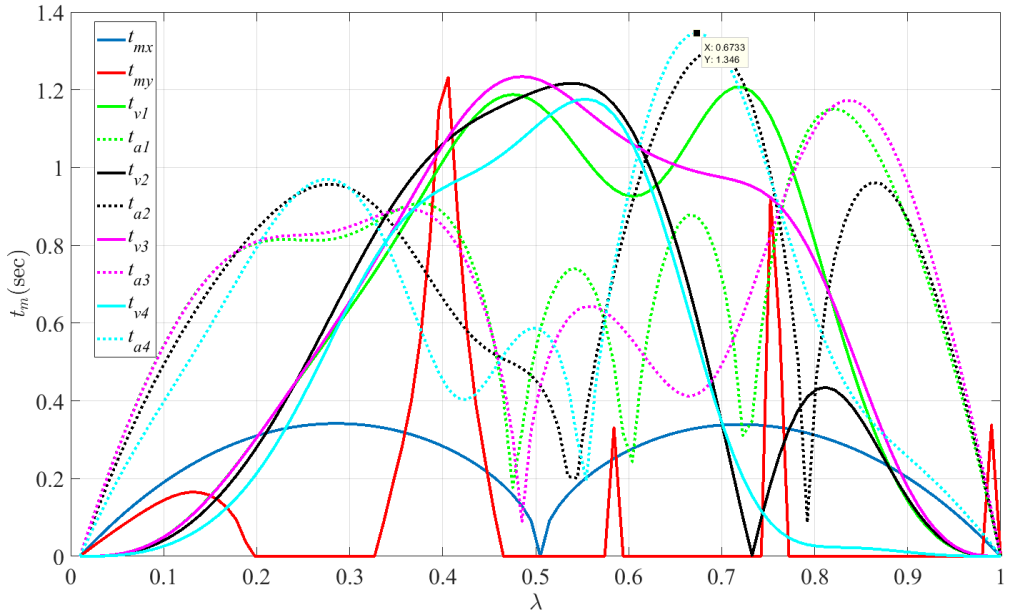

Figure 5-8: Distribution of motion minimum time based on the studied criteria in Section 5.4.

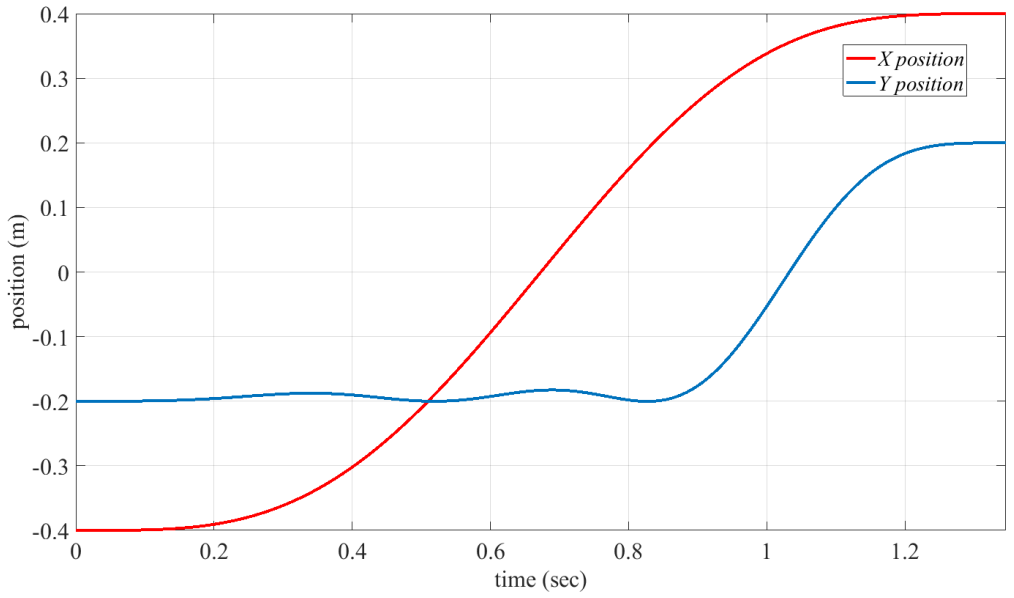

Figure 5-9: Position of the moving platform along the stiffness-optimum trajectory.

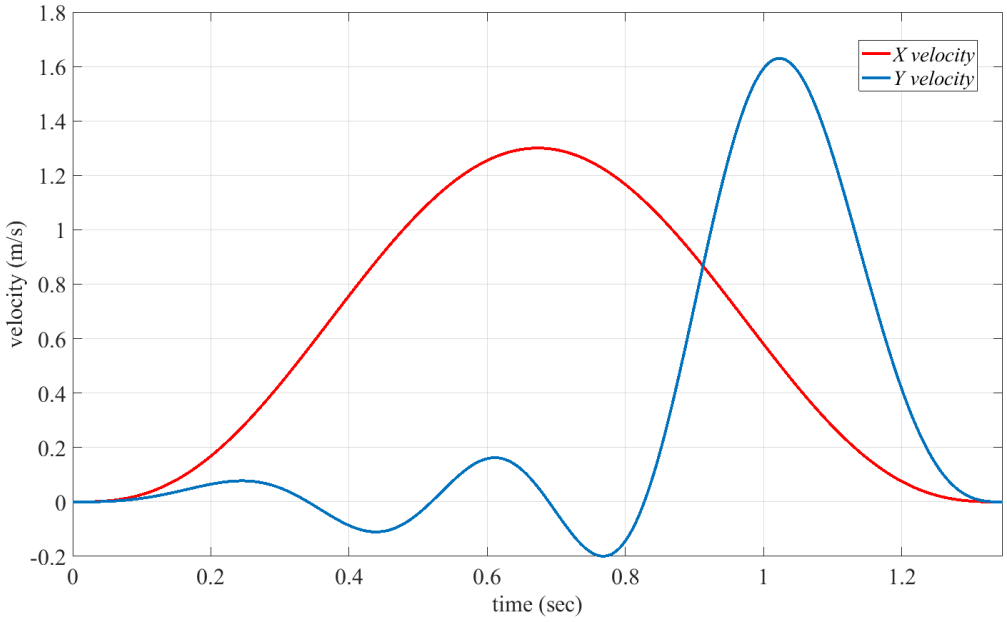

Figure 5-10: Velocity of the moving platform along the stiffness-optimum trajectory.

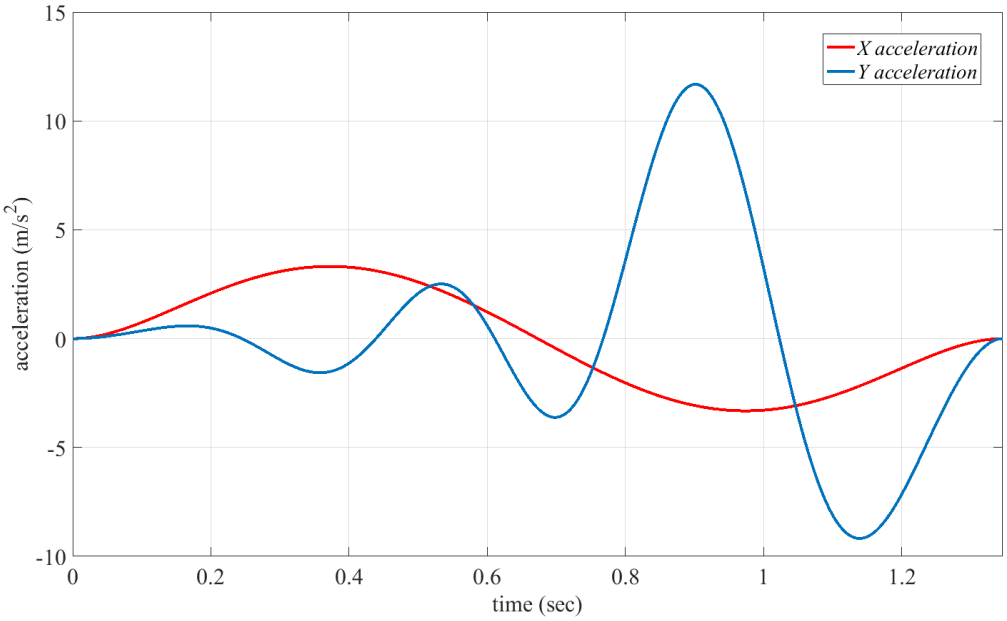

Figure 5-11: Acceleration of the moving platform along the stiffness-optimum trajectory.

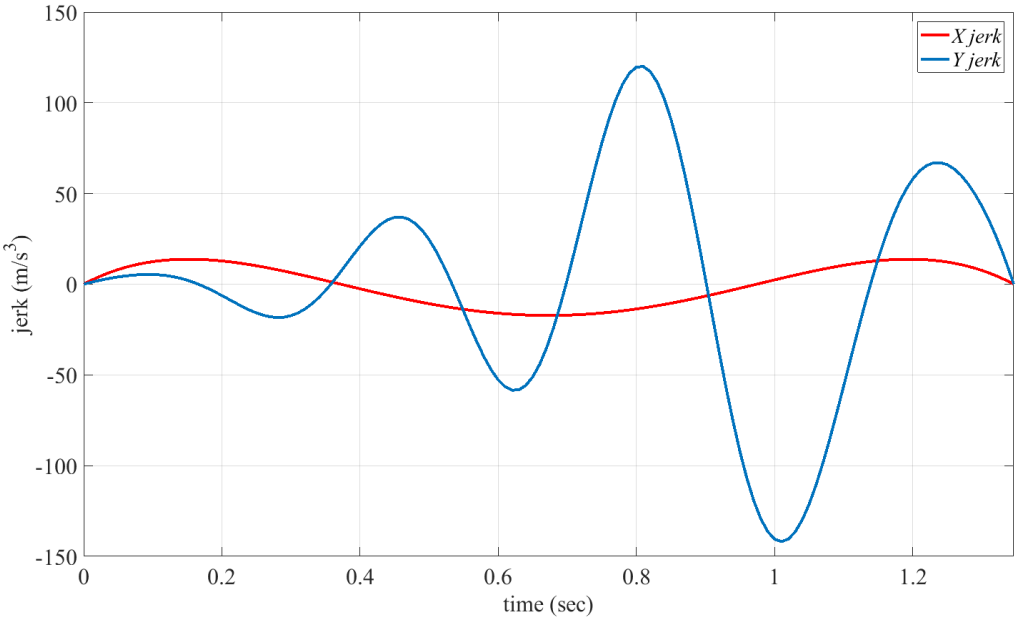

Figure 5-12: Jerk of the moving platform along the stiffness-optimum trajectory.

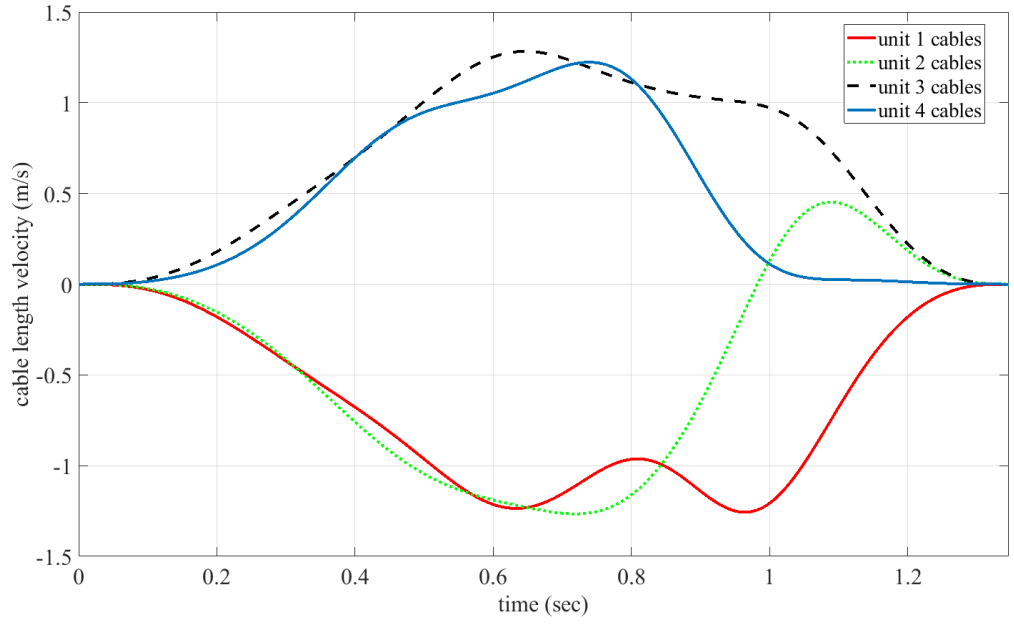

Figure 5-13: Velocity of the cables along the stiffness-optimum trajectory.

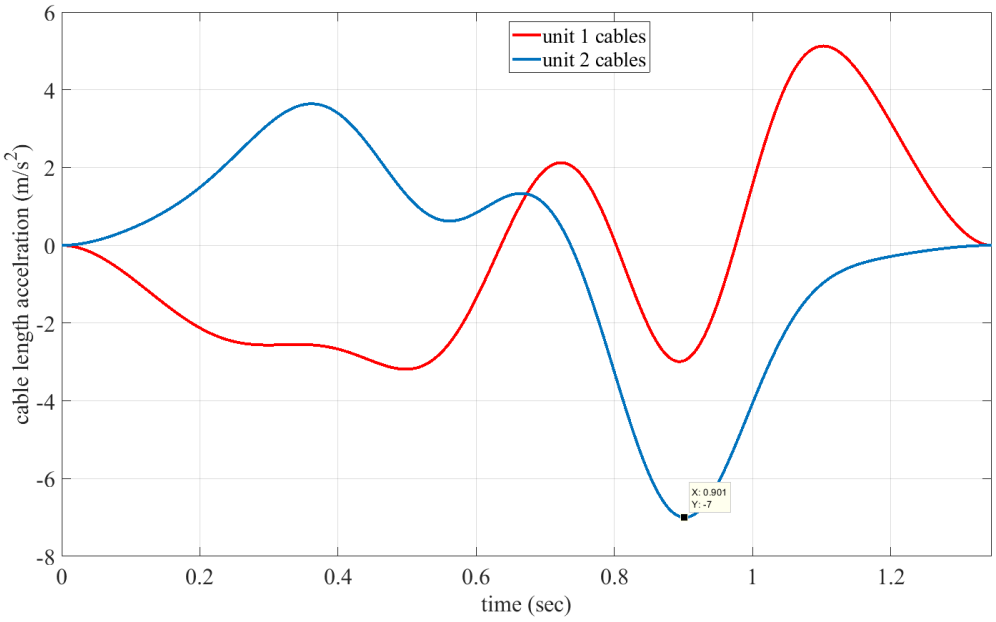

Figure 5-14: Acceleration of the cables along the stiffness-optimum trajectory.

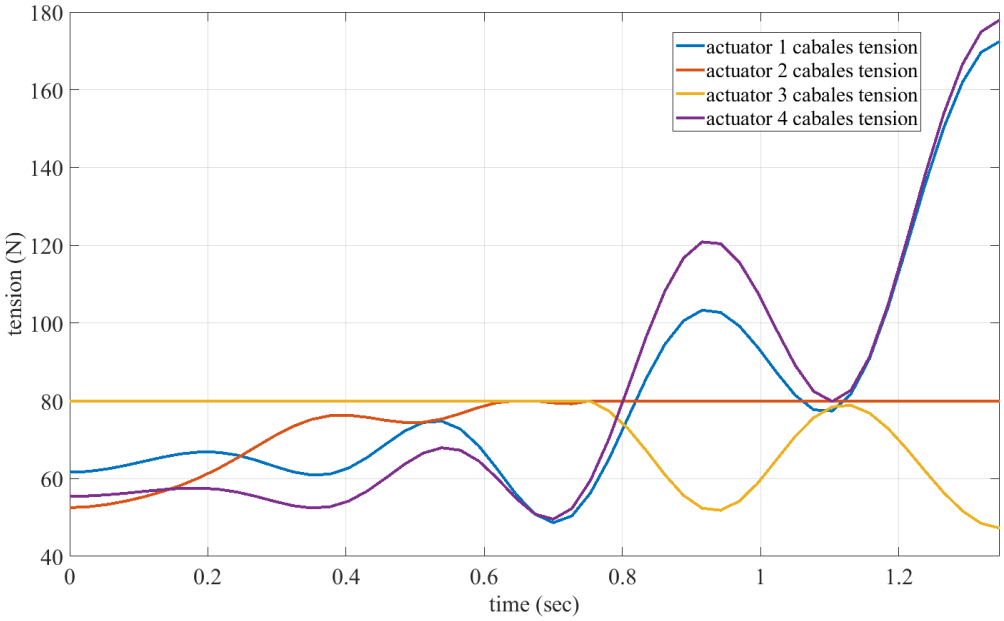

Figure 5-15: Tension of the cables along the stiffness-optimum trajectory.

Figure 5-9 to Figure 5-12 demonstrate the smoothness of the designed trajectory with zero values of velocity, acceleration and jerk in the initial and final time of motion. Figure 5-13, Figure 5-14 and Figure 5-15 demonstrate that the cables' velocity, acceleration and tension are within the allowable range. It is worth mentioning that the minimum motion time along the stiffness-optimum trajectory is around 50 percent of the minimum motion time along the straight line. Such observation shows, in spite of following a shorter distance, tracking the straight line is not providing the minimum motion time for a zero-to-zero continuous-jerk motion in general case.

5.6 Summary

The concepts of structural-stiffness-based trajectory-planning for KC-CDPRs has been proposed and studied in this chapter. In spite of considering a predetermined geometry for the moving platform's trajectory, minimizing the effects of an external disturbance on the perturbation of the moving platform was based to find the geometry of the optimal trajectory. Based on the structural stiffness model of KC-CDPRs and by considering a disturbance wrench on the moving platform, the platform's perturbation has been formulated. Based on the direction of the external disturbance force/moment vector and disturbance sensitivity of the platform in certain directions, different stiffness-based objective functions have been derived. According to the derived objective functions, two optimization problems have been formulated in the form of maximizing the minimum stiffness and maximizing the average stiffness, and the corresponding optimization algorithms have been developed.

After finding the stiffness-optimum geometry of the trajectory, a time-optimal zero-to-zero continuous-jerk motion design approach was proposed and studied. Considering the limitations of the cables' velocity, acceleration and tension, an analytic approach was developed to find the minimum feasible motion time along the determined trajectory. In order to clarify the details of the proposed approach, four examples of the warehousing KC-CDPR were studied where by using numerical and experimental results for these examples, effectiveness of the proposed approaches have been demonstrated.

Chapter 6: Conclusions and Future Work

6.1 Summary of Results and Conclusions

In this thesis, modeling, stiffness optimization, vibration and trajectory-tracking control as well as stiffness-optimization-based trajectory-planning of KC-CDPRs were studied. The main contributions of this thesis are as follows:

- A new generic dynamic modeling approach for flexible KC-CDPRs was proposed which made it possible to separate the linear vibration equations of the moving platform from its rigid body equations of motion. Based on the separated vibration model, the effects of both cables' arrangement and tension on the stiffness of the moving platform, during the motion and in static equilibrium conditions, were shown. The idea of directional stiffness maximization was proposed for solving the tensions redundancy problem enabling maximizing the stiffness of moving platform in certain directions. The proposed approach reduced the effects of external disturbances on undesired vibration of KC-CDPRs specifically in directions where the platform suffers from a low level of stiffness. Different experimental results were provided which validated the proposed modeling and tension optimization approaches.

- Based on the developed vibration model of the moving platform, a robust gain-scheduling LPV-H_∞ control structure was developed which made it possible to consider the effects of external disturbances in the control design of KC-CDPRs and also to minimize such effects on the trajectory-tracking performance. The effects of kinematically-constrained actuation method in vibration attenuation and control design simplification of KC-CDPRs was shown. This was shown practically for trajectory-tracking and vibration control of CDPRs that only a limited number of actuators can be involved where other actuators can be used to constrain the moving platform's undesired motion and vibrations. Real-time experimental results were provided which demonstrated the effectiveness of the developed control structure and actuation method.

- Stiffness-based trajectory-planning problem of KC-CDPRs was studied to find a stiffness-optimum path for the moving platform trajectory between two determined points. Following

such trajectories helped to minimize the effects of external disturbances on the perturbation of the moving platform. Time-optimal zero-to-zero jerk motion design approach was developed which made it possible to track the stiffness-optimum trajectory in the minimum feasible time where the cables' velocity, acceleration and tension limits are considered in the trajectory design. Such an approach helps to see the effects of limitations of actuators and cables on the minimum time of motion and to provide a motion with minimum vibration-simulating effects for the moving platform.

6.2 Future Work

To continue the work presented in this thesis, a few suggestions are made which are listed below:

- Improvement of the state-estimation approach: by using the model-based state-estimation techniques, a more precise estimation of the moving platform's states can be provided which can directly affect the trajectory-tracking performance of the KC-CDPR. In such an investigation, different state-estimation techniques can be proposed and tested on the KC-CDPR, where the limitations of the IMU in providing only the translational acceleration and angular velocities need to be considered.

- Considering the motion time in the proposed trajectory-planning approach: the proposed optimization algorithm considers only the directional stiffness of the moving platform for finding the optimum geometry for the trajectory, while the total time of motion can be another concern in pick-&-place applications. Accordingly, involvement of the total motion time in the defined objective function can provide a trade-off between the moving platform's stiffness and the motion time.

- Providing an adaptive control algorithm for performance improvement of the KC-CDPR: in the developed control structure of this study, it was assumed the mass and inertia of the moving platform is known, where uncertainty of the payloads can make such parameters uncertain. Accordingly, design of an adaptive algorithm to provide an online estimation of the payload mass and inertia to schedule the controller gains based on that can improve the performance of the developed control approach.

REFERENCES

[1] "Ecommerce Sales Topped $1 Trillion for First Time in 2012 - eMarketer." [Online]. Available: https://www.emarketer.com/Article/Ecommerce-Sales-Topped-1-Trillion-First-Time-2012/1009649. [Accessed: 26-Nov-2017].

[2] "How Many Ecommerce Companies Are There? - The Data Point." [Online]. Available: https://blog.rjmetrics.com/2014/06/18/how-many-ecommerce-companies-are-there/. [Accessed: 26-Nov-2017].

[3] "Automated Material Handling Equipment Market by Product ASRS, Automated Conveyors and Sortation Systems, Automated Cranes - 2023 | MarketsandMarkets." [Online]. Available: https://www.marketsandmarkets.com/Market-Reports. [Accessed: 26-Nov-2017].

[4] W. B. Lim, G. Yang, S. H. Yeo, and S. K. Mustafa, "A generic force-closure analysis algorithm for cable-driven parallel manipulators," *Mech. Mach. Theory*, vol. 46, no. 9, pp. 1265–1275, 2011.

[5] M. Arsenault, "Workspace and stiffness analysis of a three-degree-of-freedom spatial cable-suspended parallel mechanism while considering cable mass," *Mech. Mach. Theory*, vol. 66, pp. 1–13, 2013.

[6] I. Imam, G. N. Sandor, and S. N. Kramer, "Deflection and stress analysis in high speed planar mechanisms with elastic links," *J. Manuf. Sci. Eng.*, vol. 95, no. 2, pp. 541–548, 1973.

[7] B. M. Bahgat and K. D. Willmert, "Finite element vibrational analysis of planar mechanisms," *Mech. Mach. Theory*, vol. 11, no. 1, pp. 47–71, 1976.

[8] S. Nagarajan and D. A. Turcic, "Lagrangian formulation of the equations of motion for elastic mechanisms with mutual dependence between rigid body and elastic motions: Part I—element level equations," *J. Dyn. Syst. Meas. Control*, vol. 112, no. 2, pp. 203–214, 1990.

[9] R. L. W. Ii, R. L. Williams, P. Gallina, and J. Vadia, "Planar translational cable-direct-driven robots," *J. Robot. Syst.*, vol. 20, pp. 107–120, 2003.

[10] R. L. Williams and P. Gallina, "Planar cable-direct-driven robots: Design for wrench exertion," *J. Intell. Robot. Syst.*, vol. 35, no. 2, pp. 203–219, 2002.

[11] R. L. Williams, P. Gallina, and R. L. W. Ii, "Translational planar cable-direct-driven robots," *J. Intell. Robot. Syst. Theory Appl.*, vol. 37, pp. 69–96, 2003.

[12] H. Yuan, E. Courteille, and D. Deblaise, "Static and dynamic stiffness analyses of cable-driven parallel robots with non-negligible cable mass and elasticity," *MAMT*, vol. 85, pp. 64–81, 2015.

[13] Y. B. Bedoustani, H. D. Taghirad, and M. M. Aref, "Dynamics analysis of a redundant parallel manipulator driven by elastic cables," *10th Int. Conf. Control. Autom. Robot. Vision (*ICARCV*)*, 2008, pp. 536–542.

[14] X. Tang and R. Yao, “Dimensional Design on the Six-Cable Driven Parallel Manipulator of FAST,” *J. Mech. Des.*, vol. 133, no. November 2011, p. 111012, 2011.

[15] B. Zi, B. Y. Duan, J. L. Du, and H. Bao, “Dynamic modeling and active control of a cable-suspended parallel robot,” *Mechatronics*, vol. 18, no. 1, pp. 1–12, Feb. 2008.

[16] J. Albus, R. Bostelman, and N. Dagalakis, “The NIST robocrane,” *J. Robot. Syst.*, vol. 10, no. 5, pp. 709–724, 1993.

[17] P. Bosscher, R. L. Williams II, and M. Tummino, “A Concept for Rapidly-Deployable Cable Robot Search and Rescue Systems,” in *ASME International Design Engineering Technical Conferences & Computers and Information in Engineering Conference*, 2005, pp. 589–598.

[18] P. Bosscher, R. L. Williams, L. S. Bryson, and D. Castro-Lacouture, “Cable-suspended robotic contour crafting system,” *Autom. Constr.*, vol. 17, no. 1, pp. 45–55, Nov. 2007.

[19] A. Alikhani and M. Vali, “Modeling and robust control of a new large scale suspended cable-driven robot under input constraint,” *2011 8th Int. Conf. Ubiquitous Robot. Ambient Intell.*, pp. 238–243, Nov. 2011.

[20] A. Alikhani, S. Behzadipour, S. A. S. Vanini, and A. Alasty, “Workspace Analysis of a Three DOF Cable-Driven Mechanism,” *J. Mech. Robot.*, vol. 1, no. 4, p. 41005, 2009.

[21] M. Hassan and A. Khajepour, “Analysis of Large-Workspace Cable-Actuated Manipulator For Warehousing Applications,” in *ASME 2009 International Design Engineering Technical Conference*, 2009, pp. 1–9.

[22] H. D. Taghirad and M. A. Nahon, “Dynamic Analysis of a Macro – Micro Redundantly Actuated,” vol. 22, no. January 2015, pp. 949–981, 2008.

[23] Q. Duan, V. Vashista, and S. K. Agrawal, “Effect on wrench-feasible workspace of cable-driven parallel robots by adding springs,” *Mech. Mach. Theory*, vol. 86, pp. 201–210, 2015.

[24] B. Ouyang and W. Shang, “Wrench-feasible workspace based optimization of the fixed and moving platforms for cable-driven parallel manipulators,” *Robot. Comput. Integr. Manuf.*, vol. 30, no. 6, pp. 629–635, 2014.

[25] S. Perreault, P. Cardou, and C. Gosselin, “Approximate static balancing of a planar parallel cable-driven mechanism based on four-bar linkages and springs,” *Mech. Mach. Theory*, vol. 79, pp. 64–79, 2014.

[26] M. A. Khosravi and H. D. Taghirad, “Robust PID control of fully-constrained cable driven parallel robots,” *Mechatronics*, vol. 24, no. 2, pp. 87–97, 2014.

[27] R. Babaghasabha, M. A. Khosravi, and H. D. Taghirad, “Adaptive robust control of fully-constrained cable driven parallel robots,” *Mechatronics*, vol. 25, pp. 27–36, 2014.

[28] S. Perreault, P. Cardou, C. M. Gosselin, and M. J.-D. Otis, “Geometric Determination of the

Interference-Free Constant-Orientation Workspace of Parallel Cable-Driven Mechanisms," *J. Mech. Robot.*, vol. 2, no. August 2010, p. 31016, 2010.

[29] M. H. Korayem, M. Bamdad, and M. Saadat, "Workspace analysis of cable-suspended robots with elastic cable," in *IEEE International Conference on Robotics and Biomimetics, ROBIO*, 2007, pp. 1942–1947.

[30] S. Kawamura, W. Choe, S. Tanaka, and S. R. Pandian, "Development of an ultrahigh speed robot FALCON using wire drive system," in *Proceedings - IEEE International Conference on Robotics and Automation*, 1995, vol. 1, pp. 215–220.

[31] R. Verhoeven, M. Hiller, and S. Tadokoro, "Workspace, Stiffness, Singularities and Classification of Tendon-Driven Stewart Platforms," in *Advances in Robot Kinematics: Analysis and Control*, 1998, pp. 105–114.

[32] S. Behzadipour and A. Khajepour, "Stiffness of Cable-based Parallel Manipulators With Application to Stability Analysis," *J. Mech. Des.*, vol. 128, no. 1, p. 303-310, 2006.

[33] M. A. Khosraviand and H. D. Taghirad, "On the Modelling and Control of Fully Constrained Cable Driven Robots with Flexible Cables," in *2nd International Conference on Control, Instrumentation and Automation (ICCIA)*, 2011, pp. 1030–1035.

[34] M. A. Khosravi, H. D. Taghirad, and S. Member, "Dynamic Modeling and Control of Parallel Robots With Elastic Cables : Singular Perturbation Approach," *IEEE Trans. Robot.*, vol. 30, no. 3, pp. 1–11, 2014.

[35] A. Vafaei, M. A. Khosravi, and H. D. Taghirad, "Modeling and control of cable driven parallel manipulators with elastic cables: Singular perturbation theory," in *Lecture Notes in Computer Science (including subseries Lecture Notes in Artificial Intelligence and Lecture Notes in Bioinformatics)*, 2011, vol. 7101 LNAI, pp. 455–464.

[36] M. A. Khosravi, H. D. Taghirad, and R. Oftadeh, "A positive tensions PID controller for a planar cable robot: An experimental study," in *International Conference on Robotics and Mechatronics* (*ICRoM*), 2013, pp. 325–330.

[37] M. A. Khosravi and H. D. Taghirad, "Robust PID control of cable-driven robots with elastic cables," in *International Conference on Robotics and Mechatronics* (*ICRoM*), 2013, pp. 331–336.

[38] T. Bruckmann and a Pott, "A Reconfigurable Robot for Cable-Driven Parallel Robotic Research and Industrial Scenario Proofing Jean-Baptiste," *Cable-Driven Parallel Robot*, vol. 12, pp. 135–148, 2012.

[39] J. Du, C. Cui, H. Bao, and Y. Qiu, "Dynamic Analysis of Cable-Driven Parallel Manipulators Using a Variable Length Finite Element," *J. Comput. Nonlinear Dyn.*, vol. 10, no. 1, pp. 1–7, 2015.

[40] R. J. Caverly and J. R. Forbes, "Dynamic Modeling and Noncollocated Control of a Flexible

Planar Cable-Driven Manipulator," *Robotics, IEEE Transactions on*, vol. 30, no. 6. pp. 1386–1397, 2014.

[41] A. Alikhani, S. Behzadipour, F. Ghahremani, A. Alasty, and S. A. S. Vanini, "Modeling, Control and Simulation of a New Large Scale Cable- Driven Robot," *ASME Int. Des. Eng. Tech. Conf.*, pp. 1–6, 2009.

[42] J.-P. Merlet, "Kinematics of the wire-driven parallel robot MARIONET using linear actuators," *IEEE Int. Conf. Robot. Autom. (ICRA)*, pp. 3857–3862, 2008.

[43] D. Q. Nguyen, M. Gouttefarde, O. Company, and F. Pierrot, "On the simplifications of cable model in static analysis of large-dimension cable-driven parallel robots," *IEEE Int. Conf. Intell. Robot. Syst.*, pp. 928–934, 2013.

[44] X. Zhang, H. Li, R. Yao, and S. Yang, "Free Vibration Model and Experimental Study of the FAST Cable-Driven Parallel Mechanism," vol. 4, no. November, pp. 310–320, 2012.

[45] M. Hiller, S. Fang, S. Mielczarek, R. Verhoeven, and D. Franitza, "Design, analysis and realization of tendon-based parallel manipulators," *Mech. Mach. Theory*, vol. 40, no. 4, pp. 429–445, 2005.

[46] C. Gosselin and J. Angeles, "Singularity analysis of closed-loop kinematic chains," *IEEE Trans. Robot. Autom.*, vol. 6, no. 3, pp. 281–290, 1990.

[47] D. Zlatanov, R. G. Fenton, and B. Benhabib, "Singularity analysis of mechanisms and robots via avelocity-equation model of the instantaneous kinematics," *Proc. 1994 IEEE Int. Conf. Robot. Autom.*, pp. 986–991, 1994.

[48] X. Diao, O. Ma, and Q. Lu, "Singularity analysis of planar cable-driven parallel robots," *Conf. Robot. Autom. Mechatronics*, pp. 272–277, 2008.

[49] J. J. German, K. W. Jablokow, and D. J. Cannon, "The cable array robot: theory and experiment," *IEEE Int. Conf. Robot. Autom. (ICRA)*, 2001, vol. 3, pp. 2804–2810.

[50] S. R. Oh and S. K. Agrawal, "Cable-suspended planar robots with redundant cables: Controllers with positive tensions," *IEEE Trans. Robot.*, vol. 21, no. 3, pp. 457–465, 2005.

[51] S. R. Oh and S. K. Agrawal, "Generation of feasible set points and control of a cable robot," *IEEE Trans. Robot.*, vol. 22, no. 3, pp. 551–558, 2006.

[52] P. H. Borgstrom, N. P. Borgstrom, M. J. Stealey, B. Jordan, G. S. Sukhatme, S. Member, M. A. Batalin, and W. J. Kaiser, "Design and Implementation of NIMS3D , a 3-D Cabled Robot for Actuated Sensing Applications," *IEEE Trans. Robot.*, vol. 25, no. 2, pp. 325–339, 2009.

[53] D. Lau, D. Oetomo, and S. K. Halgamuge, "Generalized modeling of multilink cable-driven manipulators with arbitrary routing using the cable-routing matrix," *IEEE Trans. Robot.*, vol. 29, no. 5, pp. 1102–1113, 2013.

[54] H. D. Taghirad and M. A. Nahon, “Dynamic Analysis of a Macro–Micro Redundantly Actuated Parallel Manipulator,” *Adv. Robot.*, vol. 22, no. 9, pp. 949–981, 2008.

[55] M. A. Khosravi and H. D. Taghirad, “Dynamics analysis and control of cable driven robots considering elasticity in cables,” in *CCToMM Symposium*, pp. 1–12, 2011.

[56] S. Kawamura, H. Kino, and C. Won, “High-speed manipulation by using parallel wire-driven robots,” *Robotica*, vol. 18, pp. 13–21, 2000.

[57] R. J. Caverly, J. R. Forbes, and D. Mohammadshahi, “Dynamic Modeling and Passivity-Based Control of a Single Degree of Freedom Cable-Actuated System,” *IEEE Trans. Control Syst. Technol.*, vol. 23, no. 3. pp. 898-909, 2015.

[58] J. Du, H. Bao, C. Cui, and D. Yang, “Dynamic analysis of cable-driven parallel manipulators with time-varying cable lengths,” *Finite Elem. Anal. Des.*, vol. 48, no. 1, pp. 1392–1399, 2012.

[59] J. Du, C. Cui, H. Bao, and Y. Qiu, “Dynamic Analysis of Cable-Driven Parallel Manipulators Using a Variable Length Finite Element,” *J. Comput. Nonlinear Dyn.*, vol. 10, no. 1, pp. 1-7, 2015.

[60] G. Meunier, B. Boulet, and M. Nahon, “Control of an overactuated cable-driven parallel mechanism for a radio telescope application,” *IEEE Trans. Control Syst. Technol.*, vol. 17, no. 5, pp. 1043–1054, 2009.

[61] M. Gouttefarde and C. M. Gosselin, “Analysis of the wrench-closure workspace of planar parallel cable-driven mechanisms,” *IEEE Trans. Robot.*, vol. 22, no. 3, pp. 434–445, 2006.

[62] D. Lau, D. Oetomo, and S. K. Halgamuge, “Wrench-Closure Workspace Generation for Cable Driven Parallel Manipulators Using a Hybrid Analytical-Numerical Approach,” *J. Mech. Des.*, vol. 133, no. 7, pp. 71004, 2011.

[63] R. Kurtz and V. Hayward, “Dexterity measure for tendon actuated parallel mechanisms,” *Fifth Int. Conf. Adv. Robot. ’Robots Unstructured Environ.*, 1991.

[64] G. Barrette and C. M. Gosselin, “Determination of the Dynamic Workspace of Cable-Driven Planar Parallel Mechanisms,” *J. Mech. Des.*, vol. 127, no. 2, p. 242-248, 2005.

[65] H. D. Taghirad and Y. B. Bedoustani, “An Analytic-Iterative Redundancy Resolution Scheme for Cable-Driven Redundant Parallel Manipulators,” *IEEE Trans. Robot.*, vol. 27, no. 6, pp. 1137-1143, 2011.

[66] D. E. Whitney, “Resolved Motion Rate Control of Manipulators and Human Prostheses,” *IEEE Trans. Man-Machine Syst.*, vol. 10, no. 2, pp. 47–53, 1969.

[67] T. On, “Automatic Supervisory Control of the Configuration and Behavior of Multibody Mechanisms,” *IEEE Trans. Syst. Man. Cybern.*, vol. 7, no. 12, pp. 868–871, 1977.

[68] S. Fang, D. Franitza, M. Torlo, F. Bekes, and M. Hiller, "Motion Control of a Tendon-Based Parallel Manipulator Using Optimal Tension Distribution," *IEEE/ASME Trans. Mechatronics*, vol. 9, no. 3, pp. 561–568, 2004.

[69] C. Gosselin and M. Grenier, "On the determination of the force distribution in overconstrained cable-driven parallel mechanisms," *Meccanica*, vol. 46, no. 1, pp. 3–15, 2011.

[70] W.-J. Shiang, D. Cannon, and J. Gorman, "Dynamic analysis of the cable array robotic crane," in *IEEE Int. Conf. Robot. Autom.*, 1999, vol. 4, pp. 2495–2500.

[71] A. Pott, T. Bruckmann, and L. Mikelsons, "Closed-form force distribution for parallel wire robots," in *Computational Kinematics*, Springer, 2009, pp. 25–34.

[72] K. Yu, L. Lee, and V. Krovi, "Simultaneous trajectory tracking and stiffness control of cable actuated parallel manipulator," *ASME 2009 Int. Des. Eng. Tech. Conf. Comput. Inf. Eng. Conf.*, no. 716, pp. 55–63, 2009.

[73] K. Yu, L.-F. Lee, C. P. Tang, and V. N. Krovi, "Enhanced trajectory tracking control with active lower bounded stiffness control for cable robot," in *IEEE Int. Conf. Robot. Autom. (ICRA)*, 2010, pp. 669–674.

[74] M. Hassan and A. Khajepour, "Optimization of Actuator Forces in Cable-Based Parallel Manipulators Using Convex Analysis," *IEEE Trans. Robot.*, vol. 24, pp. 736–740, 2008.

[75] L. Mikelsons, T. Bruckmann, M. Hiller, and D. Schramm, "A real-time capable force calculation algorithm for redundant tendon-based parallel manipulators," in *IEEE Int. Conf. Robot. Autom. (ICRA)*, pp. 3869–3874, 2008.

[76] C. Gosselin, "Stiffness mapping for parallel manipulators," *IEEE Trans. Robot. Autom.*, vol. 6, no. 3, pp. 377–382, 1990.

[77] M. Griffis and J. Duffy, "Global stiffness modeling of a class of simple compliant couplings," *Mech. Mach. Theory*, vol. 28, no. 2, pp. 207–224, 1993.

[78] P. Bosscher and I. Ebert-Uphoff, "A stability measure for underconstrained cable-driven robots," *IEEE Int. Conf. Robot. Autom. (ICRA)*, 2004, vol. 5, pp. 4943–4949.

[79] M. Azadi, S. Behzadipour, and G. Faulkner, "Antagonistic variable stiffness elements," *Mech. Mach. Theory*, vol. 44, no. 9, pp. 1746–1758, Sep. 2009.

[80] M. M. Svinin, K. Ueda, and M. Uchiyama, "On the stability conditions for a class of parallel manipulators," *IEEE Int. Conf. Robot. Autom. (ICRA)*. vol. 3, 2000, pp. 2386–2391.

[81] M. M. Svinin, S. Hosoe, and M. Uchiyama, "On the stiffness and stability of Gough-Stewart platforms," *IEEE Int. Conf. Robot. Autom. (ICRA)*, 2001, vol. 4, pp. 3268–3273.

[82] S. Torres-Mendez and A. Khajepour, "Design Optimization of a Warehousing Cable-Based Robot," in *ASME International Design Engineering Technical Conferences and Computers*

and Information in Engineering Conference, 2014, pp. V05AT08A091-V05AT08A091.

[83] S. Javier and T. Méndez, "Analysis of a high stiffness warehousing cable-based robot," in *ASME International Design Engineering Technical Conferences and Computers and Information in Engineering Conference*, 2014, pp. V05AT08A088-V05AT08A088.

[84] M. Benosman and G. Le Vey, "Control of flexible manipulators: A survey," *Robotica*, vol. 22, no. 5, pp. 533–545, 2004.

[85] R. N. Banavar and P. Dominic, "An LQG/H∞ controller for a flexible manipulator," *Control Syst. Technol. IEEE Trans.*, vol. 3, no. 4, pp. 409–416, 1995.

[86] R. H. Cannon and E. Schmitz, "Initial Experiments on the End-Point Control of a Flexible One-Link Robot," *Int. J. Rob. Res.*, vol. 3, no. 3, pp. 62–75, Sep. 1984.

[87] M. Benosman, G. Le Vey, L. Lanari, and A. De Luca, "Rest-to-rest motion for planar multi-link flexible manipulator through backward recursion," *J. Dyn. Syst. Meas. Control*, vol. 126, no. 1, pp. 115–123, 2004.

[88] A. De Luca and G. Di Giovanni, "Rest-to-rest motion of a one-link flexible arm," in *IEEE/ASME International Conference on Advanced Intelligent Mechatronics*, 2001, vol. 2, pp. 923–928.

[89] A. De Luca and B. Siciliano, "Joint-based control of a nonlinear model of a flexible arm," in *American Control Conference*, 1988, pp. 935–940.

[90] S. K. Dwivedy and P. Eberhard, "Dynamic analysis of flexible manipulators, a literature review," *Mech. Mach. Theory*, vol. 41, pp. 749–777, 2006.

[91] H. Kino, T. Yahiro, F. Takemura, and T. Morizono, "Adaptive position control for fully constrained parallel wire driven systems," in *IEEE International Conference on Intelligent Robots and Systems*, 2006, pp. 79–84.

[92] H. Kino, T. Yahiro, F. Takemura, and T. Morizono, "Robust PD control using adaptive compensation for completely restrained parallel-wire driven robots: Translational systems using the minimum mumber of wires under zero-gravity condition," *IEEE Trans. Robot.*, vol. 23, no. 4, pp. 803–812, 2007.

[93] A. Alikhani and M. Vali, "Sliding Mode Control of a Cable-driven Robot via Double-Integrator Sliding Surface,", *International Conference on Control, Robotics and Cybernetics (ICCRC)*,2012, pp. 1–7.

[94] A. Ming and T. Higuchi, "Study on multiple degree-of-freedom positioning mechanism using wires. I: Concept, design and control," *Int. J. Japan Soc. Precis. Eng.*, vol. 28, no. 2, pp. 131–138, 1994.

[95] A. Ming and T. Higuchi, "Study on multiple degree-of-freedom positioning mechanism using wires. II: Development of a planar completely restrained positioning mechanism," *Int. J. Jpn.*

Soc. Precis. Eng., pp. 235–242, 1994.

[96] M. Zeinali and A. Khajepour, "Design and Application of Chattering-Free Sliding Mode Controller to Cable-Driven Parallel Robot Manipulator: Theory and Experiment," in *ASME International Design Engineering Technical Conferences and Computers and Information in Engineering Conference*, 2010, pp. 319–327.

[97] A. Ghasemi, M. Eghtesad, and M. Farid, "Constrained model predictive control of the redundant cable robots," *World Autom. Congr.*, 2008, pp. 1-6.

[98] P. Gholami, M. M. Aref, and H. D. Taghirad, "On the control of the KNTU CDRPM: A cable driven redundant parallel manipulator," *IEEE/RSJ Int. Conf. Intell. Robot. Syst.* (*IROS*), 2008 pp. 2404–2409.

[99] V. Duchaine, S. Bouchard, and C. M. Gosselin, "Computationally Efficient Predictive Robot Control," *IEEE/ASME Trans. Mechatronics*, vol. 12, no. 5, pp. 570–578, 2007.

[100] H. Kino, T. Yahiro, S. Taniguchi, and K. Tahara, "Sensorless Position Control Using Feedforward Internal Force for Completely Restrained Parallel-Wire-Driven Systems," *IEEE Trans. Robot.*, vol. 25, no. 2, pp. 467–474, Apr. 2009.

[101] D. Constantinescu and E. A. Croft, "Smooth and time-optimal trajectory-planning for industrial manipulators along specified paths," *J. Robot. Syst.*, vol. 17, no. 5, pp. 233–249, 2000.

[102] A. Gasparetto and V. Zanotto, "A technique for time-jerk optimal planning of robot trajectories," *Robot. Comput. Integr. Manuf.*, vol. 24, no. 3, pp. 415–426, 2008.

[103] A. Obradović, J. Vuković, N. Mladenović, and Z. Mitrović, "Time optimal motions of mechanical system with a prescribed trajectory," *Meccanica*, vol. 46, no. 4, pp. 803–816, 2011.

[104] S. Behzadipour and A. Khajepour, "Time-optimal trajectory-planning in cable-based manipulators," *IEEE Trans. Robot.*, vol. 22, no. 3, pp. 559–563, 2006.

[105] H. R. Fahham, M. Farid, and M. Khooran, "Time Optimal Trajectory Tracking of Redundant Planar Cable-Suspended Robots Considering Both Tension and Velocity Constraints," *J. Dyn. Syst. Meas. Control*, vol. 133, no. 1, pp. 11004-1-11004-14, 2011.

[106] L. Barbazza, F. Oscari, S. Minto, and G. Rosati, "Optimized Trajectory-planning of Pick and Place Operations to Be Performed by Cable-Driven Parallel Robots," in *Advances in Italian Mechanism Science*, Springer, 2017, pp. 287–295.

[107] E. Barnett and C. Gosselin, "Time-Optimal Trajectory-planning of Cable-Driven Parallel Mechanisms for Fully Specified Paths With G 1 -Discontinuities," *J. Dyn. Syst. Meas. Control*, vol. 137, no. 7, p. 71007, Jul. 2015.

[108] A. Sharifi and H. D. Taghirad, "Online time-optimal trajectory-planning in dynamic

workspace of cable-suspended robots," in *Second RSI/ISM International Conference on Robotics and Mechatronics* (*ICRoM*), 2014, pp. 239–244.

[109] M. Bamdad, "Time-energy optimal trajectory-planning of cable-suspended manipulators," in *Cable-Driven Parallel Robots*, Springer, 2013, pp. 41–51.

[110] S. K. Mustafa, G. Yang, S. H. Yeo, W. Lin, and I. M. Chen, "Self-calibration of a biologically inspired 7 DOF cable-driven robotic arm," *IEEE/ASME Trans. Mechatronics*, vol. 13, no. 1, pp. 66–75, 2008.

[111] S. Donohoe, S. Velinsky, and T. Lasky, "Mechatronic Implementation of a Force Optimal Underconstrained Planar Cable Robot," *IEEE/ASME Trans. Mechatronics*, vol. 21, no. 1, pp. 69-78, 2015.

[112] S. Behzadipour and A. Khajepour, "Design of reduced DOF parallel cable-based robots," *Mech. Mach. Theory*, vol. 39, no. 10, pp. 1051–1065, 2004.

[113] H. Jamshidifar, B. Fidan, G. Gungor, and A. Khajepour, "Adaptive vibration control of a flexible cable driven parallel robot," in *IFAC Proceedings Volumes (IFAC-PapersOnline)*, 2015, vol. 48, no. 3, pp. 1302–1307.

[114] O. Saber, "A Spatial Translational Cable Robot," *J. Mech. Robot.*, vol. 7, no. 3, p. 31006, 2015.

[115] H. Khakpour, L. Birglen, and S. A. Tahan, "Synthesis of differentially driven planar cable parallel manipulators," *IEEE Trans. Robot.*, vol. 30, no. 3, pp. 619–630, 2014.

[116] H. Jamshidifar, A. Khajepour, B. Fidan, and M. Rushton, "Kinematically-Constrained Redundant Cable-Driven Parallel Robots: Modeling, Redundancy Analysis, and Stiffness Optimization," *IEEE/ASME Trans. Mechatronics*, vol. 22, no. 2, pp. 921–930, 2017.

[117] H. Jamshidifar, S. Khosravani, B. Fidan, and A. Khajepour, "Vibration Decoupled Modeling and Robust Control of Redundant Cable-Driven Parallel Robots," *IEEE/ASME Trans. Mechatronics*, vol. 23, no. 2, pp. 690–701, 2018.

[118] E. D. Andersen and K. D. Andersen, "Presolving in linear programming," *Math. Program.*, vol. 71, no. 2, pp. 221–245, 1995.

[119] M. Rushton, "Vibration Control in Cable Robots Using a Multi-Axis Reaction System," MASc Thesis, University of Waterloo, 2016.

[120] C. Briat, *Linear parameter-varying and time-delay systems*, vol. 3. Springer, 2014.

[121] F. Blanchini, D. Casagrande, G. Giordano, and S. Miani, "On the LPV Control Design and Its Applications to Some Classes of Dynamical Systems," in *Developments in Model-Based Optimization and Control*, Springer, 2015, pp. 319–338.

[122] P. Gahinet, P. Apkarian, and M. Chilali, "Affine parameter-dependent Lyapunov functions

and real parametric uncertainty," *IEEE Trans. Automat. Contr.*, vol. 41, no. 3, pp. 436–442, 1996.

[123] L. Zaccarian and A. R. Teel, *Modern anti-windup synthesis: control augmentation for actuator saturation*. Princeton University Press, 2011.

[124] R. Babaghasabha, M. A. Khosravi, and H. D. Taghirad, "Adaptive robust control of fully-constrained cable driven parallel robots," *Mechatronics*, vol. 25, pp. 27–36, 2015.

[125] A. V Oppenheim, A. S. Willsky, and S. H. Nawab, *Signals and Systems*, vol. 2. Prentice-Hall Englewood Cliffs, NJ, 1983.

[126] Y. K. Thong, M. S. Woolfson, J. A. Crowe, B. R. Hayes-Gill, and D. A. Jones, "Numerical double integration of acceleration measurements in noise," *Measurement*, vol. 36, no. 1, pp. 73–92, 2004.

[127] W. T. Latt, K. C. Veluvolu, and W. T. Ang, "Drift-free position estimation of periodic or quasi-periodic motion using inertial sensors," *Sensors*, vol. 11, no. 6, pp. 5931–5951, 2011.

[128] S. Boyd and L. Vandenberghe, *Convex optimization*. Cambridge university press, 2004.